

2022

## Machine Learning Based Real-Time Quantification of Production from Individual Clusters in Shale Wells

Ayodeji Luke Aboaba

West Virginia University, aaboaba@mix.wvu.edu

Follow this and additional works at: <https://researchrepository.wvu.edu/etd>

 Part of the [Petroleum Engineering Commons](#)

---

### Recommended Citation

Aboaba, Ayodeji Luke, "Machine Learning Based Real-Time Quantification of Production from Individual Clusters in Shale Wells" (2022). *Graduate Theses, Dissertations, and Problem Reports*. 11269.

<https://researchrepository.wvu.edu/etd/11269>

This Dissertation is protected by copyright and/or related rights. It has been brought to you by the The Research Repository @ WVU with permission from the rights-holder(s). You are free to use this Dissertation in any way that is permitted by the copyright and related rights legislation that applies to your use. For other uses you must obtain permission from the rights-holder(s) directly, unless additional rights are indicated by a Creative Commons license in the record and/ or on the work itself. This Dissertation has been accepted for inclusion in WVU Graduate Theses, Dissertations, and Problem Reports collection by an authorized administrator of The Research Repository @ WVU. For more information, please contact [researchrepository@mail.wvu.edu](mailto:researchrepository@mail.wvu.edu).

# **Machine Learning Based Real-Time Quantification of Production from Individual Clusters in Shale Wells**

**Ayodeji L. Aboaba**

**Dissertation submitted  
to the Benjamin M. Statler College of Engineering and Mineral Resources  
at West Virginia University**

**in partial fulfillment of the requirements for the degree of**

**Doctor of Philosophy in  
Petroleum and Natural Gas Engineering**

**Shahab D. Mohaghegh, Ph.D., Chair**

**Samuel Ameri, M.S., P.E.**

**Kashy Aminian, Ph.D.**

**Hassan Amini, Ph.D.**

**Mehrdad Zamirian, Ph.D.**

**Scott Reeves, MBA**

**Department of Petroleum and Natural Gas Engineering**

**Morgantown, West Virginia  
2022**

**Keywords: Fuzzy Logic, Clustering, Fiber Optics, DTS, Production Logging, Real-time  
Monitoring, Hydraulic Fracturing, Machine Learning, Artificial Intelligence, Neural  
Networks.**

**©Copyright 2022 Ayodeji L. Aboaba**

## **ABSTRACT**

### **Machine Learning Based Real-Time Quantification of Production from Individual Clusters in Shale Wells**

**Ayodeji Aboaba**

Production logs have proved invaluable for identifying production and completion anomalies and problems in oil and gas wells. Conventional production logging especially in horizontal wells come with challenges such as the risks associated with lowering the logging tools into the wellbore, harsh downhole conditions, and the cost of well intervention. More importantly, measurements acquired from conventional production logging is only a snapshot of the downhole condition for that moment in time. Over the last two decades, there has been advances in downhole monitoring in oil and gas wells with the use of Fiber-Optic sensing technology such as the Distributed Temperature Sensing (DTS). Unlike a conventional production log that provides only snapshots of the well performance, DTS provides continuous temperature measurements along the entire wellbore. Unfortunately, current DTS interpretation methods are based on visualization of the temperature change in the DTS measurements, and are qualitative in nature, at best.

Whether by fluid extraction or injection, oil and gas production changes reservoir conditions, and continuous monitoring of downhole conditions is highly desirable. This research study presents a tool for real-time quantification of production from individual perforation clusters in a multi-stage shale well using Artificial Intelligence and Machine Learning. The technique presented provides continuous production log on demand thereby providing opportunities for the optimization of completions design and hydraulic fracture treatments of future planned wells. A Fiber-Optic sensing enabled horizontal well MIP-3H in the Marcellus Shale has been selected for this work. MIP-3H is a 28-stage horizontal well drilled in July 2015, as part of a Department of Energy (DOE)-sponsored project - Marcellus Shale Energy & Environment Laboratory (MSEEL). A one-day conventional production logging operation has been performed on MIP-3H using a flow scanner while the installed Fiber-Optic DTS unit has collected temperature measurements every three hours along the well since completion. An ensemble of machine learning models has been developed using as input the DTS measurements taken during the production logging operation, details of mechanical logs, completions design and hydraulic fracture treatments data of the well to develop the real-time shale gas production monitoring tool.

## **DEDICATION**

This work is dedicated to my wife, Bolanle Aboaba, who has been a constant source of support and encouragement during the challenges of graduate school and life. I am truly thankful for having you in my life. This work is also dedicated to my research advisor, Dr. Shahab Mohaghegh for the guidance and support he gave me throughout this process.

## **ACKNOWLEDGEMENTS**

I give thanks to God for the grace and strength I have received to complete this work. Throughout my research study and the writing of this dissertation, I have received a great deal of support and assistance.

I would first like to thank my advisor, Dr. Shahab Mohaghegh, whose expertise was invaluable in formulating the research questions and methodology. Your insightful feedback pushed me to sharpen my thinking and brought the best out of my work.

A special thank you also goes to my committee members who have provided immense support in various forms. This work would not have been possible without your feedback and the encouragement you gave me every step of the way.

# Table of Contents

<b>List of Tables .....</b>	<b>vii</b>
<b>Table of Figures.....</b>	<b>viii</b>
<b>Chapter 1: Introduction .....</b>	<b>1</b>
1.1 Problem Statement .....	1
1.2 Research Objective.....	2
1.3 Hydraulic Fracturing Overview .....	3
1.4 Production Logging Overview .....	4
1.5 Distributed Temperature Sensing (DTS) Technology Overview .....	4
1.6 Machine Learning Overview.....	5
1.6.1 Fuzzy Clustering .....	6
1.6.2 Random Forests .....	6
1.6.3 Artificial Neural Networks .....	7
1.7 Structure of Work.....	8
<b>Chapter 2: Literature Review.....</b>	<b>9</b>
2.1 Distributed Fiber Optic Sensing Systems .....	9
2.2 Applications of Distributed Temperature Sensing (DTS) in Petroleum Industry .....	9
2.2.1 Hydraulic Fracturing.....	10
2.2.2 Well Treatment and Stimulation.....	11
2.2.3 Leakage Detection .....	12
2.2.4 Flow Monitoring .....	13
2.3 Machine Learning based Flow Monitoring Using DTS.....	15
<b>Chapter 3: MIP-3H Data Collection .....</b>	<b>18</b>
3.1 Study Area.....	18
3.2 Completion Data .....	19
3.3 Mechanical Logs .....	20
3.4 Hydraulic Fracturing Treatment Data .....	22
3.5 DTS Measurements .....	23
3.6 Production Log.....	23
3.7 Building the Spatial-Temporal Database .....	26
<b>Chapter 4: Model Development.....</b>	<b>28</b>
4.1 Feature Engineering – Completion Data.....	28
4.2 Feature Engineering – Geomechanical Logs .....	29

4.3	Feature Engineering – Gas Production Rate Data.....	34
4.4	Database Construction for Model Development.....	36
4.5	Feature Selection.....	38
4.6	Fuzzy Classification Model using Random Forest .....	39
4.7	Regression Model using Artificial Neural Network .....	40
<b>Chapter 5: Model Validation &amp; Discussion.....</b>		<b>41</b>
5.1	Data Partitioning .....	41
5.2	Model Validation Scenario 1: Blind Stage #4 & Clusters 1 – 7 .....	42
5.3	Model Validation Scenario 2: Blind Stage #15 & Clusters 1 – 7 .....	44
5.4	Model Validation Scenario 3: Blind Stage #26 & Clusters 1 – 7 .....	47
<b>Chapter 6: Conclusion &amp; Recommendations.....</b>		<b>49</b>
6.1	Conclusion.....	49
6.2	Recommendation.....	50
<b>References.....</b>		<b>51</b>
<b>Appendix.....</b>		<b>59</b>

## List of Tables

Table 1: Summary of the Completion Design .....	19
Table 2: Available Completion Data .....	20
Table 3: Schlumberger Sonic Scanner Logs .....	21
Table 4: Selected Geomechanical Logs for Analysis .....	21
Table 5: Available Hydraulic Fracturing Treatment Data .....	22
Table 6: Snapshot of DTS Measurements at a Well Section .....	23
Table 7: MIP-3H Data Collected from MSEEL Website .....	27
Table 8: Offset Perforation Cluster Distance Features .....	29
Table 9: Generated Features from Geomechanical Logs.....	34
Table 10: Fuzzy Sets for Gas Production Rate Data.....	35
Table 11: Number and Percent of Cases Per Fuzzy Set.....	35
Table 12: Gas Production Rate Fuzzy Membership Features.....	36
Table 13: MIP-3H Database Features Post Descriptive Analytics .....	37
Table 14: MIP-3H Database Features Selected for Model Development.....	38

## Table of Figures

Figure 1: Schematics of a DTS Unit .....	5
Figure 2: Types of Nodes in a Decision Tree .....	7
Figure 3: Artificial Neural Network Architecture .....	8
Figure 4: Modeling Workflow to Estimate Flow Rate using DTS Data (Johnson et al. 2006) ....	13
Figure 5: Wells Located in the Marcellus Shale Energy and Environment Laboratory (MSEEL) Site. ....	18
Figure 6: Production Logging Tool Trajectory and Travel Time .....	24
Figure 7: Excerpt from the Flow Scanner Log Interpretation Report.....	25
Figure 8: Identifying DTS Measurements at Individual Perforation Cluster Location .....	26
Figure 9: Offset Perforation Cluster Distances .....	29
Figure 10: Traditional Completions Design with no Consideration for Lateral Heterogeneity ...	30
Figure 11: Engineered Completion Design.....	30
Figure 12: Identifying Geomechanical Log Measurement Intervals for Clustering .....	31
Figure 13: Offset Cluster Heterogeneity Index.....	32
Figure 14: Stage Heterogeneity Index .....	33
Figure 15: Gas Production Rate Distribution from Production Log .....	34
Figure 16: Fuzzy Set Memberships from Gas Production Rate Data .....	36
Figure 17: Gas Production Fuzzy Classification Model Using Random Forest .....	39
Figure 18: Gas Production Regression Model Using Artificial Neural Network .....	40
Figure 19: Data Partitioning for Model Validation Scenario 1 .....	42
Figure 20: Fuzzy Classification Training Results for Validation Scenario 1 .....	43
Figure 21: Fuzzy Classification Validation Results for Validation Scenario 1 .....	43
Figure 22: Fuzzy Classification Blind Validation Results for Validation Scenario 1 .....	43
Figure 23: Production Log vs. ANN Regression Results for Blind Validation in Scenario 1 .....	44
Figure 24: Production Log vs. ANN Regression Results for Clusters 1-7 for Validation Scenario 1 .....	44
Figure 25: Data Partitioning for Model Validation Scenario 2 .....	45
Figure 26: Fuzzy Classification Training Results for Validation Scenario 2 .....	45
Figure 27: Fuzzy Classification Validation Results for Validation Scenario 2 .....	45

Figure 28: Fuzzy Classification Blind Validation Results for Validation Scenario 2 .....	45
Figure 29: Production Log vs. ANN Regression Results for Blind Validation in Scenario 2.....	46
Figure 30: Production Log vs. ANN Regression Results for Clusters 1-7 for Validation Scenario 2.....	46
Figure 31: Data Partitioning for Model Validation Scenario 3.....	47
Figure 32: Fuzzy Classification Training Results for Validation Scenario 3 .....	47
Figure 33: Fuzzy Classification Validation Results for Validation Scenario 3 .....	47
Figure 34: Fuzzy Classification Blind Validation Results for Validation Scenario 3 .....	47
Figure 35: Production Log vs. ANN Regression Results for Blind Validation in Scenario 3.....	48
Figure 36: Production Log vs. ANN Regression Results for Clusters 1-7 for Validation Scenario 3.....	48
Figure 37: DTS Measurements in Stage 1 on Day of Production Log .....	59
Figure 38: DTS Measurements in Stage 2 on Day of Production Log .....	59
Figure 39: DTS Measurements in Stage 3 on Day of Production Log .....	60
Figure 40: DTS Measurements in Stage 4 on Day of Production Log .....	60
Figure 41: DTS Measurements in Stage 5 on Day of Production Log .....	61
Figure 42: DTS Measurements in Stage 6 on Day of Production Log .....	61
Figure 43: DTS Measurements in Stage 7 on Day of Production Log .....	62
Figure 44: DTS Measurements in Stage 8 on Day of Production Log .....	62
Figure 45: DTS Measurements in Stage 9 on Day of Production Log .....	63
Figure 46: DTS Measurements in Stage 10 on Day of Production Log .....	63
Figure 47: DTS Measurements in Stage 11 on Day of Production Log .....	64
Figure 48: DTS Measurements in Stage 12 on Day of Production Log .....	64
Figure 49: DTS Measurements in Stage 13 on Day of Production Log .....	65
Figure 50: DTS Measurements in Stage 14 on Day of Production Log .....	65
Figure 51: DTS Measurements in Stage 15 on Day of Production Log .....	66
Figure 52: DTS Measurements in Stage 16 on Day of Production Log .....	66
Figure 53: DTS Measurements in Stage 17 on Day of Production Log .....	67
Figure 54: DTS Measurements in Stage 18 on Day of Production Log .....	67
Figure 55: DTS Measurements in Stage 19 on Day of Production Log .....	68
Figure 56: DTS Measurements in Stage 20 on Day of Production Log .....	68

Figure 57: DTS Measurements in Stage 21 on Day of Production Log .....	69
Figure 58: DTS Measurements in Stage 22 on Day of Production Log .....	69
Figure 59: DTS Measurements in Stage 23 on Day of Production Log .....	70
Figure 60: DTS Measurements in Stage 24 on Day of Production Log .....	70
Figure 61: DTS Measurements in Stage 25 on Day of Production Log .....	71
Figure 62: DTS Measurements in Stage 26 on Day of Production Log .....	71
Figure 63: DTS Measurements in Stage 27 on Day of Production Log .....	72
Figure 64: DTS Measurements in Stage 28 on Day of Production Log .....	72

# Chapter 1: Introduction

## 1.1 Problem Statement

Exploration and exploitation of the shale formations in the United States has continued to accelerate since the early 2000's. Once considered to exist only as a cap rock, Shale is now proving to be one of the most important reservoir rocks in North America and throughout the world. In most Shale formations, horizontal wells are drilled through the reservoir before being hydraulically fractured at a series of discrete zones and placed on production. The subsequent zonal gas production rates have proved highly variable and inconsistent for the same shale gas reservoirs that have been completed and treated in the same way. In fact, production evaluation data have confirmed that two-thirds of gas production comes from one-third of perforation clusters, and almost one-third of all perforation clusters is not contributing to production [1]. Furthermore, studies have indicated that the completion, hydraulic fracture treatment design, operational and production issues can all significantly influence multi-fractured horizontal well production and economics. However, due to the extreme complexities encountered, determining the specifics of a completion and hydraulic fracture design that will result in the highest economic return on investment is problematic. This has resulted in increased demand for production logging (PL) in these reservoirs to better understand the basis behind higher stimulation efficiency and increased production results. Operators use production logs to evaluate fluid movement in and out of the wellbores, quantify flow rates and determine fluid properties at downhole conditions. Completion engineers can evaluate production and completion efficiency, and plan remediation or modify future completion designs based on the interpretation of production logs.

The traditional production logging technique requires occasionally lowering the logging tool into the wellbore to measure flow rate and fluid properties. This method is reactive as it is often used as a response to an event or scheduled as part of workover and well intervention plans. The timing of such infrequent measurements may not be optimal for diagnosing production problems or capturing the dynamic changes that occur in the reservoir. Occasional measurements in wells rarely detect production events as they occur and often fail to describe production behavior, or even define a trend because of the low frequency at which they are collected. Production logs in Shale gas wells are normally recorded 30 to 60 days after the stimulation process has finished [2].

In addition to the inadequacy of the traditional production logs, companies contend with high cost of well intervention and the risk of lowering expensive production logging tools into the extended reach horizontal wells in Shale. The production log must contend with semi-stagnant water trapped in the lateral section because of the wellbore trajectory, substantial wellbore debris impacting depth of data capture, and completion configurations that limit equipment options and ease of logging.

Over the last two decades, fiber-optic based sensing such as the Distributed Temperature Sensing (DTS) has opened opportunities for in-well reservoir surveillance in the oil and gas industry. A characteristic thermal gradient signature is created when fluid flows in or out of a wellbore [3]. For example, fluid flows from high-pressure reservoirs into the wellbore during production. The recovery of liquid fluids produces a warming trend in the wellbore, whereas gas recovery produces a cooling effect known as the Joule Thompson effect [4]. Such basic characteristics help to determine liquid and gas movements by using Distributed Temperature Sensing (DTS). Unlike a conventional production log that provides only snapshots of the well performance, DTS provides a continuous temperature profile of the entire wellbore in real time, which in turn, can provide an enhanced understanding of the downhole production (or injection) profile. Thermal profiling along the reservoir section and over the well itself reveals trends, which when appropriately analyzed, help corroborate reservoir inflow and well performance characteristics.

DTS data interpretation in the oil and gas industry can be divided into qualitative and quantitative methods. For example, to detect a leak in the wellbore, qualitative understanding of the leak location based on visualization of the temperature change in the DTS measurements is sufficient whereas in flow profiling, a quantitative approach is required. Most quantitative approaches combine numerical models with DTS data to convert temperature signals to the desired parameter. Unfortunately, current quantitative approaches to flow profiling using DTS data are complicated and have assumptions in the thermal models which impacts the ability of such approaches to capture the dynamics of flow over time.

## **1.2 Research Objective**

One goal for oil fields of the future is acquiring continuous and on-demand data; and making timely operational decisions as required for field and reservoir management. The objective of this

research study is to develop a workflow for real-time quantification of production from individual perforation clusters in a multi-stage Shale gas well using Artificial Intelligence and Machine Learning. This work leverages the fiber optics Distributed Temperature Sensing (DTS) technology to provide continuous production log on demand thereby providing opportunities for the optimization of completions design and hydraulic fracture treatments of future planned Shale wells. The data-driven approach utilizes spatio-temporal data collected from a 28-stage hydraulically fractured horizontal well in the Marcellus Shale, in Northern West Virginia. An ensemble of machine learning models, comprising of a random forest model and an artificial neural network model was developed using as input the downhole DTS measurements, production measurements taken during a production logging operation, details of mechanical logs, completions design and hydraulic fracture treatments data of the well. The model provides real-time measurement of shale gas production from individual perforation clusters of the well.

### **1.3 Hydraulic Fracturing Overview**

Hydraulic fracturing is a technique used in stimulating hydrocarbon production from shale gas or oil formations. Since ultra-low permeability coefficients of shale formation make it hard for hydrocarbons to transport towards the wellbore, artificial fractures are induced to the shale formation to achieve commercial gas production rate. Directional and horizontal drilling combined with hydraulic fracturing have made the production of natural gas from different shale formations achievable in some parts of the world. Hydraulic fractures are created by injecting fluid such as slick water, under high pressure. The fluid that is used in hydraulic fracturing is mixed with proppants, commonly referred to as sand. The proppant is pumped into the fractured rock to prop the fractures open and relatively permeable to formation fluids once the fracturing pressure from the injected fluid is released. In addition to the fracturing fluid and the proppant, some other chemicals (commonly referred to as additives) are added to the fluid mixture. These chemicals serve many functions during hydraulic fracturing, such as controlling the injected fluid's viscosity. A lot of factors affect the efficiency of a hydraulic fracturing treatment, some of which include formation in-situ stress, fracturing fluid properties, the type and amount of proppant, pumping schedule, reservoir fluid and rock properties, completion design among others.

## **1.4 Production Logging Overview**

While several geophysical logs such as sonic log, resistivity log and many more can be run to acquire formation and fluid properties during the exploration and development stage of a well, production logging is only performed after a well is completed and placed on production. The general purpose of production logging is to evaluate the behavior and type of fluids within the wellbore during production or injection operations. It is often used to evaluate the success of horizontal well placement and reservoir stimulation in Shale reservoirs. Once an hydraulically fractured shale well has cleaned up, a production log is run to measure the zonal production from each perforation cluster. Results from the production log are used to calibrate the petrophysical, reservoir, and fracturing models. The production logging tools are small in diameter and are run through tubing for evaluation of the well as it is producing. A production logging assembly usually comprises of a combination of a wide range of sensors which provides downhole measurements such as temperature, fluid density, fluid capacitance, pressure, fluid velocity and so on. One of such tools is the Schlumberger Flow Scan Imager (FSI) which is widely used in the industry for production logging in multiphase horizontal wells. The tool provides a phase area measurement (holdup) and phase velocity measurement of gas, oil and water in the wellbore using advanced probe and micro-spinner technology [5]. The product is a direct, down-hole calculation of multiphase production. When combined with seismic, micro-seismic, petrophysical, geological, completion and stimulation data, it becomes an invaluable tool for realizing what is required for optimal well performance [6] [7].

## **1.5 Distributed Temperature Sensing (DTS) Technology Overview**

Fiber-optic distributed-temperature systems offer excellent capabilities to increase the effectiveness of temperature surveillance. No cable movement is required, and measurements are taken by the fiber-optic cable, so many temperature surveys can be conducted for a given period. A modern fiber optic DTS system uses optical fiber as the primary sensing element. This fiber sensing element is smaller than a human hair. A DTS system senses temperature much like Doppler radar senses weather conditions. Monochromatic light pulses, generated by a laser source, are sent down the length of fiber from the surface at periodic intervals. As the light pulses strike imperfections in the fiber, some light is scattered and reflected towards the source (Rayleigh

scattering), and some light excites the molecules at the imperfection. These excited molecules scatter light at wavelengths above and below the incident light. One component of scattered light pulses is known as Brillouin scattering, and another component is Raman scattering. Brillouin scattering results in wavelengths very close to the incident wavelength and is difficult to process for temperature measurements. Raman scattering consists of two wavelengths that are about 440nm above and below the incident wavelength. These two wavelengths are known as Stokes and anti-Stokes. The longer wavelength, or stokes component, is relatively temperature insensitive, while the shorter wavelength (anti-stokes) increases intensity with an increase in temperature. Thus, by comparing the intensity of stokes and anti-stokes components, the temperature along the length of the fiber can be determined. The results from many pulses of light are averaged to determine the temperature profile along the length of fiber. Present instruments can determine the temperature at each meter interval along the fiber. A fiber-optic distributed-temperature-sensing system can be installed on the tubing or casing on either a permanent or semi-permanent basis. It can also be run as a retrievable system much like a wireline logging system. DTS system components and backscattered lights are demonstrated in the figure below [8].

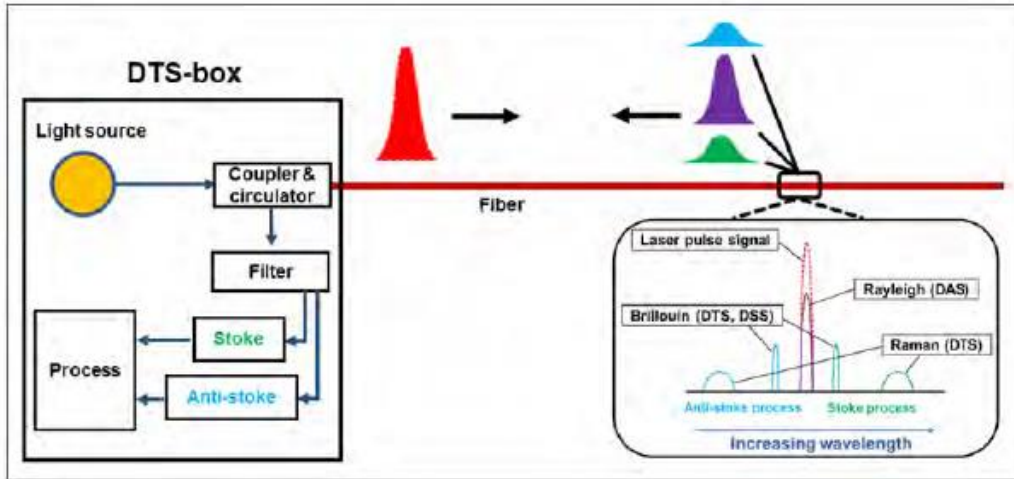


*Figure 1: Schematics of a DTS Unit*

## 1.6 Machine Learning Overview

Artificial intelligence and machine learning are widely known technologies that aim to teach machines to learn from input data. Machine learning algorithms can be classified mainly into Supervised and Unsupervised learning algorithms. Supervised learning algorithms learn a function

that, given a sample of data and desired outputs, best approximates the relationship between input features and output (also known as ground truth) observable in the data. Unsupervised learning algorithms, on the other hand, do not have labeled outputs; so, the goal is to infer the natural structure or underlying pattern present within a set of data points.

### **1.6.1 Fuzzy Clustering**

Clustering is a form of unsupervised learning technique which involves assigning data points (or objects) to clusters (groups) such that points in the same cluster are as similar as possible. The simplest form of cluster analysis is the hard clustering in which a data point exclusively belongs to a single cluster. Fuzzy clustering is useful in avoiding the arbitrariness of assigning an object or data point to only one cluster when it may be close to several. In fuzzy clustering (also called soft clustering), every object or data point belongs to every cluster with a membership weight that is between 0 (absolutely does not belong) and 1 (absolutely belongs). Cluster membership weights for any data point must sum up to 1.

In this study, the `skfuzzy` package from a popular open-source machine learning library `Scikit-learn` is used in performing fuzzy clustering tasks.

### **1.6.2 Random Forests**

A random forest is a supervised machine learning algorithm that is constructed from decision tree algorithms. It is a technique used to solve regression and classification problems. It utilizes ensemble learning, which is a technique that combines many classifiers to provide solutions to complex problems. A random forest algorithm consists of many decision trees and establishes its' outcome based on the predictions of the decision trees. It predicts by taking the average or mean of the output from various trees. Increasing the number of trees increases the precision of the outcome. A random forest eradicates the limitations of a decision tree algorithm. It reduces the overfitting of datasets and increases precision [9].

A decision tree consists of three components: decision nodes, leaf nodes, and a root node. A decision tree algorithm divides a training dataset into branches, which further segregate into other branches. This sequence continues until a leaf node is attained. The leaf node cannot be segregated further. The nodes in the decision tree represent attributes that are used for predicting the outcome.

Decision nodes provide a link to the leaves. The following diagram shows the three types of nodes in a decision tree. The Random Forest Regressor algorithm from Scikit-learn python library is used in this study.

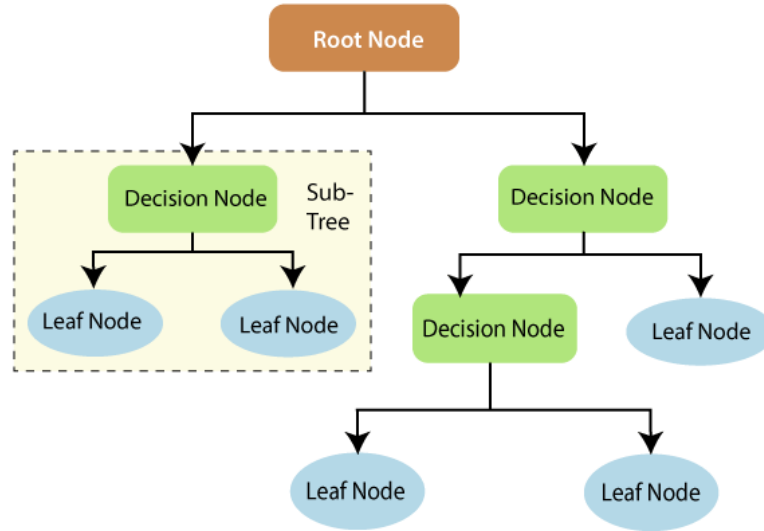


*Figure 2: Types of Nodes in a Decision Tree*

### 1.6.3 Artificial Neural Networks

One of the most common supervised learning algorithms is the Artificial Neural Network (ANN). An ANN is a simple mathematical computational algorithm that is capable of learning from input data (machine learning) as well as discovering patterns (pattern recognition) [10]. ANN is biologically inspired by the interconnections that take place between neurons in a human brain. Neurons carry and pass information from one neuron to another via synapse. The architecture of artificial neural networks consists of an input layer, one or more hidden layers, and an output layer. The input layer contains the information provided to the neural network in the form of attributes. The hidden layer is responsible for translating the information from the input layer to the output layer by a system of weighted connections and non-linear activation functions [10]. **Figure 3** shows a typical ANN with four input attributes, three neurons in the hidden layer and a single neuron in the output layer. The strength of information passed from one artificial neuron to another is assigned by its “weight”. Optimization of these weights is crucial in the development of a well-trained neural network.

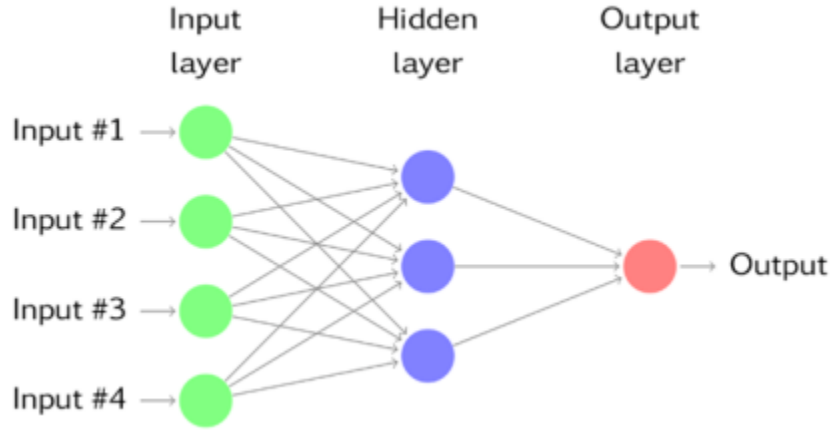


*Figure 3: Artificial Neural Network Architecture*

In this study, a machine learning library in Python called Keras is used in modeling artificial neural networks [11]. Keras is an open-source high-level neural networks API written in Python and capable of running on top of TensorFlow, CNTK, or Theano.

## 1.7 Structure of Work

This dissertation report details the research work performed in developing a purely data-driven approach to production performance monitoring in hydraulically fractured Shale wells using distributed temperature sensing measurements.

In chapter one (this chapter), the problem was defined, and the final objective of the research was articulated. A brief introduction to the key elements of the study was provided in this chapter as well, to provide a background. Chapter two provides a literature review on the applications of fiber optics DTS in the Petroleum Industry, and DTS interpretation and analysis methods. Chapter three provides detail description of the site of study, data collection and preparation. Detailed steps taken to build the predictive models are presented in Chapter four while the model validation results, and discussion follow in Chapter five. Conclusions and recommendations are provided in Chapter six.

## **Chapter 2: Literature Review**

### **2.1 Distributed Fiber Optic Sensing Systems**

Low-permeability formations such as Shale present a tremendous challenge to effective completion and reservoir drainage, especially in known heterogeneous environments that present additional complexity. Several robust diagnostic techniques exist in the market currently that are identified as guides to improve completion and stimulation efficiency in basins that require hydraulic fracturing to make low-permeability environments viable. Some of these techniques include fracture modeling, micro-seismic mapping, diagnostic fracture injection test (DFIT) analysis, radioactive and chemical tracers, and pressure matching [12]. During the past decade, fiber-optic sensing has been identified as an additional tool that can provide significant benefit to complement these more traditional approaches. Fiber optic sensing uses the physical properties of light as it travels along a fiber to detect changes in temperature, strain, and other parameters. There are various fiber optic sensing systems including Distributed Temperature Sensing (DTS), Distributed Acoustic Sensing (DAS), Distributed Vibration Sensing (DVS) or Distributed Disturbance Sensing (DDS), Distributed Strain Sensing (DSS), Distributed Pressure Sensing (DPS) and Distributed Chemical Sensing (DCS). These are all real-time technologies capable of continuous recording of property changes over time. Additionally, they are distributed sensing, meaning that the sensing and recordings take place all along the fiber. Thus, the recorded data is a function of location and time. DTS has been utilized for temperature monitoring, DAS for acoustic signal monitoring, DVS for disturbance (vibration) signature location monitoring, DSS for compaction monitoring, DPS for fluid level determination, and DCS for specific fluid molecule determination. Among these, DTS is the most matured technology and has been successfully examined for a long time.

### **2.2 Applications of Distributed Temperature Sensing (DTS) in Petroleum Industry**

DTS has been deployed for various purposes in the petroleum industry such as hydraulic fracturing characterization, well treatment or stimulation, organic/inorganic depositions, leak detection, flow monitoring, reservoir and fluid characterization in both injectors and producers. Soroush *et al.* [8] have performed an extensive literature review on various applications of DTS in the oil and gas industries.

### 2.2.1 Hydraulic Fracturing

Hydraulic fracturing characterization is one of the main applications of DTS deployment. Wang and Bussear [13] used qualitative DTS analysis for real-time monitoring of the movement and distribution of fluid in fractures during and after fracturing as well as to analyze fracture stage effectiveness. Malanya *et al.* [14] used DTS data before, during and after re-fracturing to identify new fracture positions in hydraulic fracturing. Holley *et al.* [12] used DTS to estimate fracture height during hydraulic fracturing and fluid placement during each stage in Permian basin. Fracture modeling was performed, using data acquired by fiber optics to constrain the model. Sierra *et al.* [15] presented their experience on DTS deployment for hydraulic fracturing. They believe that the location of fiber (for example, if it is conveyed with coiled tubing or permanently installed behind the casing) had a significant impact on the temperature measurements. Huckabee [16] illustrated three types of DTS installation, including temporary call-out survey, velocity string installation and permanent behind the casing. Then, they analyzed horizontal and vertical well stimulation and hydraulic fracture containments in a disposal well using DTS. They stated that DTS can be used as a complementary tool to radioactive tracer surveys. Holley *et al.* [17] [18] discussed the DTS data along with log data of an uncemented multistage hydraulic fracturing to analyze the effectiveness of the stimulation. In open hole completion, understanding of hydraulic fracturing geometry, number and locations of fractures are challenging. Therefore, DTS data is useful for overall effectiveness.

Tabatabaei and Zhu [19] developed a thermal model to use DTS data and simulate temperature behavior during fracturing and shut-in period. They interpreted fracture fluid distribution from DTS data using inversion methods (stochastic and gradient-based). Sun *et al.* [20] developed a numerical model to simulate flow and temperature. They included multi-component, multiphase flow, slippage, and mass transfer between phases in their model and finally, they analyzed the influence of different parameters on the results. Tarrahi *et al.* [21] used Ensemble Kalman Filter to characterize hydraulic fracturing using DTS data including fracture geometry (height and half length) and conductivity. Kalia *et al.* [22] developed a thermo-hydraulic model to capture the effect of Joule-Thomson and transient period and interpret DTS data in hydraulic fracturing. Holley *et al.* [23] stated that the combination of micro-seismic mapping and DTS data have the advantages of enabling real-time decision-making during fracture treatment, more accurate post-fracture

analysis and ability to combine diagnostic tools with production analysis. McCullagh *et al.* [24] used micro-seismic data to improve or calibrate temperature models (real time and warm back temperature models) which are based on DTS data to evaluate fluid distribution and hydraulic fracturing characterization of Eagle Ford.

### **2.2.2 Well Treatment and Stimulation**

DTS has been extensively used in many acid stimulation projects to monitor the stimulation job. Fahim *et al.* [25] presented the experience of Carbonate coiled tubing stimulation with DTS for Abu Dhabi onshore fields. They stated that DTS records before, during and after stimulation job indicate whether injected acid and diverter are efficient. They were able to perform a velocity interpretation of the injection profile and optimized fluid placement. Sharma *et al.* [26] presented the application of permanently installed DTS to optimize acid treatment in a case study of carbonate formation. They used Inflow Control Device (ICD) with packer completion and monitored acid injection before and after various acid stages. Santin *et al.* [27] presented the results of DTS application in one injector to monitor the stimulation job. They used DTS to ensure fluid placement in different zones, have optimum pumping schedule and rate; and assess stimulation effectiveness. Al-Najim *et al.* [28] used DTS in coiled tubing and smart fluid for the stimulation of a well with high water-cut. The viscosity of smart fluid builds up when it contacts with water and breaks down when it comes in contact with hydrocarbon. Therefore, it can plug the water zone and divert the acid toward the hydrocarbon zone. Reyes *et al.* [29] assessed stimulation effectiveness during pumping job and efficiency of fluid placement into the zones using DTS data. Grayson *et al.* [30] used a fiber optic slickline DTS system to monitor the stimulation job in a naturally fractured reservoir in California. They stated that fractures with higher conductivity show larger response than the ones with lower conductivity.

Tardy *et al.* [31] [32] used DTS in coiled tubing and couple the DTS data with inversion algorithm to quantitatively analyze acidizing and evaluate zonal coverage and fluid placement performance. In inversion algorithm, DTS recordings are transformed to zonal coverage log using numerical models. Operators have also used DTS to optimize fluid placement and distribution. For example, Glasbergen *et al.* [33] used DTS and a thermal model to quantify fluid distribution in matrix treatment. Vazquez *et al.* [34] used DTS in a case study from offshore Mexico to monitor the fluid distribution and fluid allocation in stimulation. Pinto *et al.* [35] performed lab tests using a flow

loop with installed DTS to simulate fluid placement during acid stimulation. Wang and Bussear [36] used DTS data and a modeling technique to perform qualitative analysis (using type curves) and quantitative analysis of fluid placement in acid stimulation. Tabatabaei *et al.* [37] [38] used a mathematical model and DTS data to obtain acid profile distribution in matrix acidizing. They used the heat of reaction, conduction and convection heat transfer and mass transfer to model near wellbore. They used inversion method to interpret acid distribution from DTS data. Ramondenc and Baez [39] used DTS to evaluate fluid placement in acid stimulation treatment in two case studies of carbonate formations. Lopez *et al.* [40] presented the application of inversion algorithm with thermal model to use DTS data for zonal coverage and fluid distribution quantification in acid treatment of a carbonate rock. Their fluid distribution inside the stimulated intervals agreed with the PLT data. Davies *et al.* [41] used DTS system along with PLT and water flow log to determine thief zones in acid stimulation job. They also developed a thermo-hydraulic mathematical model to determine temperature signatures associated with thief zones.

### **2.2.3 Leakage Detection**

Mao *et al.* [42] established an analytical model to obtain leakage rate around the wellbore in CO<sub>2</sub> injection at storage zones using DTS data. Their model is based on energy balance of major mechanisms including Joule-Thomson effect and heat conduction. Sun *et al.* [43] used DTS and high-pressure water jet in two wells to analyze cement quality and evaluate wellbore integrity in a geological storage project. Setiawan *et al.* [44] presented the results of DTS slickline deployment in two examples of offshore Malaysia to determine temperature anomalies and wellbore leak detection. Thompson *et al.* [45] presented the results of a case study for which DTS was used in a SAGD injector for casing and cement integrity evaluation. They observed that one injector was affected by neighboring steam chamber as temperature did not fall off.

Mishra *et al.* [46] presented the application of DTS technology in a case study for monitoring gas leakage in the pipeline and mentioned the key advantages of using this technology. These advantages include long-distance monitoring, accuracy, speed of the method, durability, and low maintenance. Bersan *et al.* [47] investigated the leak detection caused by backward erosion and seepage in piping using DTS. They used large-scale testing and with the help of numerical modeling they detected the onset of thermal anomalies. Weppenaar *et al.* [48] presented the

application of DTS in monitoring flowline, risers, and trenched section of risers to detect possible breach or damage and manage riser integrity.

#### 2.2.4 Flow Monitoring

Several authors used thermal models coupled with DTS measurements to determine flow rate. For example, Kabir *et al.* [49] utilized DTS data and a wellbore model using steady flow and unsteady heat transfer to determine the flow rate in both gas and oil reservoirs. Wang *et al.* [50] [51] used DTS data and steady-state energy balance and developed a flow profiling model. Later, Wang *et al.* [52] used Fourier series approximation to improve flow profiling while spatial resolution was preserved. They determined the best fit time interval and multipoint pressure data integration with DTS to achieve this goal. Ouyang and Belanger [53] [54] developed a thermal model for single and multiphase flow along the wells (vertical, deviated and horizontal) which uses DTS data for predicting injection and production profiles. They stated that for multiphase flow, beside DTS data, additional data is needed. Lanier *et al.* [55] used DTS data in a 1000-meter open hole horizontal producer to evaluate flow profile along the well. They used thermal model analysis and stated that only a portion of the heel was producing. Johnson *et al.* [56] used DTS data in an analytical-numerical temperature-pressure model to estimate the gas flow rate in gas reservoirs. They compared the results with PLT data and quantified zonal production. **Figure 4** shows the workflow of their simulation. They also stated that DTS transient analysis can be used to estimate oil and gas injection and production rates. By monitoring real-time temperature variations, operators can assess problems and promptly make decisions.

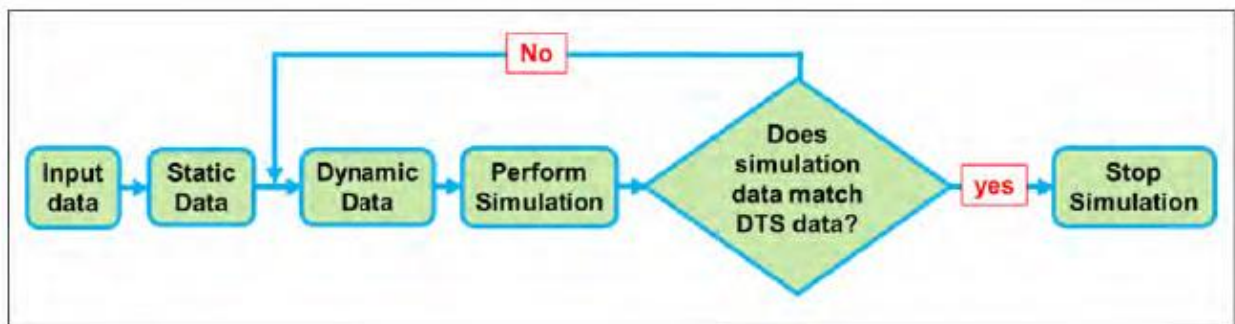


*Figure 4: Modeling Workflow to Estimate Flow Rate using DTS Data (Johnson et al. 2006)*

John *et al.* [57] integrated DTS with open hole gravel pack completion in a field of Azerbaijan for real-time production estimation. Hembling *et al.* [58] used DTS in advanced well completion systems and maximum reservoir contact wells in Saudi Arabia for efficient and accurate flow monitoring. Mehmood *et al.* [59] analyzed a case study in Pakistan for which DTS was used with coiled tubing where production logging could not be mechanically deployed.

Carlsen *et al.* [60] used permanent DTS and pressure monitoring to monitor/optimize production in horizontal wells in the Danish North Sea.

Tolan *et al.* [61] used DTS with inflow control valves to manage the amount of water into the producer in Douglas Field. Using DTS, layering, permeability variation within a single zone and zonal contribution can be investigated. DTS system has been used in various water injection projects to monitor water injection. When water is injected into a reservoir, it cools down the wellbore surrounding and the drainage radius. By shutting the injection, the reservoir and wellbore surrounding will warm back. This warm-back rate is significantly slower in porous zones which depends on the zone permeability. This mechanism has been used for permeability distribution and injection profiling. Foo *et al.* [62] discussed the application of DTS for injection profiling in Cardium Formation, Pembina field located in Alberta to detect channels and perform workover for water cut reduction. They used warm-back analysis along with storage analysis and waterfront analysis to assess the data. Khamatdinov *et al.* [63] stated that DTS can measure the real-time temperature along the wellbore at 0.01-0.1 °C temperature resolution and 1-meter spatial resolution. They used a case study in which DTS data was utilized as a history match parameter of simulation for waterflood optimization and efficient water injection.

Brown *et al.* [64] presented the results of DTS with a portable fiber unit named as Sensa tube unit. This unit which is like slickline unit with fiber inside a tube was used for water injection warm-back analysis to provide water injection profile through the production interval.

Nuñez-Lopez [65] used DTS data to monitor temperature and hence CO<sub>2</sub> flow within injection zones as well as detection of CO<sub>2</sub> leakage to overburden in the US Gulf Coast. Wiese [66] correlated heat transfer and thermodynamic conditions to DTS data in Ketzin, Germany in a CO<sub>2</sub> project. Mawalkar *et al.* [67] presented the results of real-time DTS and multi-level pressure data to monitor CO<sub>2</sub> migration into the reservoir in a CO<sub>2</sub>-EOR project in northern Michigan. They used warm-back analysis to determine where CO<sub>2</sub> enters the reservoir as well as monitor its

vertical migration. Richard and Pevzner [68] used DTS data to monitor the location of thermal anomalies for a carbon capture and storage research project.

Chin *et al.* [69] discussed the application of a dual laser DTS system in monitoring of water alternating gas (WAG) project in Malaysia. They stated that dual laser DTS eliminates the need for a double-ended fiber and tolerates the hydrogen darkening. They recorded temperature in 5-second intervals. Comparing to PLT, therefore, they eliminated the need of intervention, reduced the costs and decreased the number of personnel and increased operational efficiency.

Mehtiyev *et al.* [70] used a thermal-fluid model and Temperature Inflection Point (TIP) and analyzed the results of DTS for injection zonal allocation determination in a field in California. They stated that DTS has a higher measurement frequency, lower risk and cost compared to PLT and Radioactive Tracer Survey (RTS). Furniss *et al.* [71] used DTS to interpret the flow zone contribution qualitatively in a coal seam gas producer which is located in Surat basin, Queensland, Australia. They combined DTS with air assisted flow test by which  $kh$  (permeability-thickness) is measured for comparison purpose. Similarly, Bottomley *et al.* [72] discussed the application of permanent DTS in coal seam gas production wells to determine zonal flow allocation. This is important in commingled wells which are completed in stacked reservoir units. They developed a thermal model to obtain zonal allocation for single phase water production period. Uncertainty in geothermal gradient and fluid level, and multiphase flow were the challenges they encountered.

Brown *et al.* [73] presented the results of DTS deployment in three case studies from northern and southern Mexican regions for gas lift valves operation and gas lift optimization. Costello *et al.* [74] used hybrid DTS to monitor gas lift functionality and completion integrity. The system monitors downhole pressure, and all gas lift valves. Wang *et al.* [75] developed a software which is based on a model derived from steady state energy balance. The software has two modes: forward mode and simulation flow profiling. They used forward mode to model gas lift surveillance. They compared their model with other existing models.

### **2.3 Machine Learning based Flow Monitoring Using DTS**

Machine learning algorithms have become increasingly popular in the oil and gas industry because of their capabilities in efficiently recognizing hidden patterns in extremely complex, non-linear, and multivariate data. Sadigov *et al.* [76] used data (including DAS and DTS) collected from a flow loop facility equipped with fiber optic cables as per the completion design in Clair Ridge

reservoir. Several laboratory experiments (flow loop tests) were performed covering a range of fluid type and rate combinations expected from the actual well, to detect relative inflow rates of different fluid types along the wellbore during production. The laboratory experiments were designed to replicate reservoir conditions as closely as possible in production and injection wells in Clair Ridge. Ghahfarokhi *et al.* [77] trained a multi-layer perceptron (MLP) neural network with stage based daily DTS data, and daily flowing time to predict the well gas production for the next day in a Marcellus Shale well. Data-driven machine learning algorithms were applied to shale gas production performance analysis by integrating distributed acoustic sensing (DAS), distributed temperature sensing (DTS) fiber-optic, completions, flow scanner production log, and surface data to model daily gas production from a 28- stage stimulated horizontal well drilled in the Marcellus Shale [78]. Each completed stage was assumed to produce its share calculated from the flow scanner production log. Li *et al.* [79] developed ResNet and Convolutional LSTM networks to predict stage-based pump pressure and slurry rates using DAS, DTS and micro-seismic measurements as input. Sherman *et al.* [80] developed a physics-informed deep neural network model capable of interpreting DAS measurements in near-real time, and imaging hydraulic fracture propagation in an unconventional oil and gas reservoir. The synthetic data used in developing the neural network model was generated using a physics-based thermal-hydraulic-mechanical model to simulate synthetic DAS measurements for a range of subsurface conditions such as fracture propagation, fault slip etc.

Alkhalaf *et al.* [81] developed a methodology to use machine learning in detecting water-cut measurements from raw DAS data. The data used in the study was generated from the production logging of an oil well with fiber optics capability. Three different classification models were developed in their approach: a simple Decision Tree and two ensemble models - adaptive boost and Random Forest. Atakishiyev *et al.* [82] proposed a physics-based Machine Learning approach using DAS and DTS measurements for inflow profiling in a high-rate gas condensate well. Distributed acoustic and temperature sensing (DAS & DTS) data were acquired simultaneously while the well was producing approximately 70 MMSCF/D gas. Conventional production log data was also acquired under the same condition to validate the flow profiling results obtained from distributed fiber optics sensing measurements. The DAS and DTS data were processed to extract information regarding the presence of inflow as well as its phase and rate. The output was a set of thermal and acoustic features. The features were then labelled and used in training the machine

learning models. The library that is fed into these models consists of more than 650 experiments where independent parameters such as phase and rate were varied in a controlled lab environment. A logistic regression model was developed to predict inflow likelihood while a Ridge regressor model was trained to predict the phase rate and sand rate.

Obviously, most of the DTS applications in the Petroleum Industry have utilized qualitative interpretations or at best mathematical models which are characterized by assumptions and uncertainties in their approach. The latest developments and studies in application of machine learning to DTS interpretation shows a great potential to successful inflow profiling. However, no machine learning based approach has focused on quantifying production from Shale wells in real-time using DTS measurements, especially at the individual perforation cluster level.

## Chapter 3: MIP-3H Data Collection

### 3.1 Study Area

The well selected for this study is in the Morgantown Industrial Park (MIP) area in West Virginia, United States. The well is part of the Marcellus Shale Energy and Environment Laboratory (MSEEL); a field site and dedicated multi-disciplinary research laboratory provided by the U.S. Department of Energy with the objective of identifying and demonstrating technologies required for best practices in shale resource development, from drilling to completion through production. At the MIP site, two horizontal wells (MIP-4H and MIP-6H) were drilled in Marcellus Shale and have produced natural gas since December 2011. Two more horizontal wells (MIP-3H and MIP-5H) were drilled within the existing pad and placed on production in December 2015. MIP site also includes a vertical scientific observation well (MIP-SW) drilled approximately one-half mile to the northwest between the two new horizontal wells for the purpose of additional subsurface data collection, and micro-seismic monitoring [83]. The locations of the existing and newly drilled wells are depicted in *Figure 5*.



*Figure 5: Wells Located in the Marcellus Shale Energy and Environment Laboratory (MSEEL) Site*

The gas well chosen for this study is the MIP-3H well, which has the distributed fiber optics sensing system installed. The 28-stage horizontal well MIP-3H, with a lateral length of 6,058 feet, drilled and completed in the Marcellus Shale, contains a plethora of multi-scale and multi-sensor-

based spatio-temporal data, such as surface pressure, surface temperature, Distributed Acoustic Sensing (DAS), Distributed Temperature Sensing (DTS), petrophysical logs, geomechanical logs, and flow scanner production log for each completed stage, which were used in this study. The data used are publicly available from the MSEEL website [84].

### 3.2 Completion Data

The MIP-3H well was completed with 133 perforation clusters over 28 stages in 5 sections from the toe to the heel **Table 1**. Section A, B and D were completed using a geometric design approach in which perforation clusters are geometrically spaced with no consideration for the geomechanical properties (such as fracture closure stress and fracture intensity) along the well lateral.

Section		Stage	Cluster Count	Total Shot Count	Shot Density (shot/ft)	Stage Length (ft)	Pump schedule
E	Best Practice Applied	28	4	40	6	191	A
		27	4	40	6	184	A
		26	5	40	6	225	A
		25	5	32	6	231	A
		24	5	30	6	222	A
		23	5	40	6	237	C
		22	5	40	6	220	C
D	Sapphire VF	21	5	40	5	218	D
		20	5	40	5	240	D
C	SLB Engineered Completion	19	4	32	6	180	C
		18	4	32	8	180	C
		17	4	32	6	181	C
		16	4	26	6	178	C
		15	4	26	6	186	C
		14	5	30	6	228	A
		13	5	30	6	230	A
B	NNE 75% 100-Mesh	12	5	50	5	231	B
		11	5	50	5	232	B
		10	5	50	5	227	B
		9	5	50	5	237	B
		8	5	50	5	222	B
		7	5	50	5	224	B
A	NNE Standard 35% 100-Mesh	6	5	50	5	245	A
		5	5	50	5	234	A
		4	5	50	5	230	A
		3	5	50	5	238	A
		2	5	50	5	223	A
		1	5	50	5	233	A

*Table 1: Summary of the Completion Design*

Section C comprising of stages 13 to 19 was completed using an Engineered Completion approach. The Engineered Completion approach takes the reservoir heterogeneity into consideration and attempts to place perforation clusters in the same stage in zones of similar geomechanical properties such as fracture closure stress, fracture intensity, and gamma ray. In addition to the engineered placement of perforation clusters, a limited entry approach was taken by varying the number of shots per cluster to enhance stimulation efficiency [85]. Section E includes stages 22 to 28, in which stages were completed using either the geometric design or the limited entry approach. Each stage is approximately 200ft long with 4 or 5 perforation clusters, 3ft to 5ft in length and each consisting of 5-6 shots/foot. Stage spacing varies from 20 to 50 feet with an average of 24feet between plug depths to the nearest cluster in the previous stage. **Table 2** shows the list of available features in the completion data.

<b>Completion Data</b>
Cluster Top (ft MD)
Cluster Bottom (ft MD)
Cluster Length (ft)
Stage Length (ft)
Shot Count
Shot Orientation
Blast Shield (Perf) Depth
Blast Shield Orientation (deg)
Blast Shield Spacing (ft)

*Table 2: Available Completion Data*

### 3.3 Mechanical Logs

A series of geomechanical logs obtained from the MIP-3H well using the Sonic Scanner tool from Schlumberger is available on the MSEEL website. Measurements obtained from the Sonic Scanner tool can be used to optimize cluster placements by identifying shale anisotropy and favorable fracturing conditions based on calculated young modulus, poisson's ratio, minimum horizontal stress, pore pressure and overburden pressure. All these values can be interpreted to design a completions program that takes into account the physical properties of the shale formation. Logs available from sonic scanner measurements on the MIP-3H well are shown in **Table 3**, with their

definitions and how these values were obtained [86]. The log measurements were obtained at every 0.5ft MD of the lateral section of the well.

Logged Property:	Definition:	Calculated with:
C11 Elastic Modulus	Elastic Stiffness Coefficient in the C11 Direction	DT Compessional, DT Shear Fast and Slow
C12 Elastic Modulus	Elastic Stiffness Coefficient in the C12 Direction	DT Compessional, DT Shear Fast and Slow
C13 Elastic Modulus	Elastic Stiffness Coefficient in the C13 Direction	DT Compessional, DT Shear Fast and Slow
C33 Elastic Modulus	Elastic Stiffness Coefficient in the C33 Direction	DT Compessional, DT Shear Fast and Slow
C44 Elastic Modulus	Elastic Stiffness Coefficient in the C44 Direction	DT Compessional, DT Shear Fast and Slow
C55 Elastic Modulus	Elastic Stiffness Coefficient in the C55 Direction	DT Compessional, DT Shear Fast and Slow
C66 Elastic Modulus	Elastic Stiffness Coefficient in the C66 Direction	DT Compessional, DT Shear Fast and Slow
Borehole Deviation	Wellbore angular change from vertical (Inclination)	Direct Measurement
DT Compessional	Measured travel time for compressional waves	Direct Measurement
DTS Fast	Measured travel time for fast shear waves	Direct Measurement
DTS Slow	Measured travel time for slow shear waves	Direct Measurement
GR-Thompson	Original measurement of gamma radition	Direct Measurement
GR	Gamma Ray - Standard measurement of gamma radition	Direct Measurement
Azi	Azimuth - Angular depature from true north	Direct Measurement
Pore Pressure Gradient	Change in pore pressure per depth	Defined by tool operator
Pore Pressure	Fluid pressure within the pore space of the rock	Pore Pressure Gradient
PR Horiz	Poissons Ratio - Measure of material deformation perpendicular to applied force (Hoizontal)	DT Compessional, DT Shear Fast and Slow
PR Vert	Poissons Ratio - Measure of material deformation perpendicular to applied force (Vetical)	DT Compessional, DT Shear Fast and Slow
RHOB	Bulk Desnity - weight per given volume	Direct Measurement
TVD	True Vertical Depth from surface reference	Borehole Deviation, Azimuth
Iso Closure Stress Gradient	Closure stress per depth in Isotropic formations	Defined by tool operator
Anisio Closure Stress Gradient	Closure stress per depth in Anisotropic formations	Defined by tool operator
Iso Closure Stress	Pressure at which formation fractures close in Isotropic formations	Iso Closure Stress Gradient
Aniso Closure Stress	Pressure at which formation fractures close in Anisotropic formations	Anisio Closure Stress Gradient
Overburden Gradient	Overburden pressure per depth	Defined by tool operator
Overburden Pressure	pressure resulting from the weight of overlying formations	Overburden Gradient
YM Dynamic Hz	Young's Modulus - moving average of formation tesnise stiffness in the horizontal direction	DT Compessional, DT Shear Fast and Slow
YM Static Hz	Young's Modulus - instantaneous tesnise stiffness in the horizontal direction	DT Compessional, DT Shear Fast and Slow
YM Dynamic Vt	Young's Modulus - moving average of formation tesnise stiffness in the vertical direction	DT Compessional, DT Shear Fast and Slow
YM Static Vt	Young's Modulus - instantaneous tesnise stiffness in the vertical direction	DT Compessional, DT Shear Fast and Slow

*Table 3: Schlumberger Sonic Scanner Logs*

As shown in the table, some of the logs were direct property measurements while others have been derived (or calculated) from direct measurements. For a purely data-driven approach, it is important to avoid human biases or assumptions in measurements; we therefore focus on only geomechanical logs that are direct property measurements. **Table 4** lists the logs that have been considered useful for analysis in this study. The logs were collected from the MSEEL website [84] for every 0.5ft MD interval of the well.

Geomechanical Logs	Description
Borehole Deviation	Wellbore angular change from vertical (Inclination)
DT Compessional	Measured travel time for compressional waves
DT Fast	Measured travel time for fast shear waves
DT Slow	Measured travel time for slow shear waves
Gamma Ray-Thompson	Original measurement of gamma radiation
Gamma Ray	Standard measurement of gamma radiation
Azimuth	Angular departure from true north
Bulk Density	Rock weight per given volume

*Table 4: Selected Geomechanical Logs for Analysis*

### 3.4 Hydraulic Fracturing Treatment Data

Two types of proppants are used for hydraulic fracturing of MIP-3H: 100 mesh sand and 40/70 mesh white sand. Section A has around 38% 100 Mesh proppants and 62% 40/70 white sand, while Section B has 75% 100 Mesh Sand and 25% 40/70 white sand. The proportion of proppants varies between stages in Section C: Stages 13, 14, 15, 17, and 19 have 35% 100 mesh while Stage 16 has 67% mesh 100 and Stage 18 around 43% mesh 100. A new guar-free viscoelastic fracturing fluid known as Sapphire VF® is used in stages 20 and 21 (Section D) to maximize the well performance (Schlumberger, 2014). Sapphire fluids are designed to enhance proppants transport, deliver higher retained proppant pack permeability, improve fracture clean up, and lower the treatment pressure. Section E used Sapphire fluid, and an accelerated pumping schedule.

Proppants & Fluids	Treatment Schedule
Pad Volume (bbl.)	Fracture Gradient (psi/ft)
Total Clean Fluid (bbl.)	Initial Shut-in Pressure (ISIP) (psi)
Prop.1-Type	5 Min ISIP (psi)
Prop.1-Amount (lbs.)	10 Min ISIP (psi)
Prop.2-Type	15 Min ISIP (psi)
Prop.2-Amount (lbs.)	Breakdown Rate (BPM)
Total Proppant Amount (lbs.)	Breakdown Pressure (psi)
Flush Volume (bbl.)	Breakdown Volume (bbl.)
Screen Out (X)	Avg Treating Pressure (psi)
Acid % Strength	Max Treating Pressure (psi)
Total Acid (gals)	Avg Treating Rate (BPM)
Total Slickwater (bbl.)	Max Treating Rate (BPM)
Total Linear (bbl.)	Duration of Fracturing Treatment (secs)
Total Cross-Link (bbl.)	
Friction Reducer Amount (gals)	
Gel Amount (gals or lbs.)	
Breaker Amount (gals or lbs.)	
Scale Inhibitor (gals)	
Biocide (gals)	
Pump Down Volume (bbl.)	
Plug Depth	
Proppant Concentration (lb./ft)	
Proppant Concentration (lb./gal)	
Fluid Load (bbl./ft)	
Gel Volume (%)	
Pad Volume (%)	
Overflush Volume (bbl.)	

*Table 5: Available Hydraulic Fracturing Treatment Data*

### 3.5 DTS Measurements

The MIP-3H well is equipped with the Schlumberger WellWatcher Hyperion DTS system. The WellWatcher Hyperion portable DTS system acquisition system uses Raman spectroscopy along optical fibers in the well to measure the temperature at each fiber location. In MIP-3H, the fiber optic cable is installed behind the casing and temperature measurements have been collected since February 2016 at every 4ft or 5ft interval along the horizontal section of the well, every three hours. **Table 6** shows a snapshot of DTS measurements on a typical day, in a section of the well from 7,701 ft MD to 7,747 ft MD in 4ft or 5ft intervals.

Start_Pos	End_Pos	delta (ft)	DTS-R1	DTS-R2	DTS-R3	DTS-R4	DTS-R5	DTS-R6	DTS-R7	DTS-R8
7701	7706	5	166.32	167.26	167.07	167.81	167.3	167.96	167.27	167.34
7706	7710	4	166.39	167.11	166.92	167.78	167.99	168	167.49	167.38
7710	7715	5	166.52	167.04	167.04	167.9	168.56	168.22	167.68	167.27
7715	7720	5	166.42	167	167.23	167.88	168.48	168.45	167.59	167.32
7720	7724	4	166.42	167.12	167.03	167.66	168.27	168.12	167.59	167.27
7724	7729	5	166.44	167.04	167.04	167.76	167.8	167.85	167.4	167.51
7729	7733	4	166.52	167.29	167.21	167.67	167.65	168.2	167.5	167.49
7733	7738	5	166.57	167.3	167.4	167.82	167.97	168.12	167.85	167.68
7738	7743	5	166.71	167.28	167.58	168.11	168.26	168.22	167.73	167.58
7743	7747	4	166.62	167.26	167.39	168.47	168.49	168.3	167.75	167.51

*Table 6: Snapshot of DTS Measurements at a Well Section*

Plots of DTS measurements for all clusters in each stage on the day of production log are presented in the Appendix section. The plots show the minimum, maximum and average DTS measurements for each cluster in every stage, against the recorded gas production rate measurements from the production log.

### 3.6 Production Log

A production logging operation was performed on the MIP-3H well on March 2, 2017, using the Schlumberger Flow Scanner. The production logging interpretation report obtained from the Flow Scanner logging tool contained 5 mini-spinners, 6 water holdup measurements, 6 gas holdup measurements, relative bearing, deviation, caliper, pressure and temperature measurements that were recorded at various cable speeds [84]. Figure below is an illustration of the tool trajectory and travel time during the logging operation.

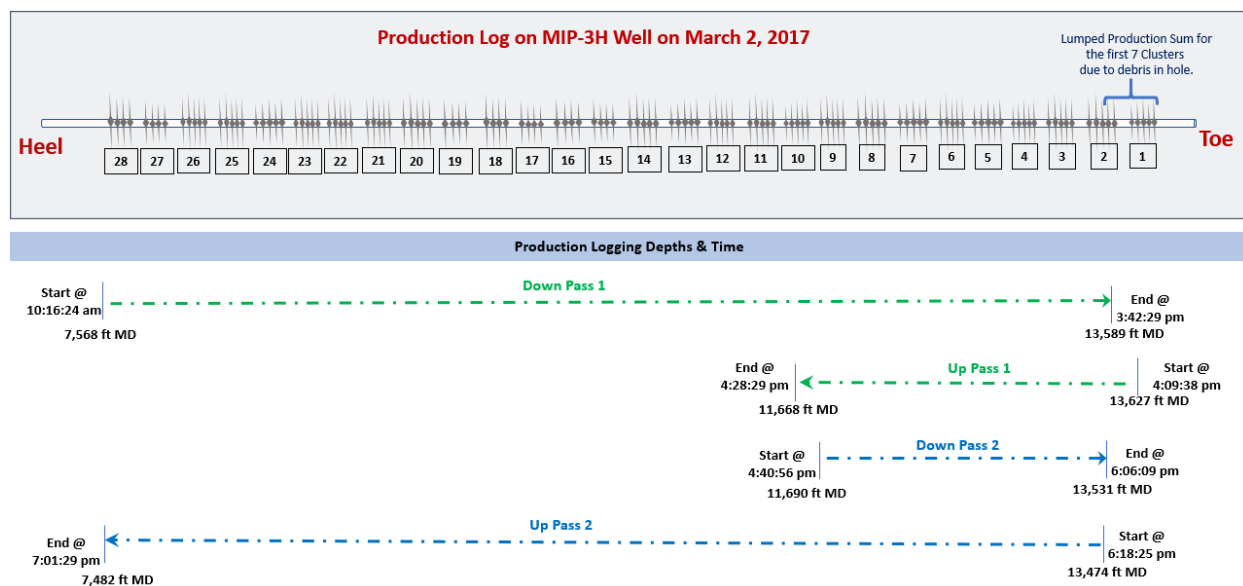


*Figure 6: Production Logging Tool Trajectory and Travel Time*

**Figure 7** shows an excerpt from the production log interpretation report. Interpreted gas rates were calculated at downhole conditions using Schlumberger's MapFLO and Mass Fraction proprietary models, and then converted to standard surface conditions. Calculated total gas rates from production log was 5,435 MCF/D while the actual reported surface rate totaled 4,763 MCF/D. The production log reported no liquids.

According to the Schlumberger log analyst report, the Flow Scanner tool could not log deeper than 13,530 ft measured depth due to debris in the lateral. As illustrated in **Figure 6** and shown in **Figure 7**, seven perforation clusters (all five clusters in Stage 1 and the first two clusters in Stage 2) were not traversed by all four passes of the Flow Scanner tool. Production rates beyond the 13,530 ft measured depth were therefore grouped and reported as a lumped production sum of 243 MCF/D for all seven clusters combined.

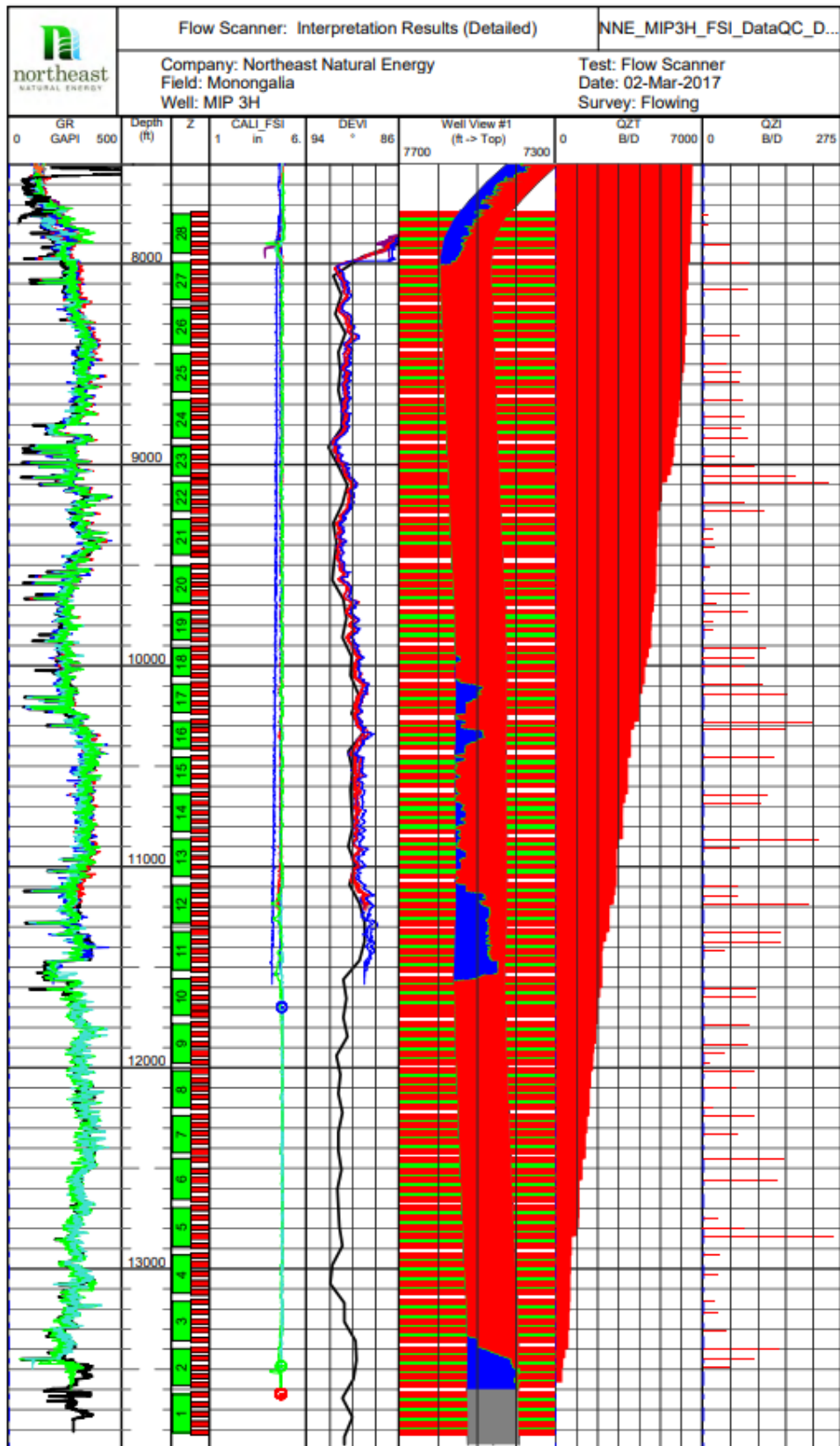
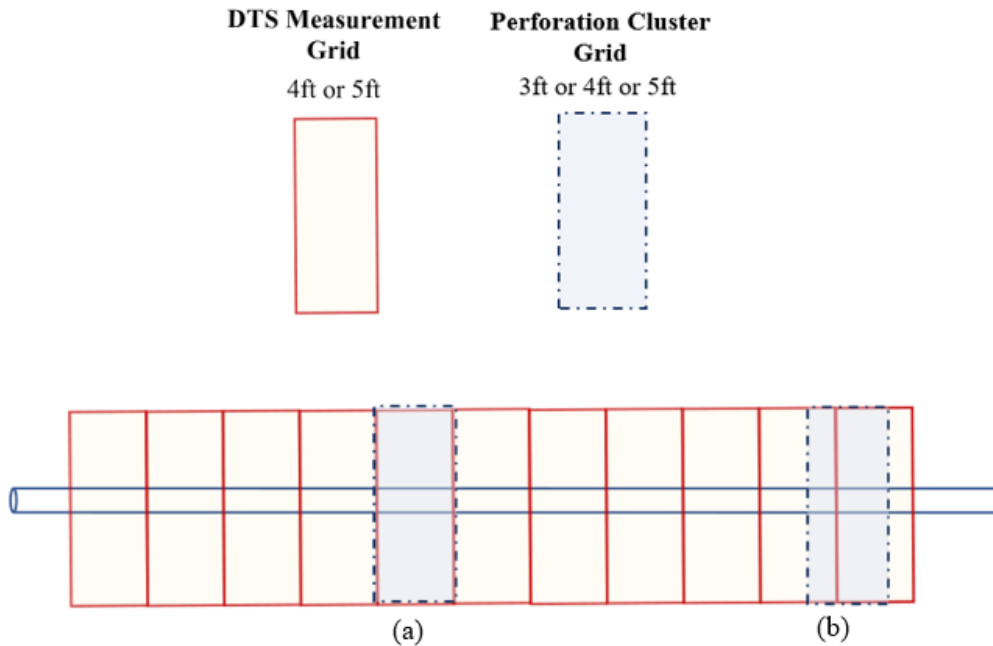


Figure 7: Excerpt from the Flow Scanner Log Interpretation Report

### 3.7 Building the Spatial-Temporal Database

The objective is to use MIP-3H completion data, geomechanical logs, hydraulic fracturing treatment data and DTS measurements to continuously predict the gas flow rate at the perforation cluster level of the well. The only source of gas production rate data at such granular resolution is a single day of production log where production rates have been reported for each perforation cluster. The spatio-temporal database to be developed therefore must be at the perforation cluster resolution. The measured depth interval of all 133 perforation clusters in MIP-3H were identified, and all attributes were prepared for each perforation cluster.

DTS measurements have been recorded in 4ft or 5ft intervals while a perforation cluster could be 3ft or 4ft or 5ft in length. As shown in **Figure 8**, this means that a perforation cluster could be located completely inside a DTS measurement grid (or interval) or overlap multiple DTS measurement grids. In scenario (a) where the perforation cluster lies within a single DTS measurement grid, the cluster is assigned the temperature measurement at that interval. In scenario (b) however, a weighted average of the measurements in the adjoining DTS intervals is calculated based on the proportion of overlapping cluster lengths.



*Figure 8: Identifying DTS Measurements at Individual Perforation Cluster Location*

The WellWatcher measured temperature along the well every three hours, so eight temperature profiles were obtained on the day of production log. The data processing described is performed for all 8 DTS measurement profiles obtained.

Like the DTS data, the geomechanical log data were prepared at the perforation cluster level. The original resolution of the log measurements is 0.5ft interval. This means that each perforation cluster covers multiple log measurement intervals. The log measurements were upscaled to the perforation cluster resolution by taking the simple average of measurement intervals within a cluster, for each geomechanical log.

The attributes in the original database prepared from MIP-3H data collected from the MSEEL website is shown in **Table 7**. All the database attributes have been prepared for each of the 133 hydraulic fracturing perforation clusters in the well. As already mentioned, gas production rates for clusters 1 through 7 were reported as a lumped sum value.

Completion Data		Proppants & Fluids	Treatment Schedule
Cluster Top (ft MD)		Pad Volume (bbl.)	Fracture Gradient (psi/ft)
Cluster Bottom (ft MD)		Total Clean Fluid (bbl.)	Initial Shut-in Pressure (ISIP) (psi)
Cluster Length (ft)		Prop.1-Type	5 Min ISIP (psi)
Stage Length (ft)		Prop.1-Amount (lbs.)	10 Min ISIP (psi)
Shot Count		Prop.2-Type	15 Min ISIP (psi)
Shot Orientation		Prop.2-Amount (lbs.)	Breakdown Rate (BPM)
Blast Shield (Perf) Depth		Total Proppant Amount (lbs.)	Breakdown Pressure (psi)
Blast Shield Orientation (deg)		Flush Volume (bbl.)	Breakdown Volume (bbl.)
Blast Shield Spacing (ft)		Screen Out (X)	Avg Treating Pressure (psi)
		Acid % Strength	Max Treating Pressure (psi)
		Total Acid (gals)	Avg Treating Rate (BPM)
		Total Slickwater (bbl.)	Max Treating Rate (BPM)
		Total Linear (bbl.)	Duration of Fracturing Treatment (secs)
		Total Cross-Link (bbl.)	
		Friction Reducer Amount (gals)	
		Gel Amount (gals or lbs.)	
		Breaker Amount (gals or lbs.)	
		Scale Inhibitor (gals)	
		Biocide (gals)	
		Pump Down Volume (bbl.)	
		Plug Depth	
		Proppant Concentration (lb./ft)	
		Proppant Concentration (lb./gal)	
		Fluid Load (bbl./ft)	
		Gel Volume (%)	
		Pad Volume (%)	
		Overflush Volume (bbl.)	
Geomechanical Logs		Fiber Optics (DTS Measurements)	
Borehole Deviation		DTS-M1 (12 am)	
DT Compressional		DTS-M2 (3 am)	
DT Fast		DTS-M3 (6 am)	
DT Slow		DTS-M4 (9 am)	
Gamma Ray-Thompson		DTS-M5 (12 pm)	
Gamma Ray		DTS-M6 (3 pm)	
Azimuth		DTS-M7 (6 pm)	
Bulk Density		DTS-M8 (9 pm)	
		Gas Production Rate	
		Gas (1000 ft <sup>3</sup> /d)	

*Table 7: MIP-3H Data Collected from MSEEL Website*

## Chapter 4: Model Development

Several factors influence the production performance of a shale well. These factors among others include the completion design (such as number of clusters per stage, cluster length and spacing), the hydraulic fracturing treatment design (such as amount of proppant and fracturing fluid, treatment pressure and rate), the reservoir characteristics (such as fracture density, mechanical rock properties). Optimizing production from shale wells is often challenging due to the complex relationship among these performance driving factors. Modeling the complex relationship between the set of input parameters that contribute to the production performance of shale well using temperature (DTS) measurements was completed in two main steps. The first step involved developing a random forest machine learning model to qualitatively determine the quality of production from a perforation cluster based on the temperature (DTS) measurement at the perforation cluster location. The second step involves coupling the random forest model in previous step to an artificial neural network to quantify the gas production from a perforation cluster based on the temperature (DTS) measurements and the qualitative assessment of the quality of production.

Machine learning algorithms cannot work without data. Little to nothing can be achieved if there are too few features to represent the underlying pattern in the data to a machine learning algorithm. Before building the machine learning models, comprehensive descriptive analytics of the MIP-3H dataset was performed and more features that further represents the underlying complex relationship among the shale performance influencing factors are generated. Following sections detail the steps taken to generate more features for model development.

### 4.1 Feature Engineering – Completion Data

Cluster spacing is essential to fracturing performance. If the cluster spacing is too small, the stimulated area between major fractures will be overlapped, and the efficiency of fracturing stimulation will be decreased. If the cluster spacing is too large, the area between major fractures cannot be stimulated completely and reservoir recovery extent will be adversely impacted. To provide additional completions design information on MIP-3H well into the proposed model, the offset perforation cluster distances immediately before and after each focal perforation cluster is generated. *Figure 9* shows an illustration of the offset cluster distances termed “Left Cluster

Distance (LCD)” and “Right Cluster Distance (RCD)”. The cluster distances accounts for whether the offset perforation cluster is in the same stage as the focal cluster or not.

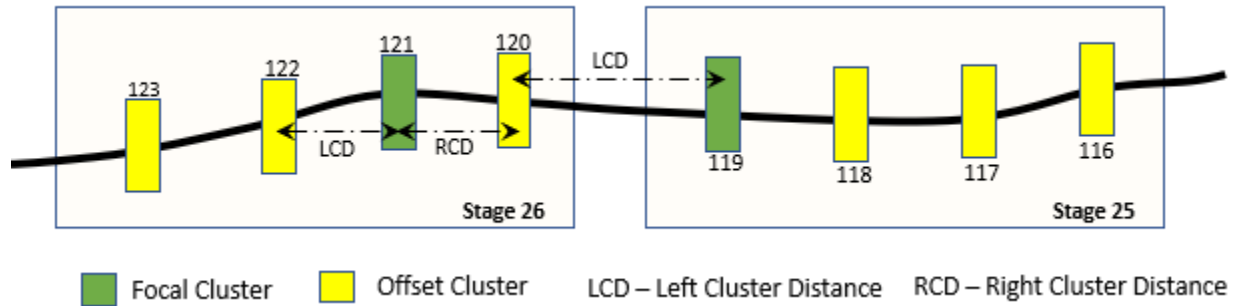


*Figure 9: Offset Perforation Cluster Distances*

The generated features listed in *Table 8* were added to the spatial-temporal database.

Generated Features
Left Cluster Distance (ft)
Right Cluster Distance (ft)

*Table 8: Offset Perforation Cluster Distance Features*

## 4.2 Feature Engineering – Geomechanical Logs

Lateral heterogeneity is often a key variable in shale well productivity. Geometrically spacing perforation clusters and stages without considering the toe-to-heel heterogeneity often results in a number of perforation clusters that do not contribute to well performance. This is because when multiple perforation clusters are placed in rocks of different stress, and treated simultaneously, the fluid will preferentially enter the clusters with the lowest stress. This causes the low-stress areas to be overstimulated relative to the clusters in higher stressed areas. *Figure 10* is an illustration of the traditional completions design approach where the lateral heterogeneity is not considered in the cluster placement. To overcome this challenge, the engineered completions design approach is usually applied by targeting rock with similar properties within the same stage. This increases the chances of more even proppant and fluid distribution across all perforation clusters, leading to enhanced production. *Figure 11* provides an illustration of the engineered completion design.

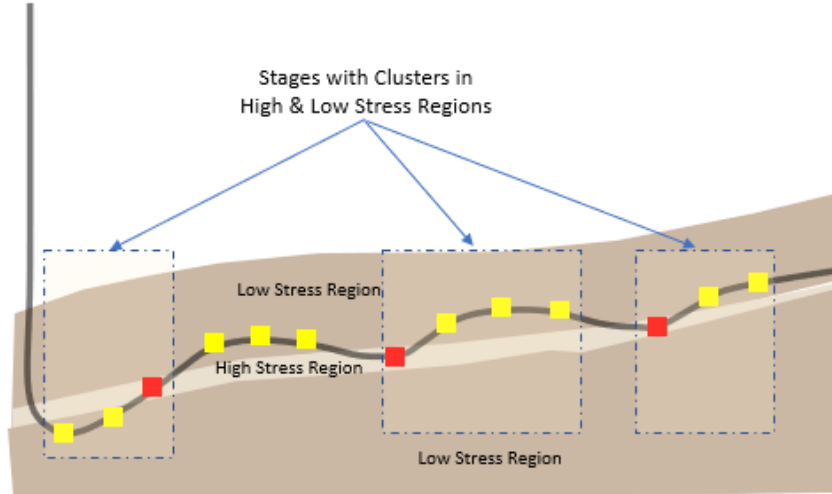


*Figure 10: Traditional Completions Design with no Consideration for Lateral Heterogeneity*

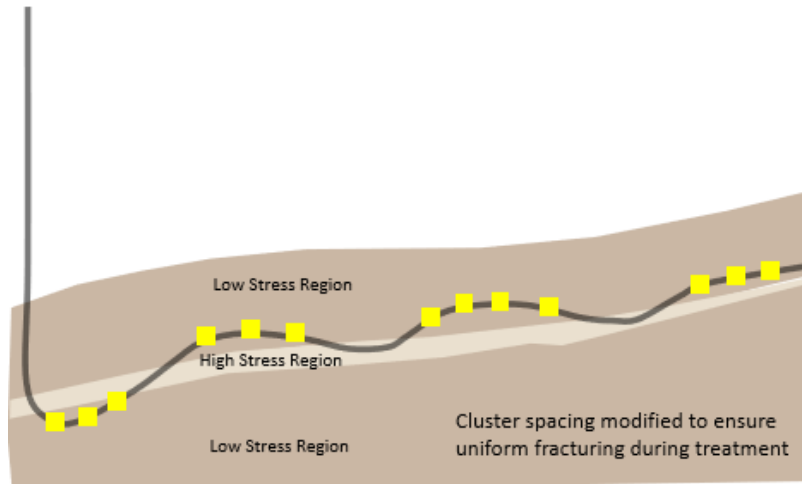


*Figure 11: Engineered Completion Design*

As stated in the previous chapter, some stages in the MIP-3H well were completed using the engineered completion design. To incorporate the effectiveness of the completion design for each stage into the proposed model, an unsupervised machine learning technique called Fuzzy Clustering is used to characterize the degree of heterogeneity (Heterogeneity Index) at each perforation cluster in the MIP-3H well, based on the geomechanical log measurements around the perforations. A brief description of the Fuzzy Clustering technique is provided in chapter one.

To capture the degree of lateral heterogeneity in geomechanical rock properties along the well, log measurements in intervals of 1ft immediately before and after each perforation cluster were identified as shown in **Figure 12**. The geomechanical logs used in the fuzzy clustering algorithm include DT-Compressional, Fast Shear Slowness, Slow Shear Slowness, Borehole Deviation and Bulk Density.

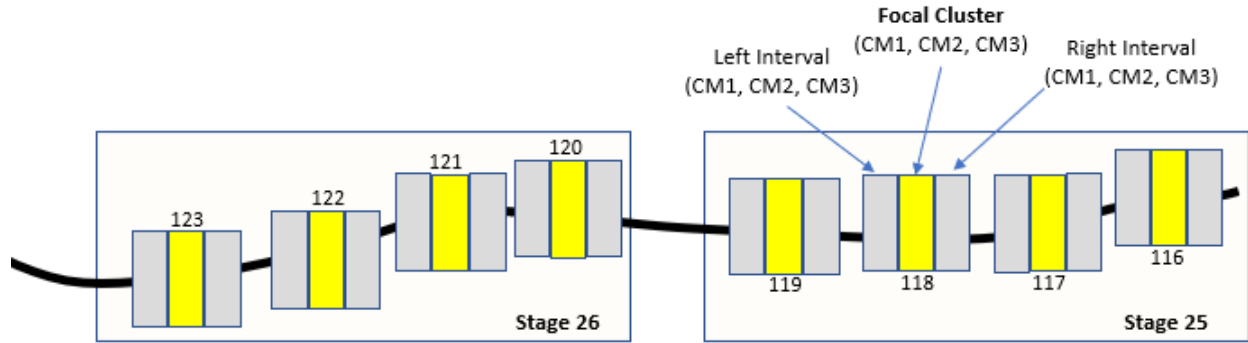


**Figure 12: Identifying Geomechanical Log Measurement Intervals for Clustering**

Clustering is used to identify groups in data such that data points that are close together are grouped in the same cluster. In hard clustering, each data point is clustered or grouped to any one cluster and cannot belong to more than one cluster. In fuzzy clustering (also known as soft clustering), each data point can belong to multiple clusters (or groups) with its probability of belonging to each cluster (or group). The Fuzzy C-means (FCM) clustering algorithm is used to classify the geomechanical log measurements at the perforation clusters, the left intervals, and right intervals into three fuzzy groups or clusters. The output of the fuzzy clustering is three numbers (values between 0 and 1) for each perforation cluster or interval representing the degrees of membership in each of the three fuzzy clusters or groupings. The degree of cluster memberships are represented as CM1, CM2 and CM3 as shown in **Figure 12**. Classifying the geomechanical log measurements at the perforation clusters and surrounding intervals provides the opportunity of identifying the degree of heterogeneity around the perforations by answering following questions.

- a. How similar are the geomechanical rock properties in a perforation cluster compared with the rock properties in areas surrounding the cluster?

- b. How similar are the geomechanical rock properties in a perforation cluster compared with the rock properties in its immediate neighboring clusters?
- c. How similar are the geomechanical rock properties in a perforation cluster compared with the rock properties in every other cluster in the same stage?

The first question can be addressed by first identifying the Heterogeneity Index between the focal cluster and the left interval (that is, the Left Heterogeneity Index), as well as between the focal cluster and the right interval (that is, the Right Heterogeneity Index), and summing up the heterogeneity indices. The Left Heterogeneity Index or the Right Heterogeneity Index is calculated by taking the absolute difference between the cluster memberships of the Focal Cluster and the corresponding left or right interval. This is presented in the following equations:

$$\text{Left Interval Heterogeneity Index} = |\text{FC}_{\text{CM1}} - \text{LI}_{\text{CM1}}| + |\text{FC}_{\text{CM2}} - \text{LI}_{\text{CM2}}| + |\text{FC}_{\text{CM3}} - \text{LI}_{\text{CM3}}|$$

$$\text{Right Interval Heterogeneity Index} = |\text{FC}_{\text{CM1}} - \text{RI}_{\text{CM1}}| + |\text{FC}_{\text{CM2}} - \text{RI}_{\text{CM2}}| + |\text{FC}_{\text{CM3}} - \text{RI}_{\text{CM3}}|$$

$$\text{Focal Cluster Heterogeneity Index} = \text{Left Interval Heterogeneity Index} + \text{Right Interval Heterogeneity Index}$$

where FC = Focal Cluster, LC = Left Interval, RI = Right Interval

In a similar manner, the similarity between the geomechanical rock properties in a perforation cluster compared with the rock properties in its immediate neighboring clusters can be determined as depicted in **Figure 13** and following equations.

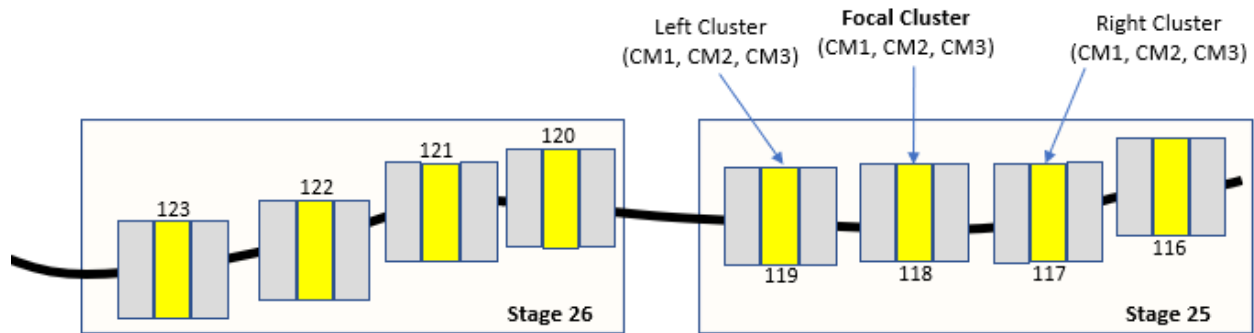


*Figure 13: Offset Cluster Heterogeneity Index*

$$\text{Left Cluster Heterogeneity Index} = |\text{FC}_{\text{CM1}} - \text{LC}_{\text{CM1}}| + |\text{FC}_{\text{CM2}} - \text{LC}_{\text{CM2}}| + |\text{FC}_{\text{CM3}} - \text{LC}_{\text{CM3}}|$$

$$\text{Right Cluster Heterogeneity Index} = |\text{FC}_{\text{CM1}} - \text{RC}_{\text{CM1}}| + |\text{FC}_{\text{CM2}} - \text{RC}_{\text{CM2}}| + |\text{FC}_{\text{CM3}} - \text{RC}_{\text{CM3}}|$$

$$\text{Offset Cluster Heterogeneity Index} = \text{Left Cluster Heterogeneity Index} + \text{Right Cluster Heterogeneity Index}$$

where FC = Focal Cluster, LC = Left Interval, RI = Right Interval

The similarity between the geomechanical rock properties in a perforation cluster compared with the rock properties in every other cluster in the same stage can be determined as depicted in **Figure 14** and following equations.

$$\text{Same Stage Cluster 119 HI} = |\text{FC}_{\text{CM1}} - \text{SSC}(119)_{\text{CM1}}| + |\text{FC}_{\text{CM2}} - \text{SSC}(119)_{\text{CM2}}| + |\text{FC}_{\text{CM3}} - \text{SSC}(119)_{\text{CM3}}|$$

$$\text{Same Stage Cluster 117 HI} = |\text{FC}_{\text{CM1}} - \text{SSC}(117)_{\text{CM1}}| + |\text{FC}_{\text{CM2}} - \text{SSC}(117)_{\text{CM2}}| + |\text{FC}_{\text{CM3}} - \text{SSC}(117)_{\text{CM3}}|$$

$$\text{Same Stage Cluster 116 HI} = |\text{FC}_{\text{CM1}} - \text{SSC}(116)_{\text{CM1}}| + |\text{FC}_{\text{CM2}} - \text{SSC}(116)_{\text{CM2}}| + |\text{FC}_{\text{CM3}} - \text{SSC}(116)_{\text{CM3}}|$$

$$\text{Stage Heterogeneity Index} = \text{Sum of all Same Stage Cluster HI} = \text{SSC}(119) + \text{SSC}(117) + \text{SSC}(116)$$

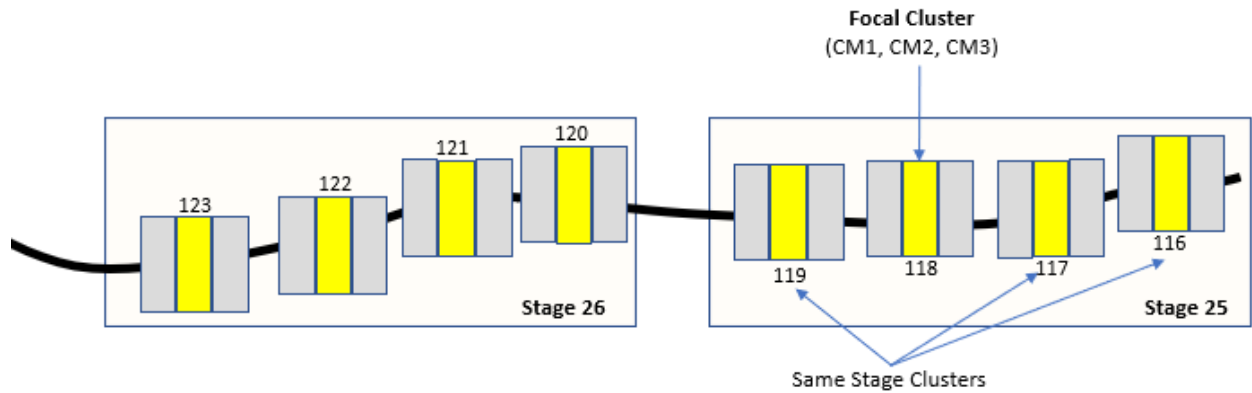


**Figure 14: Stage Heterogeneity Index**

The generated features listed in **Table 9** were added to the spatial-temporal database.

Generated Features
Fuzzy Memberships (CM1, CM2, CM3)
Left Interval Heterogeneity Index
Right Interval Heterogeneity Index
Focal Cluster Heterogeneity Index
Right Cluster Heterogeneity Index
Left Cluster Heterogeneity Index
Offset Cluster Heterogeneity Index
Stage Heterogeneity Index

*Table 9: Generated Features from Geomechanical Logs*

### 4.3 Feature Engineering – Gas Production Rate Data

Initial attempts at modeling the gas production rate yielded poor results due to imbalance in the production rate data. **Figure 15** shows the distribution of production rate data for all 126 perforation clusters. Approximately 44% of the perforation clusters have zero gas production rate value and so the distribution is largely skewed to the left. Initial modeling results showed overfitting to the zero producing clusters such that perforation clusters were being predicted to be non-producing when in fact they were producing. To address this issue, a fuzzy logic system (based on fuzzy sets theory) was designed to infer the quality of gas production from the perforation clusters based on temperature (DTS) measurements, before predicting the actual gas production rates. More details are presented in following section.

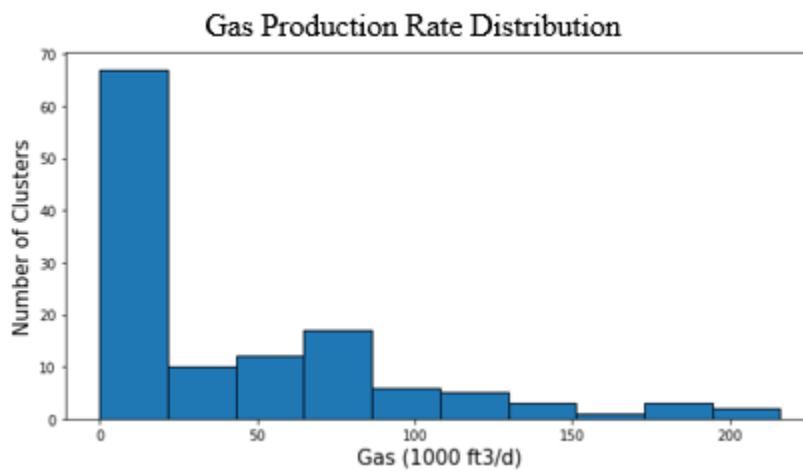


*Figure 15: Gas Production Rate Distribution from Production Log*

Fuzzy sets can be considered as an extension and oversimplification of classical sets. It can be best understood in the context of set membership. Basically, it allows partial membership which means that it contains elements that have varying degrees of membership in the set. Classical set contains elements that satisfy precise properties of membership while fuzzy set contains elements that satisfy imprecise (or vague) properties of membership. The membership function which defines how each point (production rate value) in the input space is mapped to membership value between 0 and 1 is shown in **Figure 16**. The input space is the universal set (U), which contains all the possible elements of interest, in this case the range of values of gas production rate. **Table 10** shows the range of values with which the fuzzy sets were constructed. Perforation clusters with gas production rates up to 10 (1000 ft<sup>3</sup>/d) are classified to be in the “Low Production Category”, clusters with gas production rates from 5 (1000 ft<sup>3</sup>/d) to 110 (1000 ft<sup>3</sup>/d) are classified to be in the “Mid Production Category” while clusters with gas production rates from 85 (1000 ft<sup>3</sup>/d) to 216 (1000 ft<sup>3</sup>/d) are classified to be in the “High Production Category”. **Table 11** shows the percentage and number of perforation clusters in each fuzzy set. The output of the fuzzy logic classification is the degrees of membership in each of the three fuzzy sets or categories. These additional input features shown in **Table 12** were added to the database.

Fuzzy Set	Rise	Top	Top/Fall	Fall
Low Producing	0	0	0	10
Mid Producing	5	20	80	110
High Producing	85	120	216	216

*Table 10: Fuzzy Sets for Gas Production Rate Data*

Fuzzy Set	# Cases	% Cases
Low Prod.	58	46
Mid Prod.	56	44
High Prod.	22	17

*Table 11: Number and Percent of Cases Per Fuzzy Set*

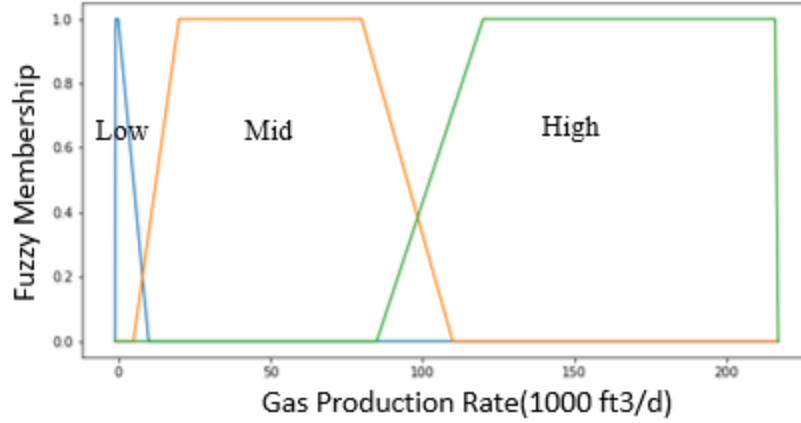


Figure 16: Fuzzy Set Memberships from Gas Production Rate Data

Fuzzy Set Membership
Low Production Category Membership
Mid Production Category Membership
High Production Category Membership

Table 12: Gas Production Rate Fuzzy Membership Features

#### 4.4 Database Construction for Model Development

Following the addition of new generated features, the current database contains a total of 133 records, 78 input features and the gas production rate as the output feature. A total of 126 perforation clusters has gas production rate measurements. Considering that the objective is to quantify the gas production rate based on fiber optic temperature (DTS) measurements, a single day of production log is all that is available to use in terms of source of production rate measurements. A small sample of 126 perforation clusters does not provide enough opportunity for a machine learning algorithm to learn the complex relationship and patterns in the dataset. To address this challenge, a fundamental assumption in conventional production logging is adopted; the fact that the production rate measurements taken during a few hours of the logging operation are assumed to remain the same on the day of production log and beyond. For each perforation cluster in the dataset, the measured gas production rate is assumed to remain constant throughout the 8 temperature (DTS) measurements taken on the day of production log. This increases the number of samples with gas production rate measurements from 126 to 1,008 and decreases the

number of input features from 78 to 71. A snapshot of the features contained in the database is presented in **Table 13** below.

Number of Features = 11		Number of Features = 16	
Completion Data	Generated Features	Geomechanical Logs	Generated Features
Cluster Top (ft)	Left Cluster Distance (ft)	Borehole Deviation	Fuzzy Memberships (CM1, CM2, CM3)
Cluster Bottom (ft)	Right Cluster Distance (ft)	DT Compressional	Left Interval Heterogeneity Index
Cluster Length (ft)		DT Fast	Right Interval Heterogeneity Index
Stage Length (ft)		DT Slow	Focal Cluster Heterogeneity Index
Shot Count		Gamma Ray- Thompson	Right Cluster Heterogeneity Index
Shot Orientation		Gamma Ray	Left Cluster Heterogeneity Index
Blast Shield (Perf) Depth		Azimuth	Offset Cluster Heterogeneity Index
Blast Shield Orient (deg)		Bulk Density	Stage Heterogeneity Index
Blast Shield Spacing (ft)			

Number of Features = 40		Number of Features = 1	
Proppants & Fluids	Treatment Schedule	Fibre Optics (DTS)	
Pad Volume (bbls)	Fracture Gradient (psi/ft)	Temperature Measurement (DTS)	
Total Clean Fluid (Bbls)	Initial Shut-in Pressure (ISIP) (psi)		
Prop. 1-Type	5 Min ISIP (psi)		
Prop. 1-Amount (lbs)	10 Min ISIP (psi)		
Prop. 2-Type	15 Min ISIP (psi)		
Prop. 2-Amount (lbs)	Breakdown Rate (BPM)		
Total Proppant Amount (lbs)	Breakdown Pressure (psi)		
Flush Volume (bbls)	Breakdown Volume (Bbls)		
Screen Out (X)	Avg Treating Pressure (psi)		
Acid % Strength	Max Treating Pressure (psi)		
Total Acid (gals)	Avg Treating Rate (BPM)		
Total Slickwater (bbls)	Max Treating Rate (BPM)		
Total Linear (bbls)	Duration of Fracturing Treatment (secs)		
Total Cross-Link (Bbls)			
Friction Reducer Amount (gals)			
Gel Amount (gals or lbs)			
Breaker Amount (gals or lbs)			
Scale Inhibitor (gals)			
Biocide (gals)			
Pump Down Volume (Bbls)			
Plug Depth			
Proppant Concentration (Lb/ft)			
Proppant Concentration (Lb/gal)			
Fluid Load (bbls/ft)			
Gel Volume (%)			
Pad Volume (%)			
Overflush Volume (bbls)			

Number of Features = 3		Number of Features = 1	
Fuzzy Set Membership (Generated)		Gas Production Rate	
Low Production Category Membership		Gas (1000 ft3/d)	
Mid Production Category Membership			
High Production Category Membership			

**Table 13: MIP-3H Database Features Post Descriptive Analytics**

## 4.5 Feature Selection

Feature selection is an important part of building machine learning models. Adding redundant variables reduces the generalization capability of the model and may also reduce the overall performance. Furthermore, adding more and more variables to a model increases the overall complexity of the model. To find the best set of features in the database that sufficiently represents the shale production performance phenomena, a few steps were taken including performing a key performance indicator (KPI) analysis on each category of features, performing several trial-and-error modeling with different combinations of features, as well as feature selection based on petroleum engineering domain knowledge. The following features were selected for model development.

Number of Features = 6	
Completion Data	Generated Features
Cluster Top (ft)	Left Cluster Distance (ft)
Cluster Bottom (ft)	Right Cluster Distance (ft)
Cluster Length (ft)	
Shot Count	

Number of Features = 16	
Geomechanical Logs	Generated Features
Borehole Deviation	Fuzzy Memberships (CM1, CM2, CM3)
DT Compressional	Left Interval Heterogeneity Index
DT Fast	Right Interval Heterogeneity Index
DT Slow	Focal Cluster Heterogeneity Index
Gamma Ray-Thompson	Right Cluster Heterogeneity Index
Gamma Ray	Left Cluster Heterogeneity Index
Azimuth	Offset Cluster Heterogeneity Index
Bulk Density	Stage Heterogeneity Index

Number of Features = 19	
Proppants & Fluids	Treatment Schedule
Pad Volume (bbls)	Breakdown Pressure (psi)
Total Clean Fluid (Bbls)	Breakdown Volume (Bbls)
Prop.1-Amount (lbs)	Avg Treating Pressure (psi)
Prop.2-Amount (lbs)	Max Treating Pressure (psi)
Total Proppant Amount (lbs)	Avg Treating Rate (BPM)
Flush Volume (bbls)	Max Treating Rate (BPM)
Total Slickwater (bbls)	
Pump Down Volume (Bbls)	
Proppant Concentration (Lb/ft)	
Proppant Concentration (Lb/gal)	
Fluid Load (bbls/ft)	
Gel Volume (%)	
Pad Volume (%)	

Number of Features = 1	
Fibre Optics (DTS)	
Temperature Measurement (DTS)	

Number of Features = 3	
Fuzzy Set Membership	
Low Production Category Membership	
Mid Production Category Membership	
High Production Category Membership	

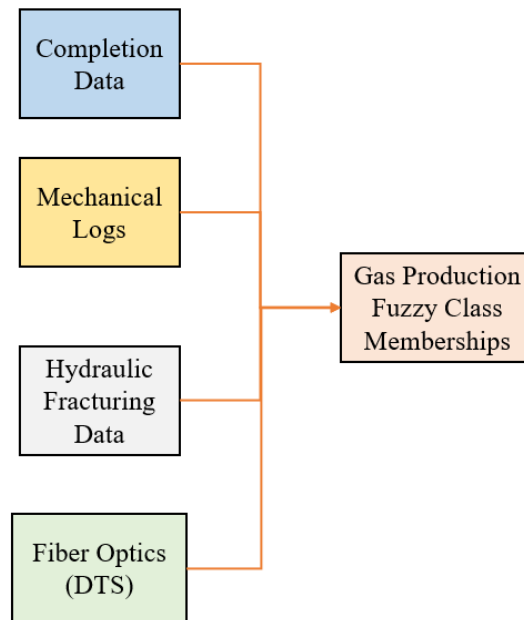
Number of Features = 1	
Gas Production Rate	
Gas (1000 ft <sup>3</sup> /d)	

Table 14: MIP-3H Database Features Selected for Model Development

## 4.6 Fuzzy Classification Model using Random Forest

As previously mentioned at the beginning of this chapter, a coupled random forest – neural network model was developed to meet the objective of this research work. Some background information has been provided on the random forest algorithm in chapter one. The skewness and unbalance of the gas production rate data as shown earlier in this chapter makes machine learning susceptible to overfitting. The random forest algorithm is an ensemble method which offers a parallel and sequential training schemes that increases the variance and reduces the bias in the model.

As shown in **Figure 17**, the random forest regressor model takes as input the completion design, mechanical log measurements and hydraulic fracturing treatment design pertaining to a perforation cluster and predicts the quality of production from the perforation cluster based on the temperature (DTS) measurements at the perforation cluster location. The output of the model is the degree of memberships in the three different gas production fuzzy classes (that is Low Production Category, Mid Production Category and High Production Category), for each perforation cluster in the well.



*Figure 17: Gas Production Fuzzy Classification Model Using Random Forest*

## 4.7 Regression Model using Artificial Neural Network

The regression model uses all the input to the fuzzy classification model (random forest model) as well as the gas production rate fuzzy class memberships as input to quantify the gas production rate from a perforation cluster based on the temperature (DTS) measurements. The network is designed fully connected with a single hidden layer, rectilinear activation function in the hidden layer and sigmoid activation function in the output layer. The structure of the final model is shown in *Figure 18*.

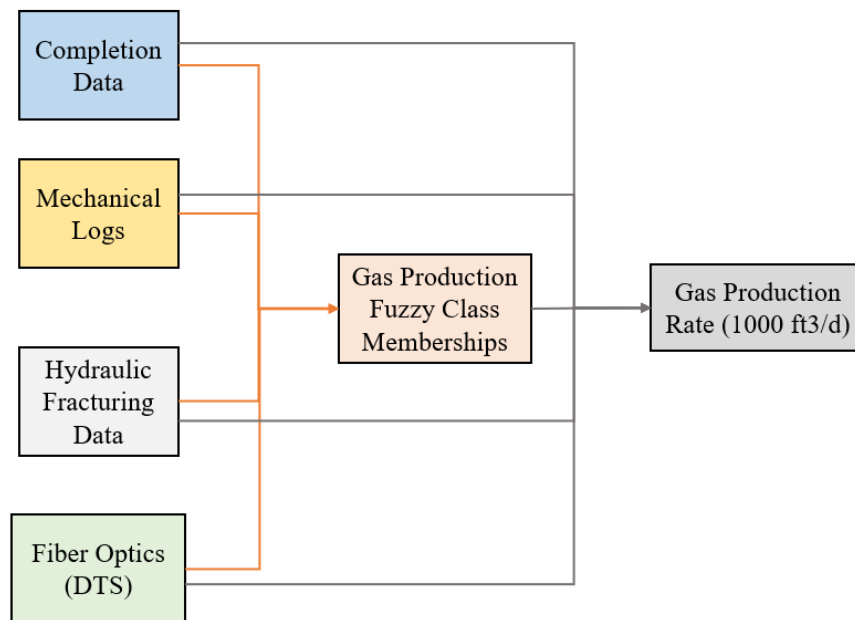


*Figure 18: Gas Production Regression Model Using Artificial Neural Network*

## **Chapter 5: Model Validation & Discussion**

The model validation step is a very crucial part of the whole process of developing the data-driven models. Considering the limited amount of data available for modeling the complex relationship between the set of input parameters that contribute to the production performance of hydraulically fractured shale well using temperature (DTS) measurements, it is important to validate that the developed machine learning models are stable. The validation step helps to check whether the model results quantifying hypothesized relationships between variables (completions design, mechanical logs, hydraulic fracturing treatment, fiber optics (DTS)) and gas production rate, are acceptable as descriptions of the data. A unique approach to model validation is taken, and in multiple steps. This chapter details steps taken to validate the models and results are presented.

### **5.1 Data Partitioning**

Prior to training the production fuzzy classification model (Random Forest model) and the production regression model (Artificial Neural Network), blind validation samples were identified and separated out from the entire dataset. The blind validation samples are perforation clusters whose data are never used in training the models. The remaining dataset contains what is referred to as the development samples which must further be divided into training, calibration, and validation samples. The training samples are perforation clusters whose data is used to teach the machine learning algorithms patterns in the dataset by establishing correlations between the input and output features. The calibration data is used to monitor the performance of a neural network as it learns and determines when to stop the training process. The validation samples are the most important as these are used to validate the performance of the trained model. The validation data checks the ability of the model to generalize on out of sample data and has no bearing on the machine learning model's training or calibration. The models are deployed on the blind validation samples only when a satisfactory result is obtained on the validation dataset.

Considering that the gas production rate data is highly skewed with approximately 44% of the perforation clusters not producing, it is important to ensure that the percentage of each fuzzy production class (Low, Mid, High) in each partition (training, calibration and validation) described above is consistent; this helps the machine learning models to learn the correct pattern in the dataset and prevent overfitting to a particular fuzzy production class. The training and calibration data

contains 80% of samples from each fuzzy production class, while the validation partition contain 10% of samples from each fuzzy production class.

Three model validation scenarios were performed using a stage and perforation clusters 1 through 7 as blind validation in each scenario. The blind stage (blind perforation clusters from a stage) was picked towards the toe (stage #4), the heel (stage #26) and the middle (stage #15) of the well lateral. Following sections show an illustration of the data partitioning and the model results for each validation scenario.

## 5.2 Model Validation Scenario 1: Blind Stage #4 & Clusters 1 – 7

A total of 12 perforation clusters used as blind validation with 5 clusters in Stage #4 and clusters 1 through 7. Total number of development samples is 968 (121 perforation clusters and 8 DTS measurements per cluster). The training and calibration data contains 80% of samples from each fuzzy production class, while the validation partition contains 10% of samples from each fuzzy production class.

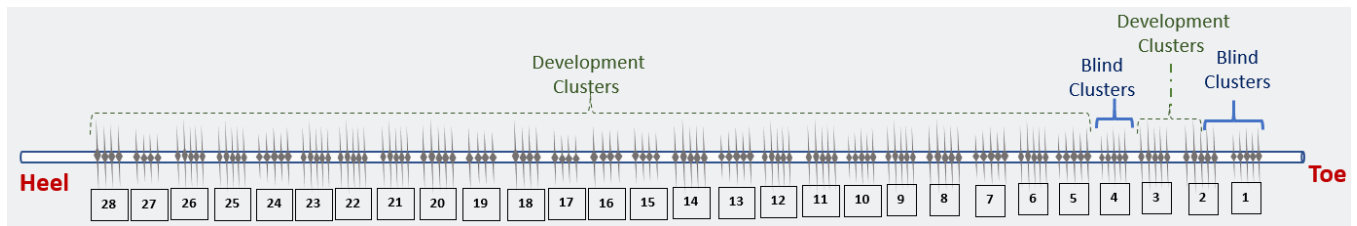


*Figure 19: Data Partitioning for Model Validation Scenario 1*

For better visualization, the gas production fuzzy classification model (Random Forest) results are presented using a confusion matrix. A confusion matrix is a summary of prediction results on a classification problem. The number of correct and incorrect predictions are summarized with count values and broken down by each class. Though the output from the fuzzy classification model is degree of membership in each class, the hard cluster memberships are shown in the confusion matrix only for the purpose of checking the accuracy of the model. The fuzzy (soft) cluster memberships are used as input into the regression (artificial neural network) model.

Training Samples				
ACTUAL		PREDICTED		
		Low Prod.	Mid Prod.	High Prod.
	Low Prod.	389	0	0
	Mid Prod.	7	339	0
	High Prod.	0	0	130

*Figure 20: Fuzzy Classification Training Results for Validation Scenario 1*

Validation Samples				
ACTUAL		PREDICTED		
		Low Prod.	Mid Prod.	High Prod.
	Low Prod.	51	0	0
	Mid Prod.	1	37	0
	High Prod.	0	0	14

*Figure 21: Fuzzy Classification Validation Results for Validation Scenario 1*

Blind Validation Samples				
ACTUAL		PREDICTED		
		Low Prod.	Mid Prod.	High Prod.
	Low Prod.	24	0	0
	Mid Prod.	0	16	0
	High Prod.	0	0	0

*Figure 22: Fuzzy Classification Blind Validation Results for Validation Scenario 1*

The following bar graph in presents the results of the regression model compared with the production log measurements for the blind perforation clusters in stage #4. The model has an average percent error of 3.2%. **Figure 24** compares the total model predictions for perforation clusters 1 through 7 against the lumped production sum for these clusters as reported in the production log. The predictions compare very nicely at less than 1% error.

## Model Prediction Results for Stage #4 & Clusters 1 - 7

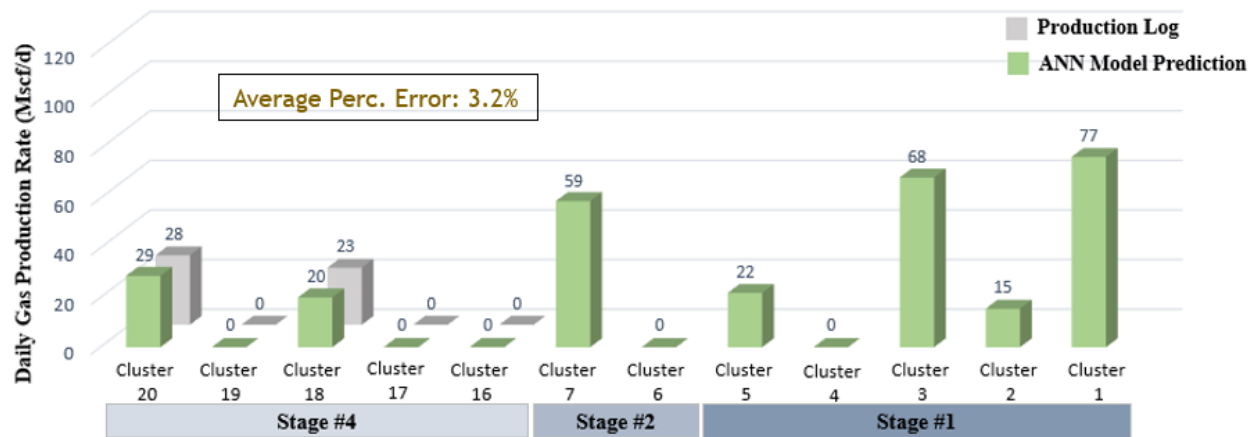


Figure 23: Production Log vs. ANN Regression Results for Blind Validation in Scenario 1

## Total Daily Gas Production Rate from Clusters 1 - 7

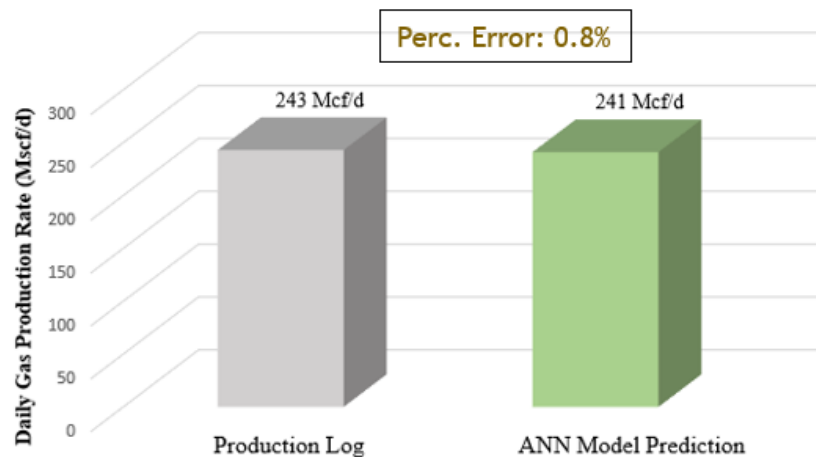


Figure 24: Production Log vs. ANN Regression Results for Clusters 1-7 for Validation Scenario 1

### 5.3 Model Validation Scenario 2: Blind Stage #15 & Clusters 1 – 7

A total of 11 perforation clusters used as blind validation with 4 clusters in Stage #15 and clusters 1 through 7. Total number of development samples is 976 (122 perforation clusters and 8 DTS measurements per cluster). The data partition is as described in the Scenario 1.

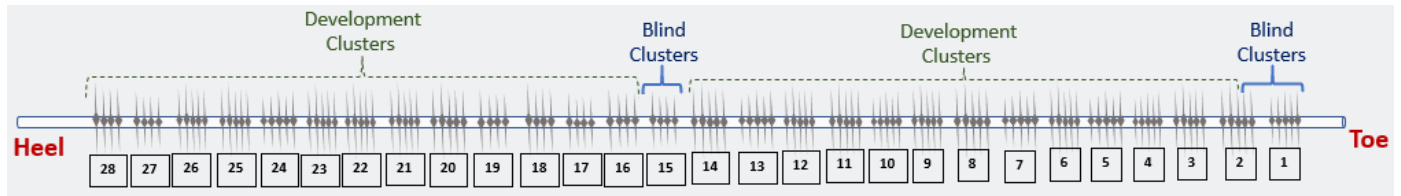


Figure 25: Data Partitioning for Model Validation Scenario 2

		Training Samples		
		PREDICTED		
		Low Prod.	Mid Prod.	High Prod.
ACTUAL	Low Prod.	389	0	0
	Mid Prod.	0	360	0
	High Prod.	0	7	116

Figure 26: Fuzzy Classification Training Results for Validation Scenario 2

		Validation Samples		
		PREDICTED		
		Low Prod.	Mid Prod.	High Prod.
ACTUAL	Low Prod.	51	0	0
	Mid Prod.	0	40	0
	High Prod.	0	1	12

Figure 27: Fuzzy Classification Validation Results for Validation Scenario 2

		Blind Validation Samples		
		PREDICTED		
		Low Prod.	Mid Prod.	High Prod.
ACTUAL	Low Prod.	24	0	0
	Mid Prod.	0	0	0
	High Prod.	0	0	8

Figure 28: Fuzzy Classification Blind Validation Results for Validation Scenario 2

The following bar graph presents the results of the regression model compared with the production log measurements for the four blind perforation clusters in stage #15. The model shows an average percent error of less than 1%. **Figure 30** compares the total model predictions for perforation

clusters 1 through 7 against the lumped production sum reported in the production log. The predictions compare very nicely at less than 1% error.

### Model Prediction Results for Stage #15 & Clusters 1 - 7



Figure 29: Production Log vs. ANN Regression Results for Blind Validation in Scenario 2

### Total Daily Gas Production Rate from Clusters 1 - 7

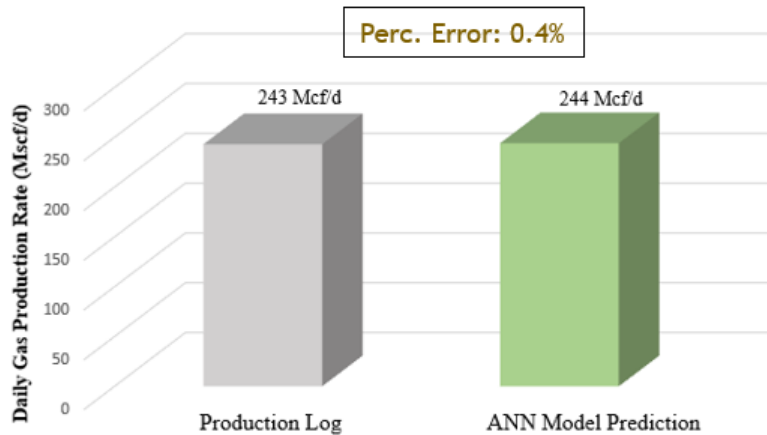


Figure 30: Production Log vs. ANN Regression Results for Clusters 1-7 for Validation Scenario 2

## 5.4 Model Validation Scenario 3: Blind Stage #26 & Clusters 1 – 7

A total of 12 perforation clusters used as blind validation with 4 clusters in Stage #26 and clusters 1 through 7. Total number of development samples is 968 (121 perforation clusters and 8 DTS measurements per cluster). The data partition is as described in the Scenario 1.

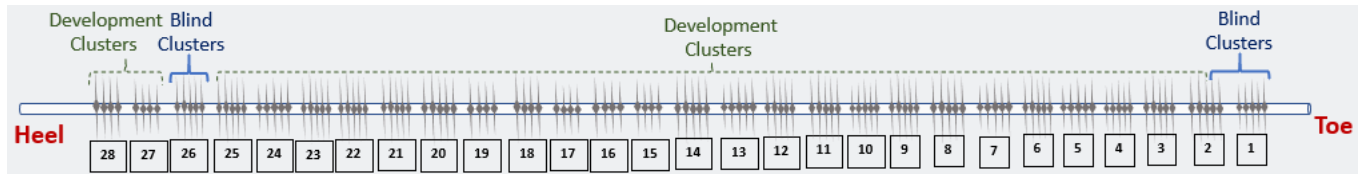


Figure 31: Data Partitioning for Model Validation Scenario 3

		Training Samples		
		PREDICTED		
		Low Prod.	Mid Prod.	High Prod.
ACTUAL	Low Prod.	382	0	0
	Mid Prod.	0	353	0
	High Prod.	0	0	130

Figure 32: Fuzzy Classification Training Results for Validation Scenario 3

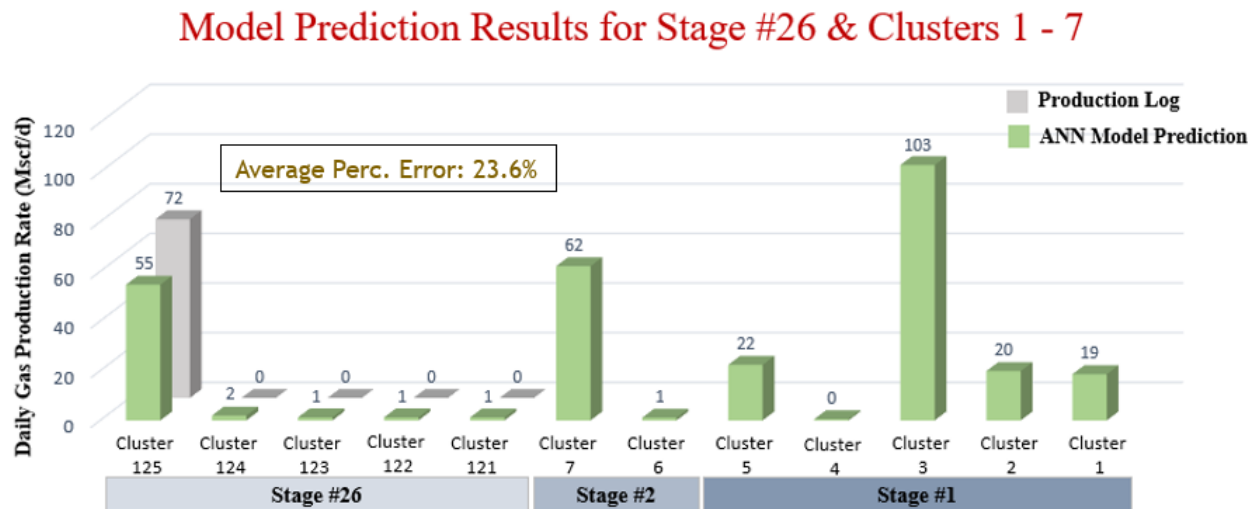
		Validation Samples		
		PREDICTED		
		Low Prod.	Mid Prod.	High Prod.
ACTUAL	Low Prod.	50	0	0
	Mid Prod.	0	39	0
	High Prod.	0	0	14

Figure 33: Fuzzy Classification Validation Results for Validation Scenario 3

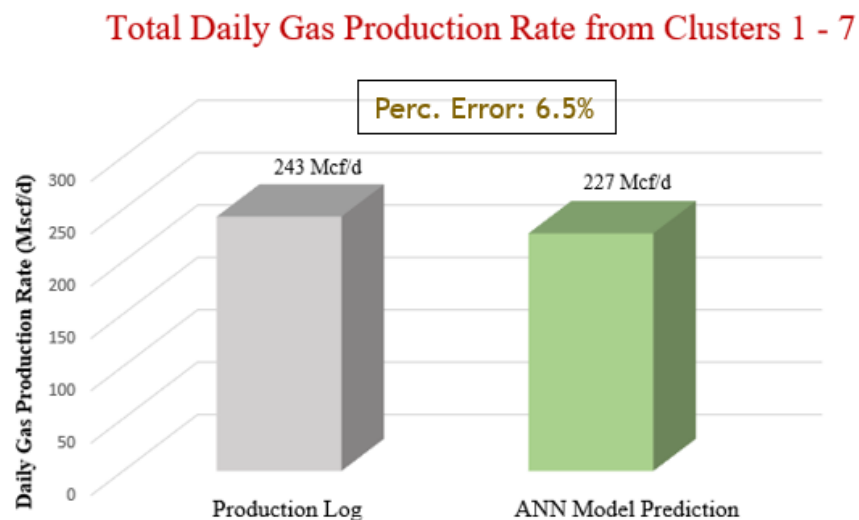
		Blind Validation Samples		
		PREDICTED		
		Low Prod.	Mid Prod.	High Prod.
ACTUAL	Low Prod.	32	0	0
	Mid Prod.	0	8	0
	High Prod.	0	0	7

Figure 34: Fuzzy Classification Blind Validation Results for Validation Scenario 3

**Figure 35** presents the results of the regression model compared with the production log measurements for the five blind perforation clusters in stage #26. The model shows an average percent error of 23.6%. **Figure 36** compares the total model predictions for perforation clusters 1 through 7 against the lumped production sum reported in the production log. The model predictions show an error of 6.5% compared to the production log.



*Figure 35: Production Log vs. ANN Regression Results for Blind Validation in Scenario 3*



*Figure 36: Production Log vs. ANN Regression Results for Clusters 1-7 for Validation Scenario 3*

## **Chapter 6: Conclusion & Recommendations**

### **6.1 Conclusion**

Based on the validation results shown in Chapter five, the developed machine learning models reliably predict the gas production rate from individual perforation clusters in the MIP-3H well given the completion data, mechanical logs, hydraulic fracturing treatment data relating to the well, as well as real-time temperature (DTS) measurements along the well lateral. The on-demand real-time production logging model presented in this research study provides a useful alternative to the reactive traditional production logging tool as real-time production measurement makes it easier to diagnose production problems and take timely remedial actions. The unique modeling approach taken to generate features that represent the complex relationship between the model input shale performance factors and gas production rate indicates that machine learning algorithms such as fuzzy set theory and artificial neural networks are capable of identifying complex data patterns with high accuracy when properly applied.

Some limitations were identified in the modeling approach taken in this study. One of such limitations is the fact that the developed models are constrained to a single day of production log. This means a very limited amount of data is available to learn the complex relationship between gas production rate and the several production performance driving factors in a shale well. Though the fuzzy classification machine learning technique was useful in finding the complex patterns in the dataset, a more significant issue regarding data availability is the fact that the model may not generalize on some days other than the production logging day. This limitation may be more evident for days where the range of temperature (DTS) measurements recorded by the Fiber Optics cable is significantly different than it was on the day of production logging. Additionally, production rate measurements obtained from a single day of production log could be highly prone to noise from various sources such as human bias during the logging operation or log interpretation. For instance, calculated total gas rates from the production log was 5,435 MCF/D while the actual reported surface rate totaled 4,763 MCF/D as stated in Section 3.6. The single day production log measurements have approximately 15% error which could be lower if multiple day production logs were taken. The noise in production log measurements could impact the performance or reliability of the developed predictive models.

## 6.2 Recommendation

Machine learning algorithms cannot learn patterns without sufficient data. Solving a complex problem such as in this study using a data driven approach often requires that the right data is collected at the right frequency. To have a more robust and generalized real-time predictive model, more days of actual production log measurements is highly desirable. A more generalizable predictive model will require a well-designed plan for data gathering such that multiple production measurements are taken over a period of say weeks or months such that the measurements capture a wide range of temperature (DTS) values as much as possible, for all perforation clusters in the well. Obtaining multiple production logs over a period rather than a single day will provide the opportunity to incorporate well operational conditions into the modeling workflow. Operational conditions such as surface pressure and temperature, casing pressure and tubing pressure could provide a lot more information about the production performance of the well.

The cooling effect created when gas flows into the wellbore was used in modeling gas production based on DTS measurements in this study. When water flows in well, it creates a warm effect which needs to be accounted for in wells with significant amount of water production. The MIP-3H well used in this study is a dry gas well. After the initial production and outside of the clean-up associated with the production logging, the well produces less than 10 barrels of water per day. Water production from this well was considered insignificant for analysis purpose. For further studies, it is recommended that a real-time predictive production logging model considers the impact of the produced water on temperature (DTS) measurements along the wellbore.

The workflow and predictive model developed in this study help to determine which perforation clusters are producing and at what rate, at any given point in time based on DTS measurements. A more interesting and important question for Shale resource development and optimization would be “Why are certain perforation clusters or stages producing more or less than others?”. The workflow and predictive model presented in this study could be extended as a completion design and hydraulic fracturing optimization tool for Shale wells. Information available from some other sources such as Fiber Optics Distributed Acoustic Sensing (DAS) and Seismic data could be incorporated into the workflow presented in this study for further detailed analysis of key shale performance indicators in MIP-3H.

## References

- [1] G. W. a. E. R. S. Camron Miller, "Evaluation of Production Log Data from Horizontal Wells Drilled in Organic Shales," *SPE International*, 2011.
- [2] C. Chadwick and C. Whittaker, "Production Logging Challenges in Horizontal Shale Gas Wells," in *SPWLA 52nd Annual Logging Symposium*, Colorado, 2011.
- [3] D. Denney, "DTS technology: Improving Acid Placement," *Journal of Petroleum Technology*, vol. 64, no. 06, pp. 96-99, 2012.
- [4] U. Djuraeva, S. Jufara and P. Vasantb, "A review on conceptual and practical oil and gas reservoir monitoring methods," *Journal of Petroleum Science and Engineering*, vol. 152, pp. 586-601, 2017.
- [5] C. Miller, G. Waters and E. Rylander, "Evaluation of Production Log Data from Horizontal Wells Drilled in Organic Shales; SPE 144326," in *SPE International*, 2011.
- [6] H. J. J. R. K. A. Waters G., "Use of Horizontal Well Image Tools To Optimize Barnett Shale Reservoir Exploitation. SPE 103202," in *SPE Annual Technical Conference and Exhibition*, San Antonio, Texas, 2006.
- [7] A. Inamdar, R. Malpani, K. Atwood, K. Brook, A. Erwemi, T. Ogundare and D. Purcell, "Evaluation of Stimulation Techniques Using Microseismic Mapping in the Eagle Ford Shale. SPE 136873," in *SPE Tight Gas Completions Conference*, San Antonio, Texas, 2010.
- [8] M. Soroush., M. Mohammadtabar., .. M. Roostaei, S. Hosseini. and M. Mahmoudi., "An Industry Overview of Downhole Monitoring Using Distributed Temperature Sensing: Fundamentals and Two Decades Deployment in Oil and Gas Industries.," in *SPE International*, Bakersfield, 2021.
- [9] O. Mbaabu, "Introduction to Random Forest in Machine Learning," Section, 2021. [Online]. Available: <https://www.section.io/engineering-education/introduction-to-random-forest-in-machine-learning/>. [Accessed 9 March 2022].
- [10] S. Sharma, "Artificial Neural Network (ANN)," [Online]. Available: <https://www.datasciencecentral.com/profiles/blogs/artificial-neural-network-ann-in-machine-learning>. [Accessed 24 February 2022].
- [11] F. Chollet, "Keras," 2015. [Online]. Available: <https://keras.io>.
- [12] E. Holley, T. Jones, J. Dodson and J. Salazar, "Using Distributed Optical Sensing to Constrain Fracture Models and Confirm Reservoir Coverage in the Permian Basin," in *Society of Petroleum Engineers*, 2014.

- [13] X. Wang and T. Bussear, "Real Time Horizontal Well Monitoring Using Distributed Temperature Sensing (DTS) Technology," in *Offshore Technology Conference*, 2011.
- [14] G. Malanya, K. Butula, K. Burdin, M. Khaziev, S. Kuzmin, I. Kaeshkov and M. Kremenetskiy, "Successful Experience of Estimating Injection Flow Profile in Horizontal Wells Completed with Multistage Fracs in Conventional Reservoirs Using CT Conveyed Distributed Temperature Sensing," in *Society of Petroleum Engineers*, 2016.
- [15] J. R. Sierra, J. D. Kaura, D. Gualtieri, G. Glasbergen, D. Sarker and D. Johnson, "DTS Monitoring of Hydraulic Fracturing: Experiences and Lessons Learned.," in *Society of Petroleum Engineers*, 2008.
- [16] P. T. Huckabee, "Optic Fiber Distributed Temperature for Fracture Stimulation Diagnostics and Well Performance Evaluation," in *Society of Petroleum Engineers*. doi: 10.2118/118831-MS, 2009.
- [17] E. H. Holley, M. M. Molenaar, E. Fidan and B. M. Banack, "Interpreting Uncemented Multistage Hydraulic-Fracturing Completion Effectiveness Using Fiber-Optic DTS Injection Data.," in *Society of Petroleum Engineers*, 2012.
- [18] E. H. Holley, M. M. Molenaar, E. Fidan and B. Banack, "Interpreting Uncemented Multistage Hydraulic Interpreting Uncemented Multistage Hydraulic," in . *Society of Petroleum Engineers*, 2013.
- [19] M. Tabatabaei and D. Zhu, "Fracture Stimulation Diagnostics in Horizontal Wells Using DTS Data," in *Society of Petroleum Engineers*, 2011.
- [20] H. Sun, W. Yu and K. Sepehrnoori, "A New Comprehensive Numerical Model for Fracture Diagnosis with Distributed Temperature Sensing DTS.," in *Society of Petroleum Engineers*, 2017.
- [21] M. Tarrahi, E. Gildin, J. Moreno and S. Gonzales, " Dynamic Integration of DTS Data for Hydraulically Fractured Reservoir Characterization with the Ensemble Kalman Filter.," in *Society of Petroleum Engineers*., 2014.
- [22] N. Kalia, S. Gorgi, E. Holley, A. S. Cullick and T. Jones, "Wellbore Monitoring in Unconventional Reservoirs: Value of Accurate DTS Interpretation and Risks Involved," in *Society of Petroleum Engineers*, 2014.
- [23] E. Holley, H. Zimmer, U. Mayerhofer and M. J. Samson, "Integrated Analysis Combining Microseismic Mapping and Fiber-Optic Distributed Temperature Sensing (DTS)," in *Society of Petroleum Engineers*., 2010.
- [24] C. L. McCullagh, A. N. Tutuncu and T. H. Song, "Coupling Distributed Temperature Sensing (DTS) based Wellbore Temperature Models with Microseismic Data for Enhanced Characterization of Hydraulic Fracture Stimulation," in *American Rock Mechanics Association*., 2014.

- [25] M. A. Fahim, A. A. Keshka, A. Al Marzooqi, A. Alvi, D. Abdallah, G. Brown and F. Ali Neyaei, "Distributed Temperature Sensing (DTS) Enables Injectivity Visualization To Enhance Stimulation Efficiency," in *Society of Petroleum Engineers*, 2011.
- [26] H. K. Sharma, A. K. Al-Zain, N. N. K. Al-Salman, M. S. Al-Harbi and R. Said, "A Successful Application of Permanently Installed Distributed Temperature Sensing (DTS) for Optimization of Acid Treatment in Power Water Injector With Advanced Well Completion: Case Study," in *Society of Petroleum Engineers*, 2010.
- [27] Y. Santin, K. Matar, E. Montes, S. Gorgi, J. Joya, M. Bu-Mijdad and M. Al-Dashti, "Reliable Carbonate Stimulation Using Distributed Temperature Sensing Diagnostics and Real-Time Fiber-Optic Coiled Tubing Intervention in Kuwait," in *Society of Petroleum Engineers*, 2018.
- [28] A. Al-Najim, A. Zahedi, T. Al-Khonaini, A. Al-Sharqawi, P. M. J. Tardy, A. Abdur Rahman and F. S. Alhadyani, "A New Methodology for Stimulation of a High-Water-Cut Horizontal Oil Well through the Combination of a Smart Chemical System with Real-Time Temperature Sensing: A Case Study of South Umm Gudair Field, PZ Kuwait.," in *Society of Petroleum Engineers*, 2012.
- [29] R. P. Reyes, V. J. Yeager, G. Glasbergen, J. L. Parrish and R. Tucker, "DTS Sensing: An Introduction To Permian Basin With A West-Texas Operator," in *Society of Petroleum Engineers*, 2011.
- [30] S. Grayson, Y. Gonzalez, K. England, R. Bidyk and S. F. Pitts, "Monitoring Acid Stimulation Treatments in Naturally Fractured Reservoirs with Slickline Distributed Temperature Sensing," in *Society of Petroleum Engineers*, 2015.
- [31] P. M. J. Tardy, P. Ramondenc, X. Weng, R. Burgos, F. Baez and K. Y. Ganjeh, "Inversion of DTS Logs To Measure Zonal Coverage During and After Wellbore Treatments With Coiled Tubing," in *Society of Petroleum Engineers*, 2011.
- [32] P. M. J. Tardy, P. Ramondenc, X. Weng, R. Burgos, F. Baez and K. Y. Ganjeh, "Inversion of Distributed-Temperature-Sensing Logs To Measure Zonal Coverage During and After Wellbore Treatments With Coiled Tubing.," in *Society of Petroleum Engineers*, 2012.
- [33] G. Glasbergen, D. Gualtieri, M. S. Van Domelen and J. Sierra, " Real-Time Fluid Distribution Determination in Matrix Treatments Using DTS.," in *Society of Petroleum Engineers*, 2009.
- [34] J. Vazquez, L. Inda, E. Medina, I. E. Narvaez and J. Gleaves, " Real-Time Monitoring of Naturally Fractured Carbonate Reservoir Stimulation Using Distributed Temperature Sensing: Case Study from Offshore Mexico," in *Society of Petroleum Engineers*, 2017.
- [35] H. Pinto, C. Frederico Eira, F. Rosas, F. Carneiro and D. Bobula, "Use of Laboratory Scale Apparatus for Simulation of Downhole Stimulation Monitoring With Distributed Temperature Surveys.," in *Society of Petroleum Engineers*, 2014.

- [36] X. Wang and T. R. Bussear, " Real-time Evaluation of Acid Stimulation Performance in Extended-Reach Carbonate Wells with DTS-enabled Intelligent Completions.," in *Society of Petroleum Engineers.*, 2013.
- [37] M. Tabatabaei, D. Zhu and D. Hill, " Interpretation of Temperature Data during Acidizing Treatment of Horizontal Wells for Stimulation Optimization," in *International Petroleum Technology Conference*, 2011.
- [38] M. Tabatabaei, D. Zhu and A. D. Hill, "Theoretical Basis for Interpretation of Temperature Data During Acidizing Treatment of Horizontal Wells," in *Society of Petroleum Engineers*, 2013.
- [39] P. Ramondenc and F. Baez, " Using Fiber-Optic-Enabled Coiled Tubing to Quantify Fluid Placement and Optimize Stimulation Effectiveness During Matrix Stimulation Treatments in Carbonate Reservoirs.," in *Society of Petroleum Engineers*, 2013.
- [40] V. H. Lopez, M. A. Castillo, R. Custodio, S. P. Worden, M. Gerardo Romandia, P. Ramondenc and F. L. Rueda, "First Real-Time DTS Inversion Job Worldwide," in *Society of Petroleum Engineers*, 2013.
- [41] J. Davies, H. Van Dongen, A. Oftedal and N. Kalia, "Interwell Communication as a Means to Detect a Thief Zone Using DTS in a Danish Offshore Well.," in *Offshore Technology Conference*, 2013.
- [42] Y. Mao, M. Zeidouni and I. Duncan, "Temperature analysis for early detection and rate estimation of CO<sub>2</sub> wellbore leakage.," *International Journal of Greenhouse Gas Control*, vol. 67, pp. 20-30, 2017.
- [43] Y. Sun, Z. Xue and T. Hashimoto, "Fiber optic distributed sensing technology for real-time monitoring water jet tests: Implications for wellbore integrity diagnostics.," *Journal of Natural Gas Science and Engineering*, vol. 58, pp. 241 - 250, 2018.
- [44] T. Setiawan, S. E. Lidwin, G. T. Wei, S. W. Widodo, R. Sandanasamy, T. Rakela and J. C. Vaca, "Identification of Shallow Gas Leaks Through Multiple Strings Using Slickline With Fiber-Optic Distributed Temperature Sensing.," in *Society of Petroleum Engineers*, 2016.
- [45] S. Thompson, A. Bello, M. Medina and T. Greig, "Well Integrity Evaluation Using Distributed Temperature Sensing (DTS) on an Operating SAGD Injector Well Influenced by Neighboring Steam Chambers.," in *Society of Petroleum Engineers*, 2015.
- [46] A. Mishra, S. H. Al Gabani and A. Jumaa Al Hosany, "Pipeline Leakage Detection Using Fiber Optics Distributed Temperature Sensing DTS.," in *Society of Petroleum Engineers*, 2017.
- [47] S. Bersan, A. R. Koelewijn, M. Putti and P. Simonini, "Large-Scale Testing of Distributed Temperature Sensing for Early Detection of Piping," *J. Geotech. Geoenviron. Eng.*, vol. 145, no. 9, 2019.

- [48] N. I. T. S. A. B. A. M. Weppenaar, "Full-Scale Testing of Distributed Temperature Sensing in Flexible Risers and Flowlines.," in *Offshore Technology Conference*, 2013.
- [49] C. S. Kabir, B. Izgec, A. R. Hasan, X. Wang and J. Lee, "Real-Time Estimation of Total Flow Rate and Flow Profiling in DTS-Instrumented Wells.," in *International Petroleum Technology Conference*, 2008.
- [50] X. Wang, J. Lee and G. Vachon, "Distributed Temperature Sensor (DTS) System Modeling and Application.," in *Society of Petroleum Engineers*., 2008.
- [51] X. Wang, J. Lee, B. Thigpen, G. P. Vachon, S. H. Poland and D. Norton, "Modeling Flow Profile using Distributed Temperature Sensor (DTS) System.," in *Society of Petroleum Engineers*, 2008.
- [52] X. Wang, T. R. Bussear and A. R. Hasan, "Technique To Improve Flow Profiling Using Distributed Temperature Sensors.," in *Society of Petroleum Engineers*, 2010.
- [53] L. Ouyang and D. Belanger, "Flow Profiling via Distributed Temperature Sensor (DTS) System Expectation and Reality.," in *Society of Petroleum Engineers*, 2004.
- [54] L. Ouyang and D. Belanger, "Flow Profiling by Distributed Temperature Sensor (DTS) System Expectation and Reality.," in *Society of Petroleum Engineers*, 2006.
- [55] G. H. Lanier, G. Brown and L. Adams, "Brunei Field Trial of a Fibre Optic Distributed Temperature Sensor (DTS) System in a 1,000m Open Hole Horizontal Oil Producer.," in *Society of Petroleum Engineers*, 2003.
- [56] D. O. Johnson, J. R. Sierra, J. D. Kaura and D. Gualtieri, "Successful Flow Profiling of Gas Wells Using Distributed Temperature Sensing Data.," in *Society of Petroleum Engineers*, 2006.
- [57] C. P. John, L. W. Ramnath, R. V. Khankishiyev, H. Hasanov, J. Stephenson and P. D. A. Keatinge, "Integration of Distributed Temperature Sensing Technology with Open Hole Gravel Packed Completions - The ACG Field Experience.," in *Society of Petroleum Engineers*, 2015.
- [58] D. E. Hembling, G. Berberian, N. Carter and G. J. Naldrett, "Enabling Efficient Permanent Production Monitoring of Advanced Well Completions In Saudi Arabia Using Fiber-Optic Distributed Temperature Sensing.," in *Society of Petroleum Engineers*, 2008.
- [59] A. Mehmood, D. Ali, S. A. Mallah, K. Rashid, A. Mhiri, P. Ramondenc and R. S. A. Khan, "Overcoming Production Logging Challenges in Completions with Mechanical Restrictions Using Distributed Temperature Sensing: A Case Study from North Pakistan.," in *Society of Petroleum Engineers*, 2018.
- [60] M. K. S. S. R. L. M. F. Carlsen, "Production Optimisation of a Long Horizontal Well Using Permanent Down-hole Distributed Temperature and Pressure Monitoring and Surface Controlled Zones.," in *Society of Petroleum Engineers*, 2013.

- [61] M. Tolan, M. Boyle and G. Williams, "The Use of Fiber-Optic Distributed Temperature Sensing and Remote Hydraulically Operated Interval Control Valves for the Management of Water Production in the Douglas Field.," in *Society of Petroleum Engineers*, 2001.
- [62] D. B. Foo, J. Krislock, T. J. Meador and T. Cheng, "Horizontal Well Injection Profiling Using Distributed Temperature Sensing.," in *Society of Petroleum Engineers.*, 2014.
- [63] R. Khamatdinov, X. Wang, I. Mostafa and M. A. Chughtai, "Optimizing Waterflood Management by Modeling Historical Temperature of the Water Injection Front using Distributed Temperature Sensing DTS System.," in *Society of Petroleum Engineers*, 2016.
- [64] G. A. Brown, V. L. S. Carvalho, A. S. Wray, A. Sanchez and G. Gutierrez Murillo, "Slickline With Fiber-Optic Distributed Temperature Monitoring for Water-Injection and Gas Lift Systems Optimization in Mexico.," in *Society of Petroleum Engineers*, 2005.
- [65] V. Nuñez-Lopez, J. Muñoz-Torres and M. Zeidouni, "Temperature monitoring using Distributed Temperature Sensing (DTS) technology.," *Energy Procedia*, vol. 63, p. 3984–3991, 2014.
- [66] B. Wiese, "Thermodynamics and heat transfer in a CO<sub>2</sub> injection well using distributed temperature sensing (DTS) and pressure data.," *International Journal of Greenhouse Gas Control*, vol. 21, p. 232–242, 2014.
- [67] S. Mawalkar, D. Brock, A. Burchwell, M. Kelley, S. Mishra, N. Gupta, R. Pardini and B. Shroyer, "Where is that CO<sub>2</sub> flowing? Using Distributed Temperature Sensing (DTS) technology for monitoring injection of CO<sub>2</sub> into a depleted oil reservoir.," *International Journal of Greenhouse Gas Control*, vol. 85, p. 132–142, 2019.
- [68] L. Richard and R. Pevzner, "Evaluation of Sensitivity of Downhole Temperature Estimates from Distributed Temperature Sensing measurements.," *Energy Procedia*, vol. 154, p. 106–111, 2018.
- [69] M. W. S. Chin, G. C. Woon, K. Wood and B. Gorgi, "Integrated EOR Approach via Application and Installation of Distributed Fiber-Optic Technology.," in *Offshore Technology Conference*, 2016.
- [70] N. Mehtiyev, M. Rahman and D. A. Bourgoynne, "Determination of Water Injection Zonal Allocation From Distributed Temperature Sensing Data.," in *Society of Petroleum Engineers*, 2012.
- [71] J. P. Furniss, J. Schouten, W. Bottomley and H. Taylor, "Reservoir Characterisation Using Distributed Temperature Sensing in CSG Development: Application in the Surat Basin, Queensland, Australia.," in *Society of Petroleum Engineers.*, 2014.
- [72] W. Bottomley, J. P. Furniss, I. Oguiche and M. Konopczynski, "Reservoir Characterisation Using Permanent Distributed Temperature Sensing in Coal Seam Gas Development: Success and Challenges in the Surat Basin," in *Society of Petroleum Engineers*, 2017.

- [73] G. A. Brown, V. L. S. Carvalho, A. S. Wray, A. Sanchez and G. Gutierrez Murillo, "Slickline With Fiber-Optic Distributed Temperature Monitoring for Water-Injection and Gas Lift Systems Optimization in Mexico.," in *Society of Petroleum Engineers*, 2005.
- [74] C. Costello, P. Sordyl, C. T. Hughes, M. R. Figueroa, E. P. Balster and G. Brown, "Permanent Distributed Temperature Sensing (DTS) Technology Applied in Mature Fields - A Forties Field Case Study.," in *Society of Petroleum Engineers*., 2012.
- [75] X. Wang, J. Lee, B. Thigpen, G. P. Vachon, S. H. Poland and D. Norton, "Modeling Flow Profile using Distributed Temperature Sensor (DTS) System," in *Society of Petroleum Engineers*, 2008.
- [76] T. Sadigov, J. Ramsay, C. Cerrahoglu, M. Salt and P. Thiruvengathanathan, "Production Optimisation Using a 24/7 Distributed Fibre Optic DFO Sensing Based Multiphase Inflow Profiling Capability," in *SPE International*, Denver, Colorado, 2020.
- [77] P. Ghahfarokhi, T. Carr, S. Bhattacharya, J. Elliott, A. Shahkarami and K. Martin, "A Fiber-optic Assisted Multilayer Perceptron Reservoir Production Modeling: A Machine Learning Approach in Prediction of Gas Production from the Marcellus Shale," in *Unconventional Resources Technology Conference*, Houston, Texas, 2018.
- [78] S. Bhattacharyaa, P. Ghahfarokhi, T. Carr and S. Pantaleonea, "Application of predictive data analytics to model daily hydrocarbon production using petrophysical, geomechanical, fiber-optic, completions, and surface data: A case study from the Marcellus Shale, North America," *Journal of Petroleum Science and Engineering*, vol. 176, pp. 702-715, 2019.
- [79] W. Li, H. Lu, Y. Jin and F. Hveding, "Deep Learning for Quantitative Hydraulic Fracture Profiling from Fiber Optic Measurements," in *Unconventional Resources Technology Conference*, Houston, Texas, 2021.
- [80] C. Sherman, R. Mellors and J. Morris, "Subsurface Monitoring via Physics-Informed Deep Neural Network Analysis of DAS," in *American Rock Mechanics Association*, New York, New York, 2019.
- [81] M. Alkhalaf, F. Hveding and M. Arsalan, "Machine Learning Approach to Classify Water Cut Measurements using DAS Fiber Optic Data," in *SPE International*, Abu Dhabi, UAE, 2019.
- [82] F. Atakishiyev, C. C. A. Delfino, Z. Hasanov, A. Wallace and A. Mendoza, "Flow Diagnostics in High Rate Gas Condensate Well Using Distributed Fiber-Optic Sensing and its Validation with Conventional Production Log," in *SPE International*, 2021.
- [83] S. Amini, P. Kavousi and T. Carr, "Application of Fiber-optic Temperature Data Analysis in Hydraulic Fracturing Evaluation: A Case Study in Marcellus Shale," in *Unconventional Resources Technology Conference*, 2017.

- [84] T. Carr, "Marcellus Shale Energy and Environment Laboratory," MSEEL, National Energy and Technology Laboratory, West Virginia University, Northeast Natural Energy, Schlumberger, 2015. [Online]. Available: [www.mseel.org/](http://www.mseel.org/).
- [85] O. Anifowoshe, M. Yates, L. Xu, P. Dickenson, J. Akin, B. Carney, J. Hewitt, I. Costello and Z. Arnold, "Improving Wellbore Stimulation Coverage in the Marcellus: Integrating Lateral Measurements with Enhanced Engineered Completion Design and Fiber Optic Evaluation," in *Society of Petroleum Engineers*, 2016.
- [86] C. Palmer, "Using AI and Machine Learning to Indicate Shale Anisotropy and Assist in Completions Design," West Virginia University, 2020.
- [87] J. Y. Julian, "Downhole Leak Determination Using Fiber-Optic Distributed-Temperature Surveys at Prudhoe Bay,," in *Society of Petroleum Engineers*, Alaska, 2007.
- [88] Q. Wu, S. Nair, E. Oort, A. Guzik and K. Kishida, "Concurrent Real-Time Distributed Fiber Optic Sensing of Casing Deformation and Cement Integrity Loss,," in *Society of Petroleum Engineers*, 2019.

## Appendix

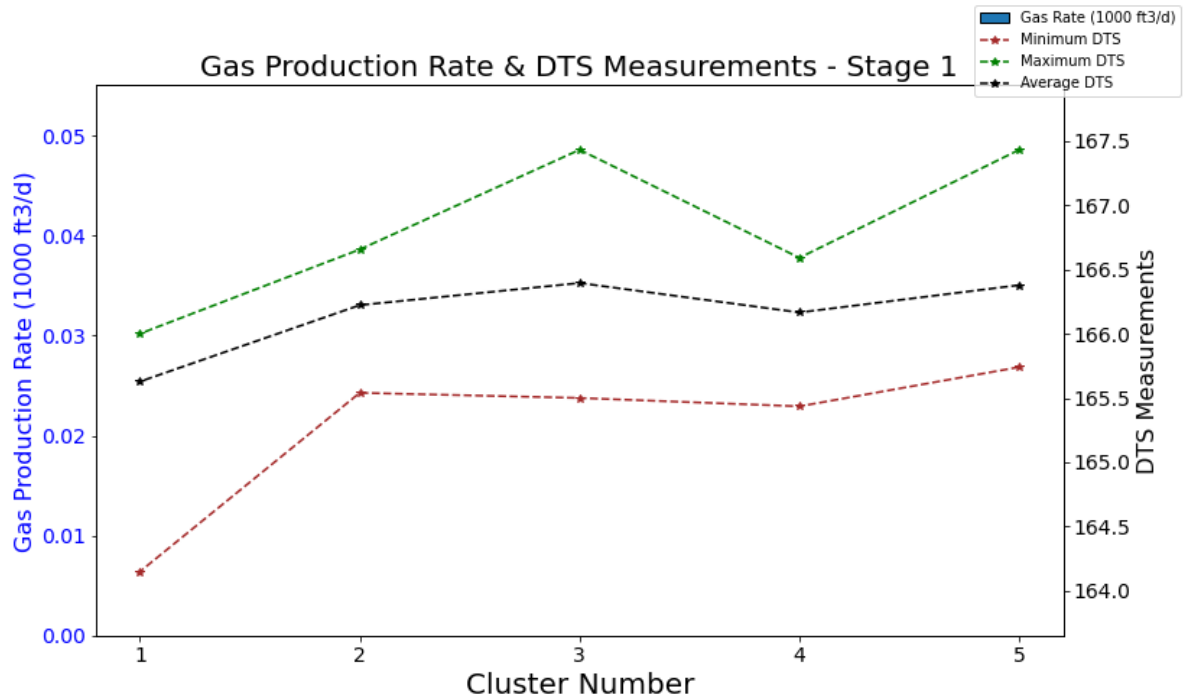


Figure 37: DTS Measurements in Stage 1 on Day of Production Log

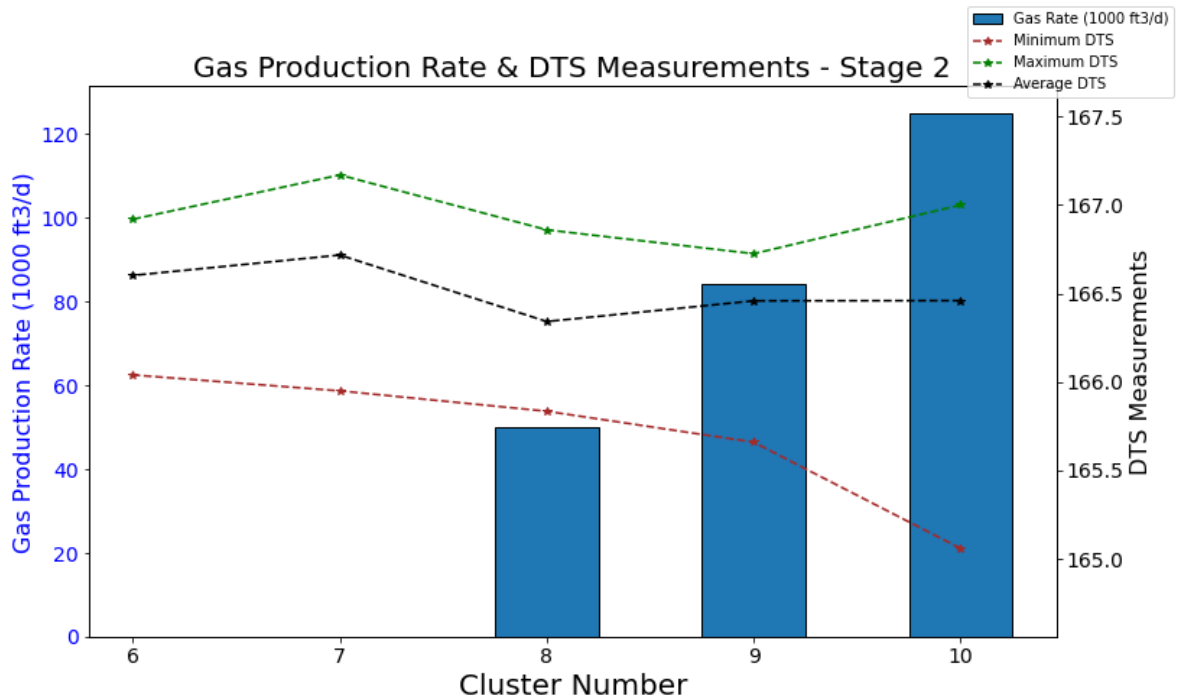


Figure 38: DTS Measurements in Stage 2 on Day of Production Log

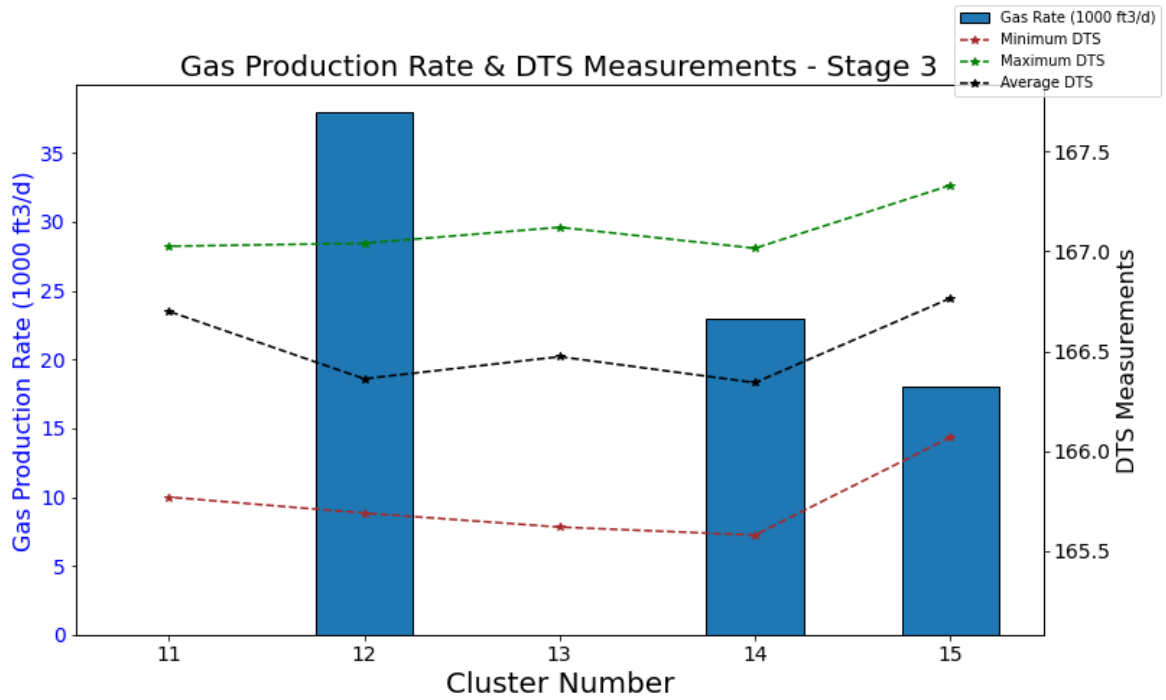


Figure 39: DTS Measurements in Stage 3 on Day of Production Log

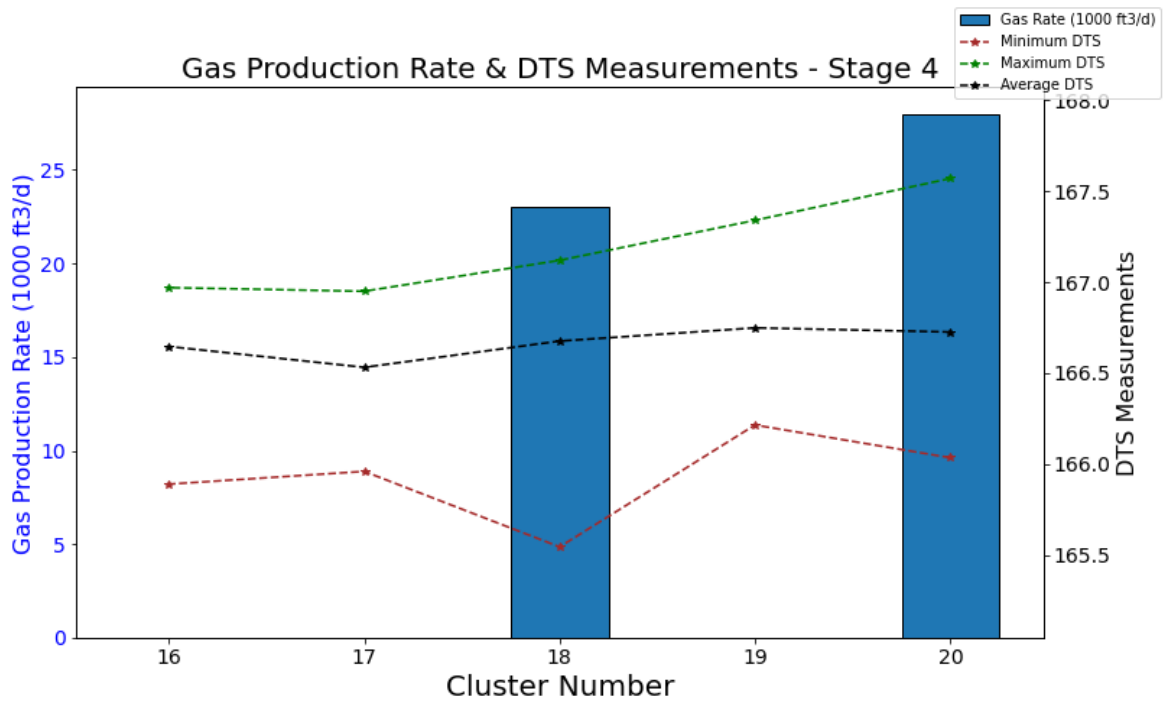


Figure 40: DTS Measurements in Stage 4 on Day of Production Log

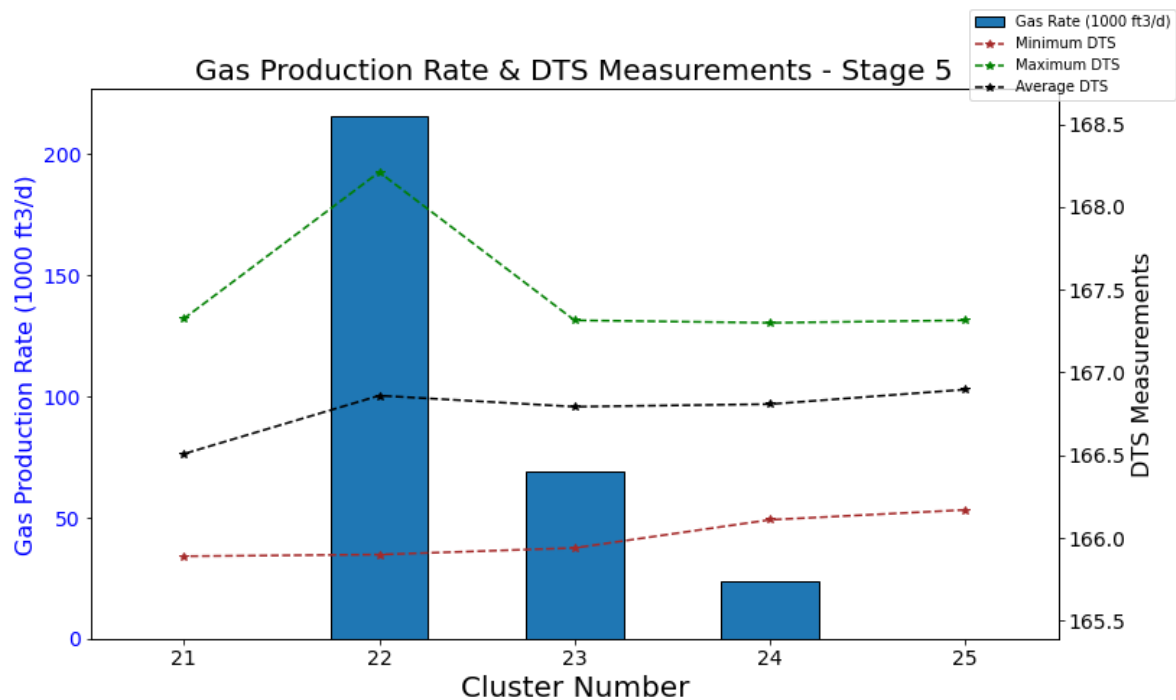


Figure 41: DTS Measurements in Stage 5 on Day of Production Log

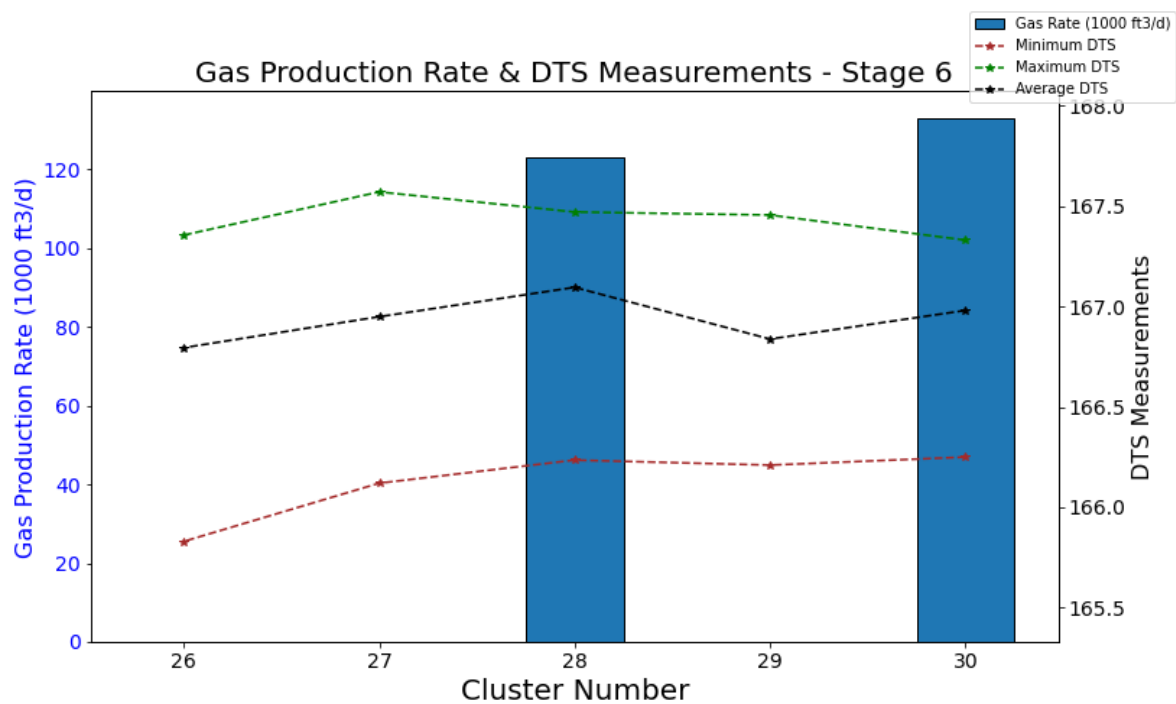


Figure 42: DTS Measurements in Stage 6 on Day of Production Log

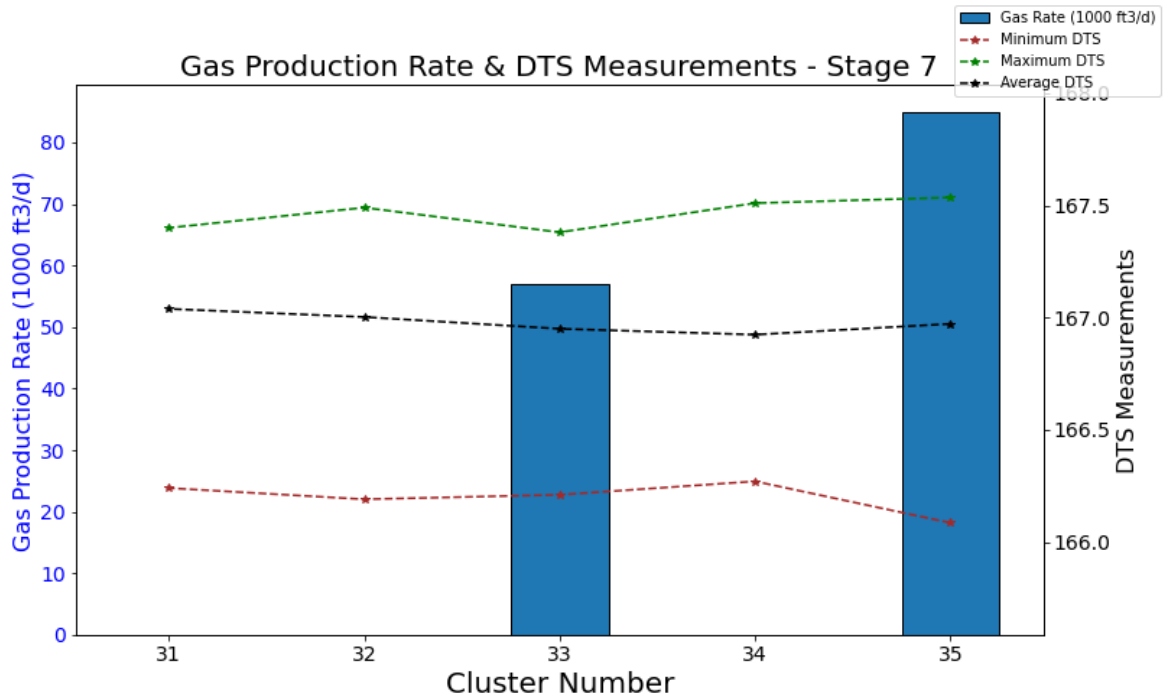


Figure 43: DTS Measurements in Stage 7 on Day of Production Log

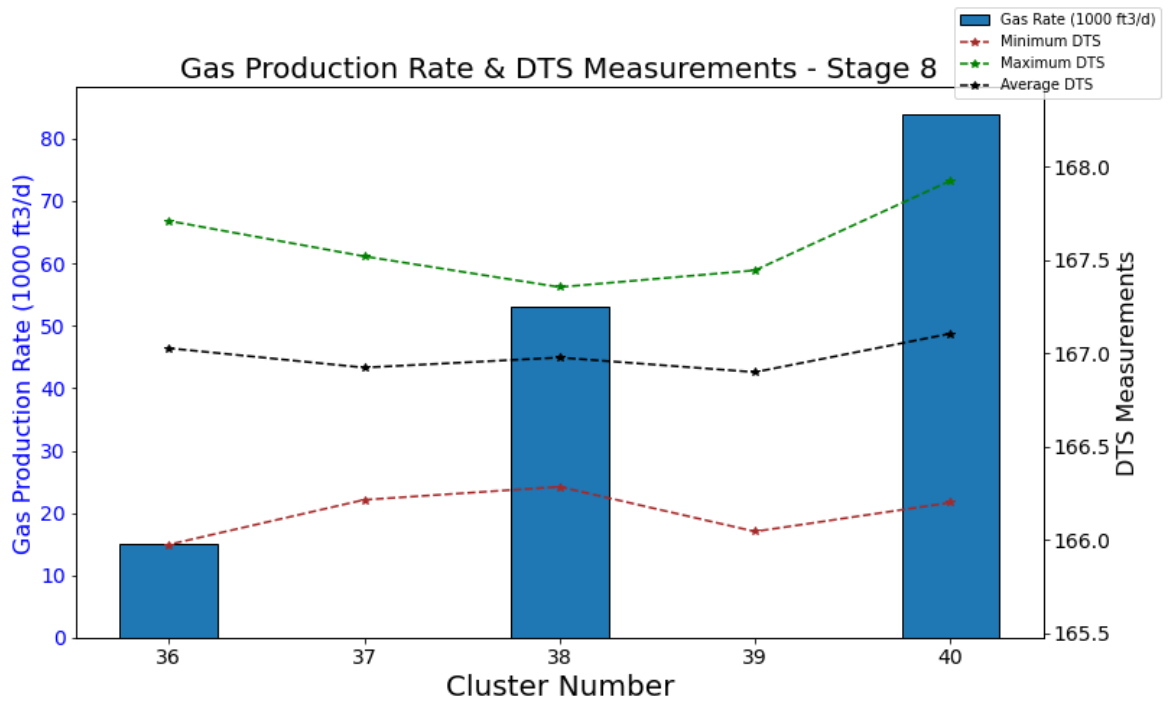


Figure 44: DTS Measurements in Stage 8 on Day of Production Log

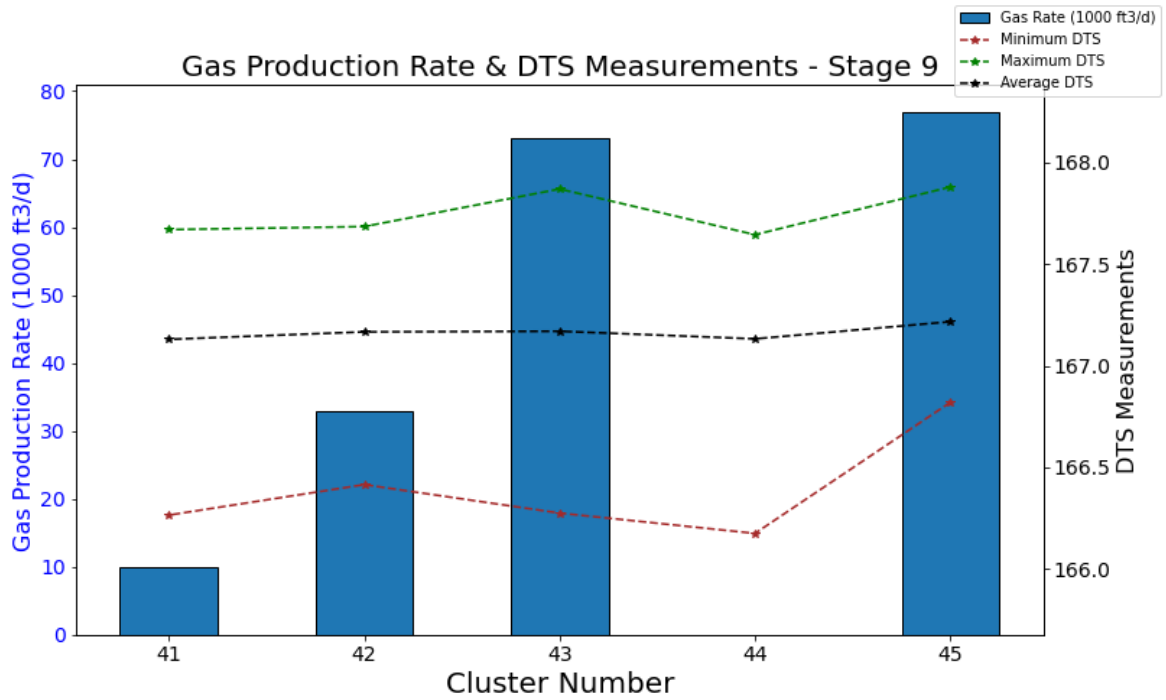


Figure 45: DTS Measurements in Stage 9 on Day of Production Log

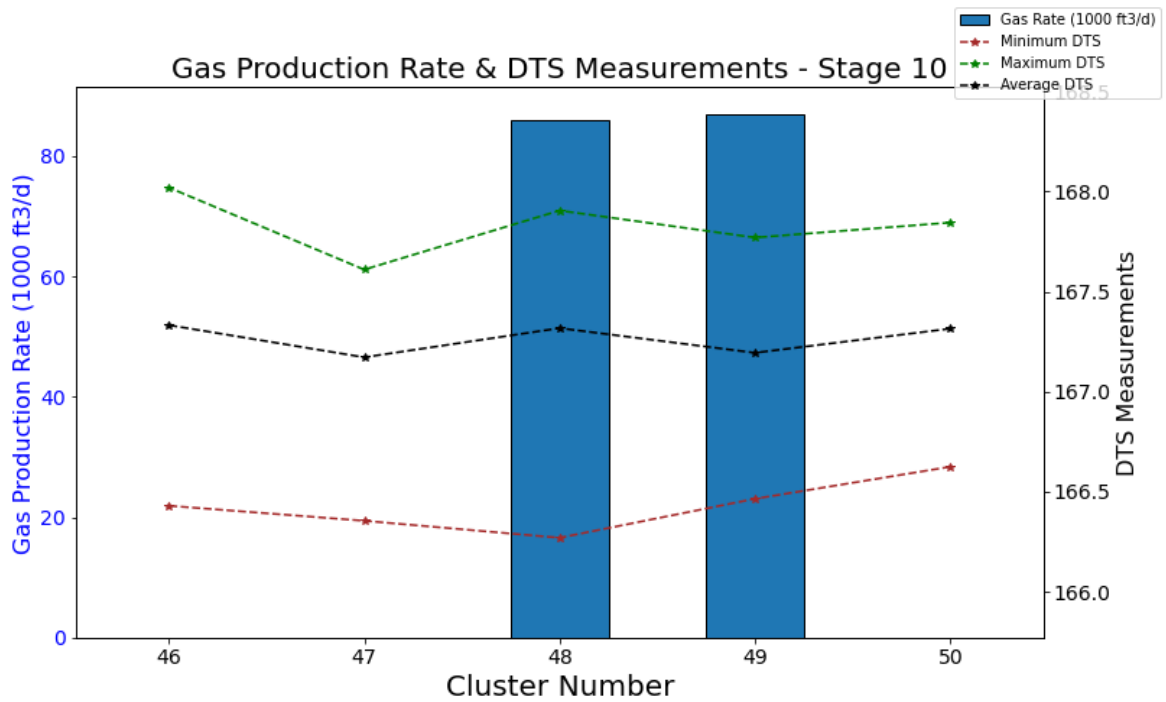
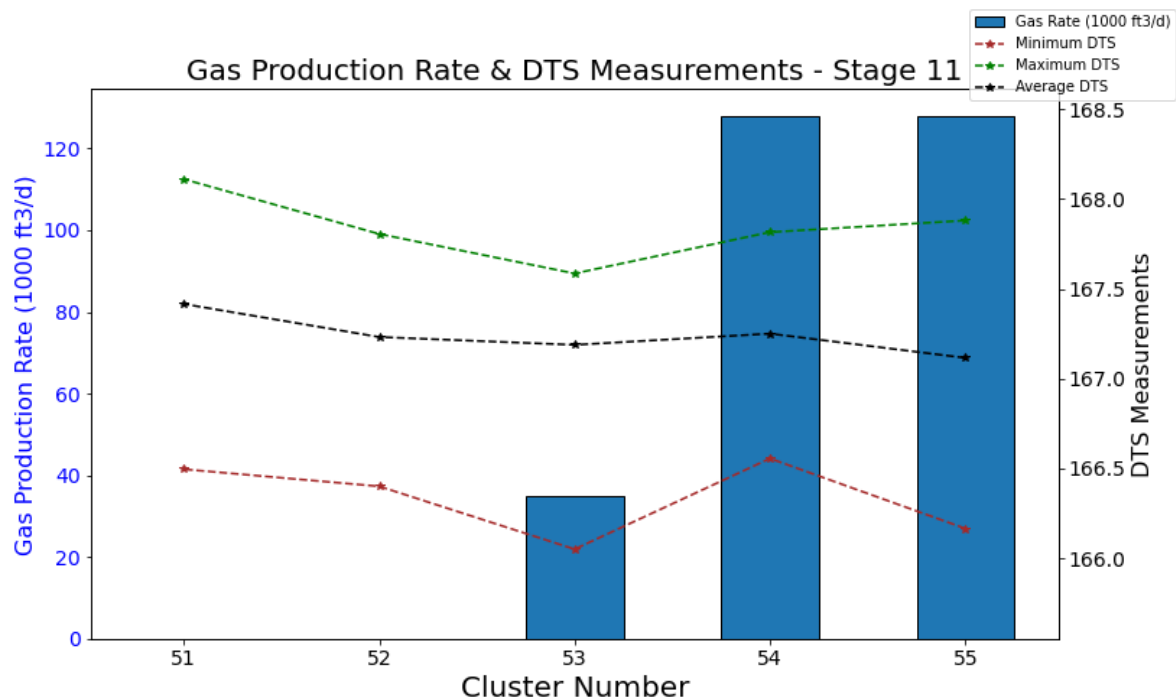
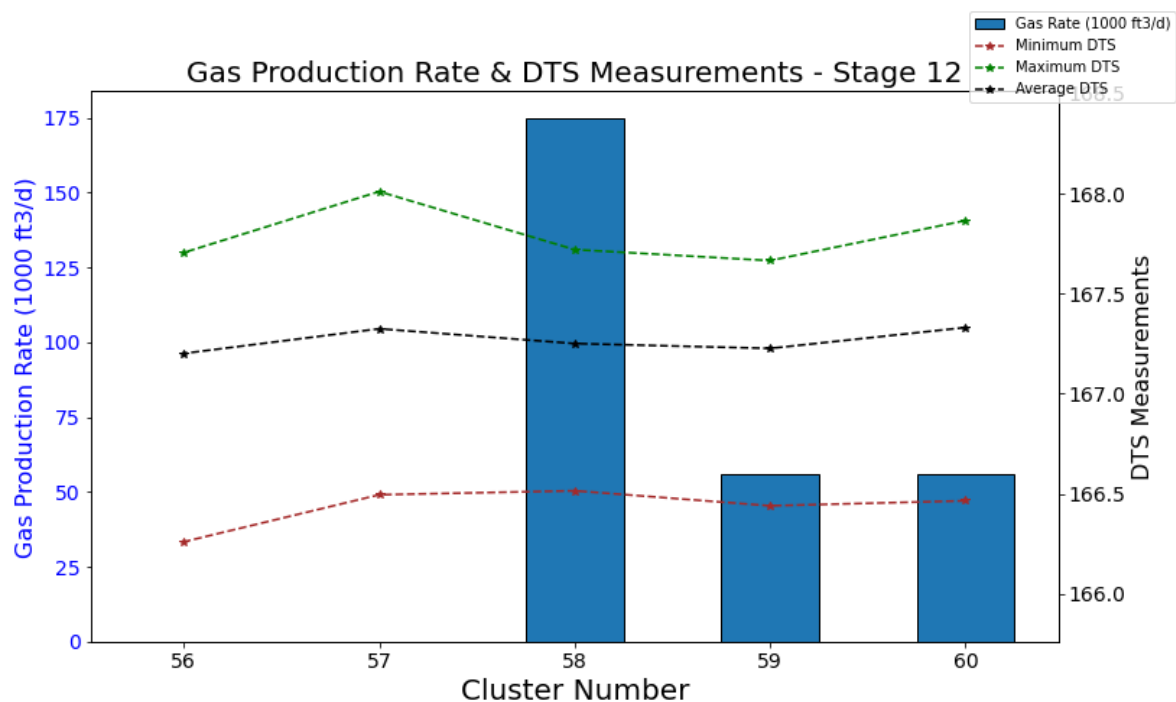


Figure 46: DTS Measurements in Stage 10 on Day of Production Log



*Figure 47: DTS Measurements in Stage 11 on Day of Production Log*



*Figure 48: DTS Measurements in Stage 12 on Day of Production Log*

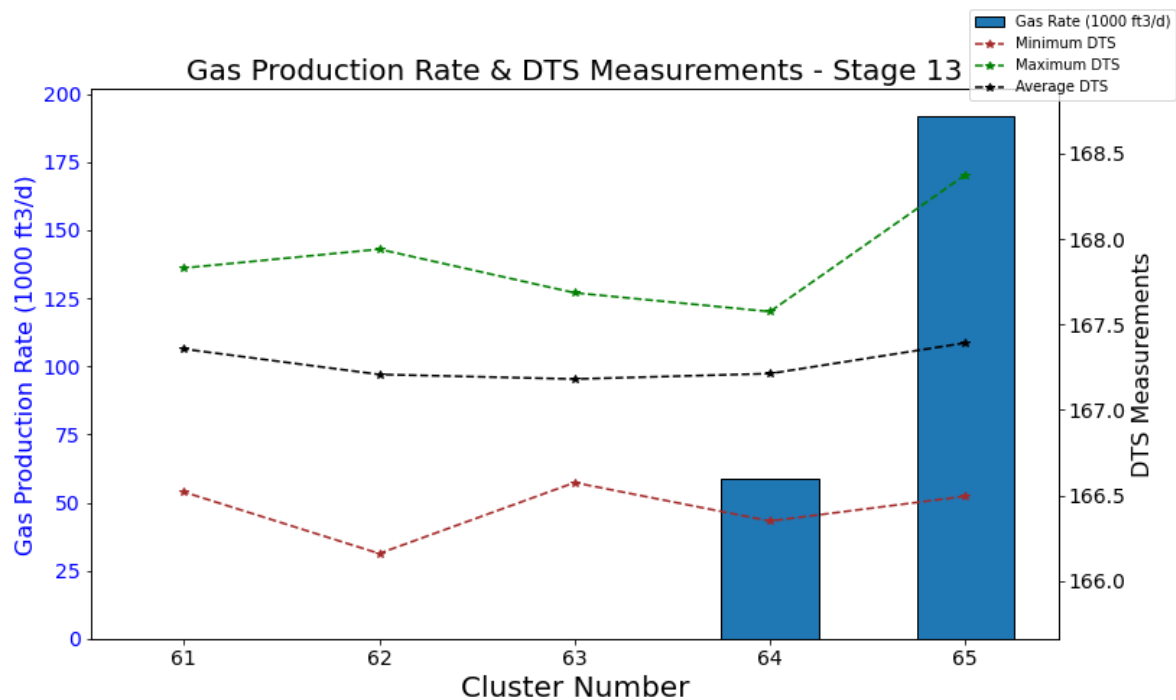


Figure 49: DTS Measurements in Stage 13 on Day of Production Log

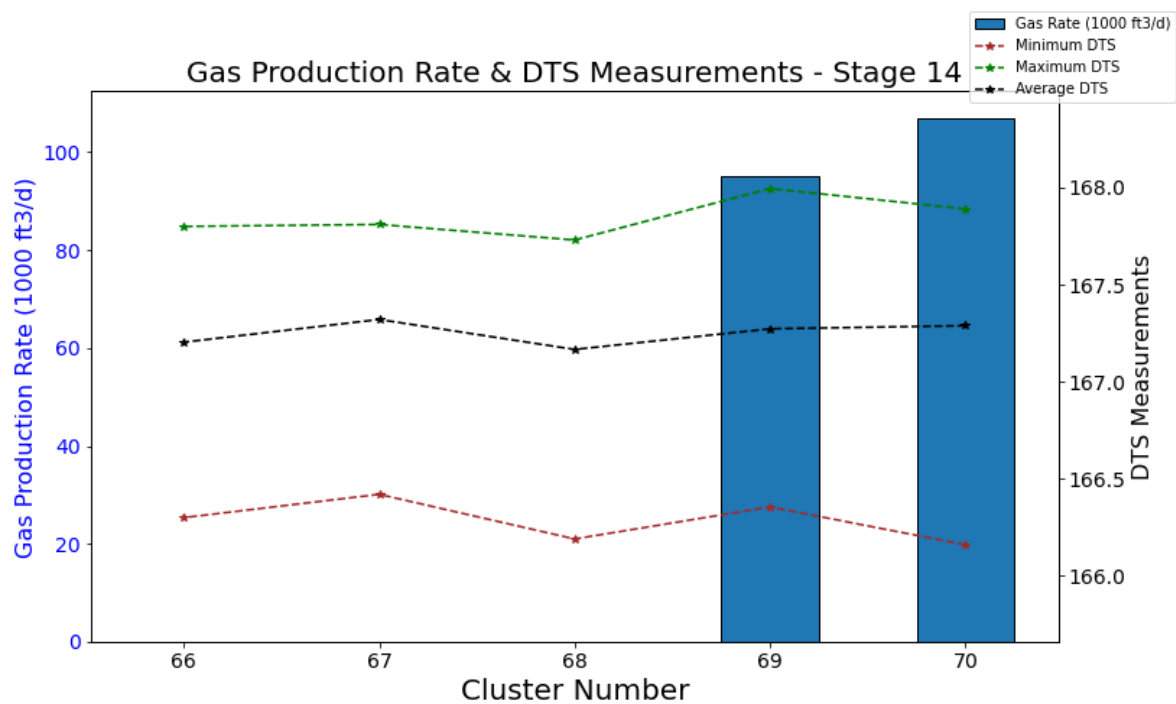
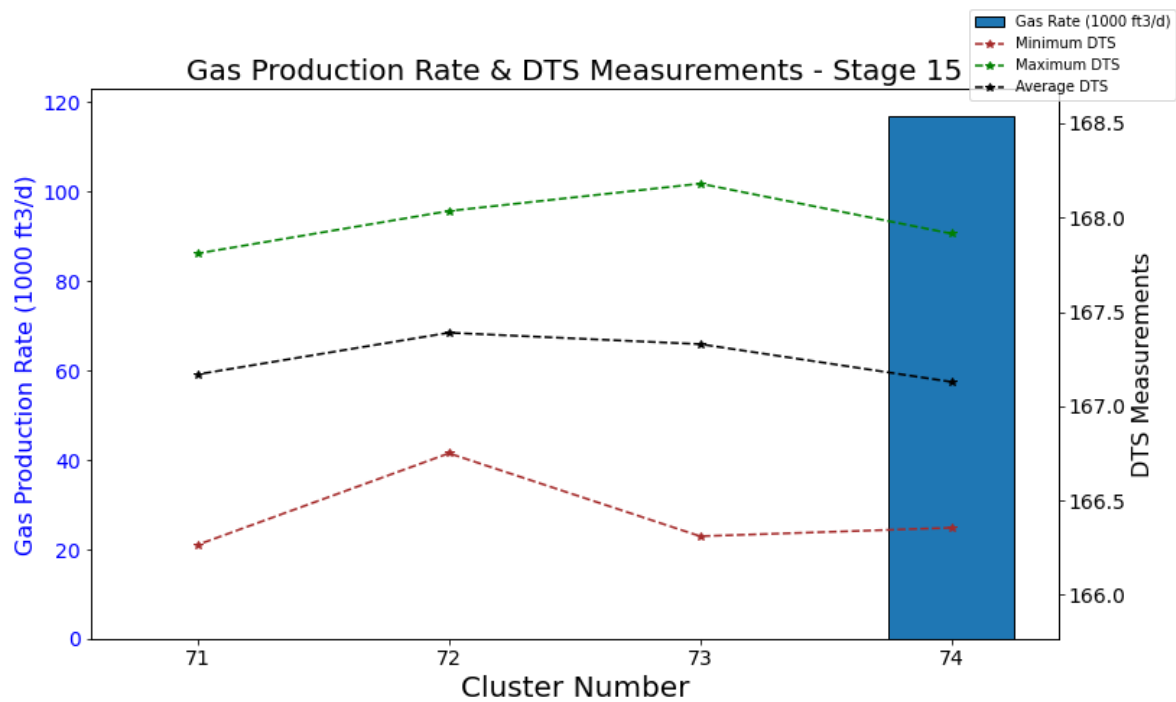
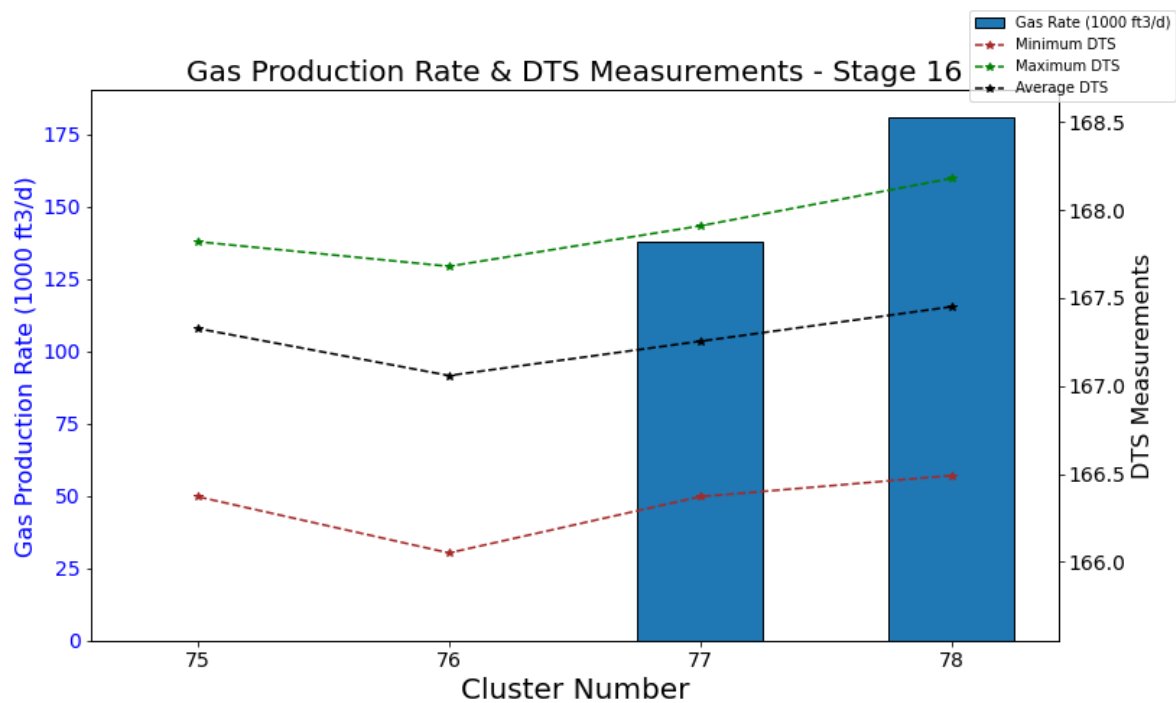


Figure 50: DTS Measurements in Stage 14 on Day of Production Log



*Figure 51: DTS Measurements in Stage 15 on Day of Production Log*



*Figure 52: DTS Measurements in Stage 16 on Day of Production Log*

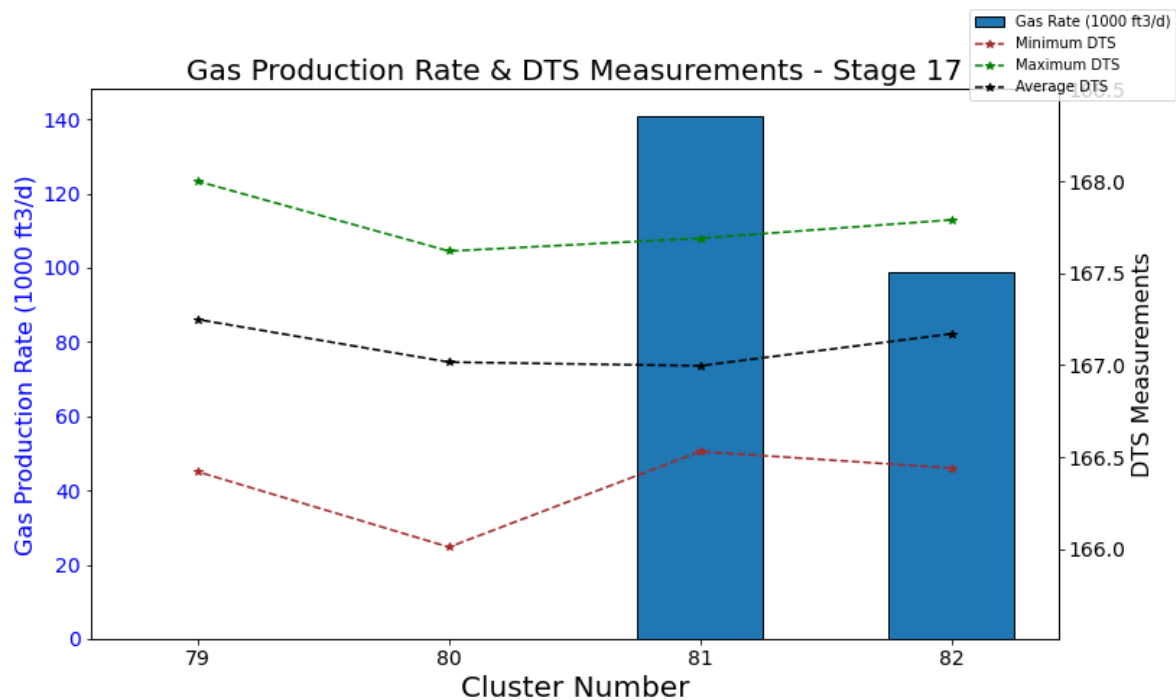


Figure 53: DTS Measurements in Stage 17 on Day of Production Log

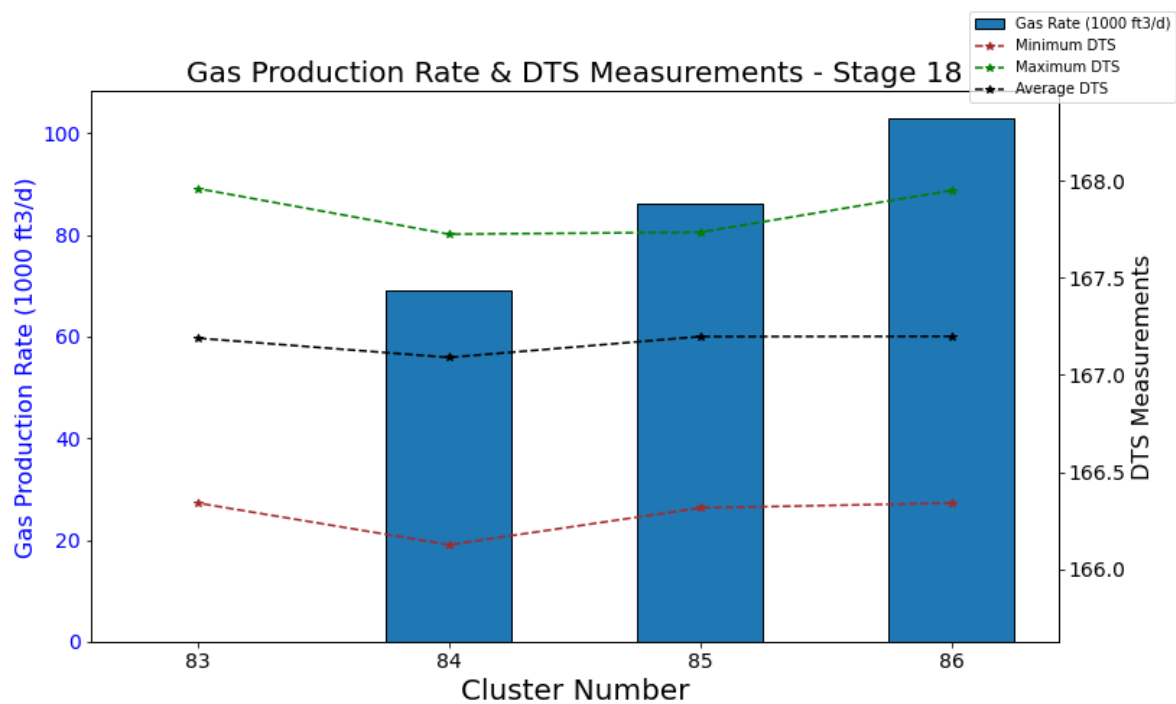
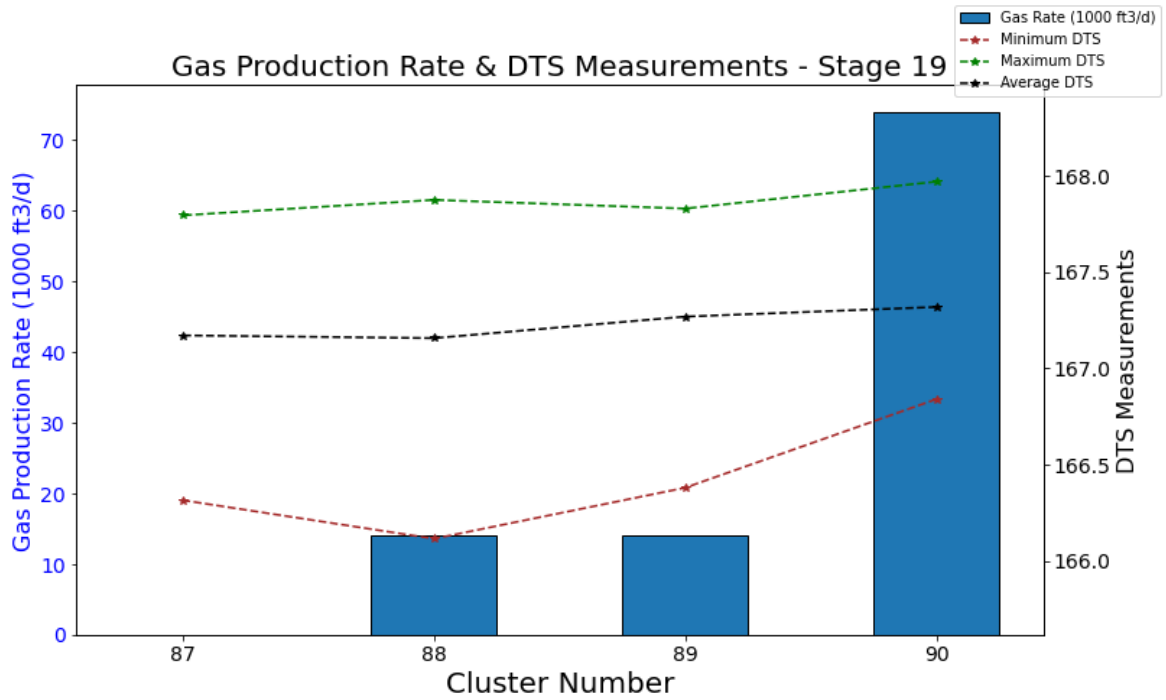
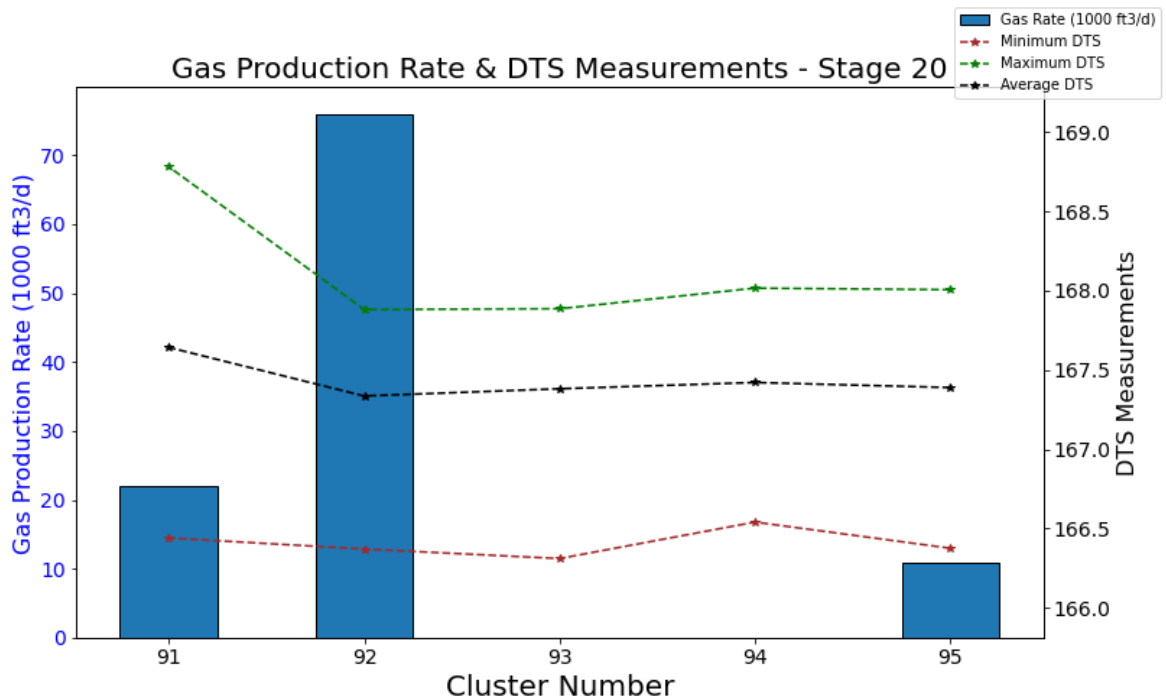


Figure 54: DTS Measurements in Stage 18 on Day of Production Log



*Figure 55: DTS Measurements in Stage 19 on Day of Production Log*



*Figure 56: DTS Measurements in Stage 20 on Day of Production Log*

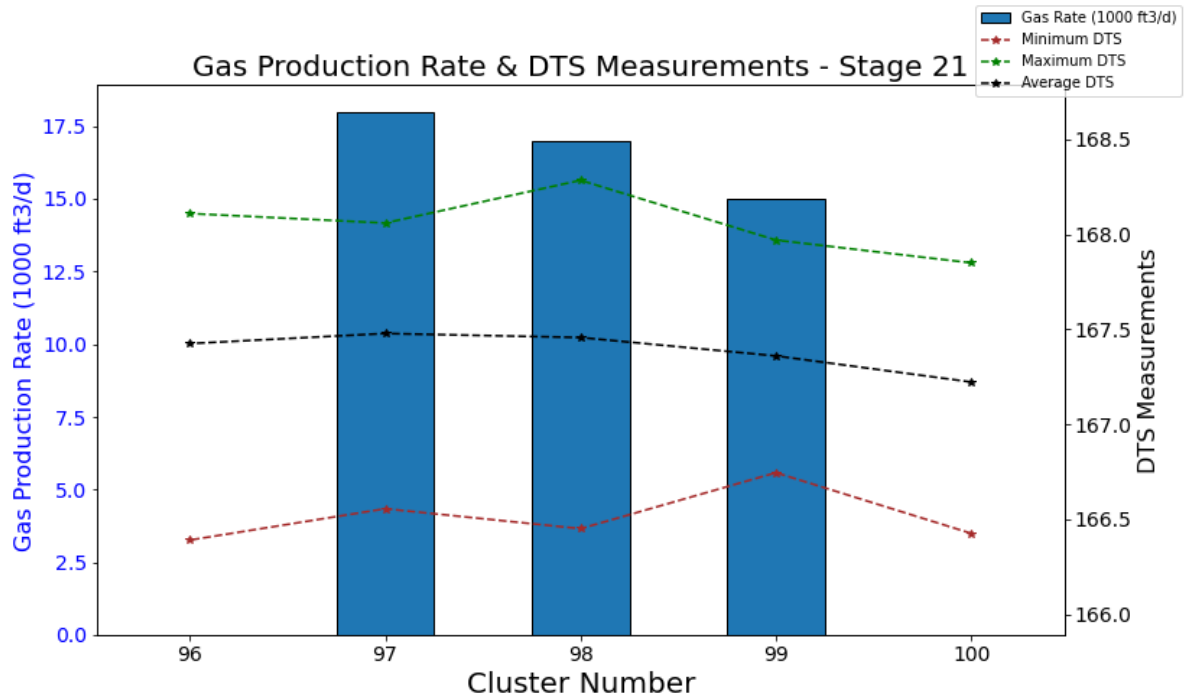


Figure 57: DTS Measurements in Stage 21 on Day of Production Log

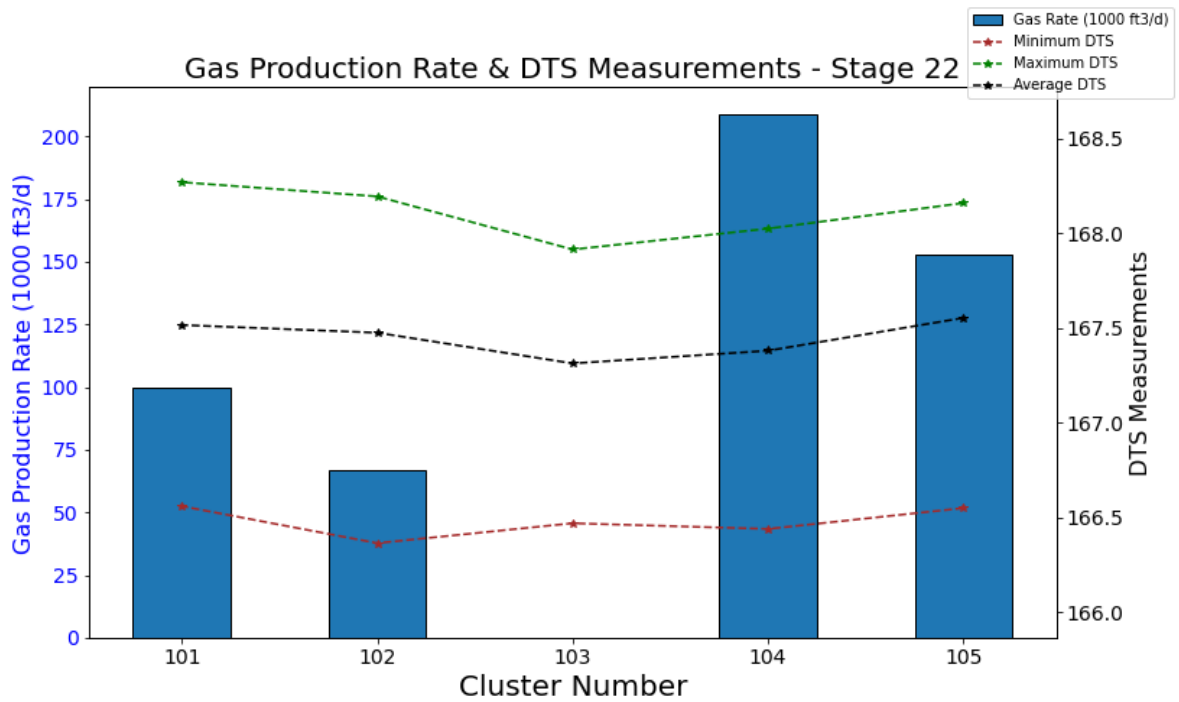
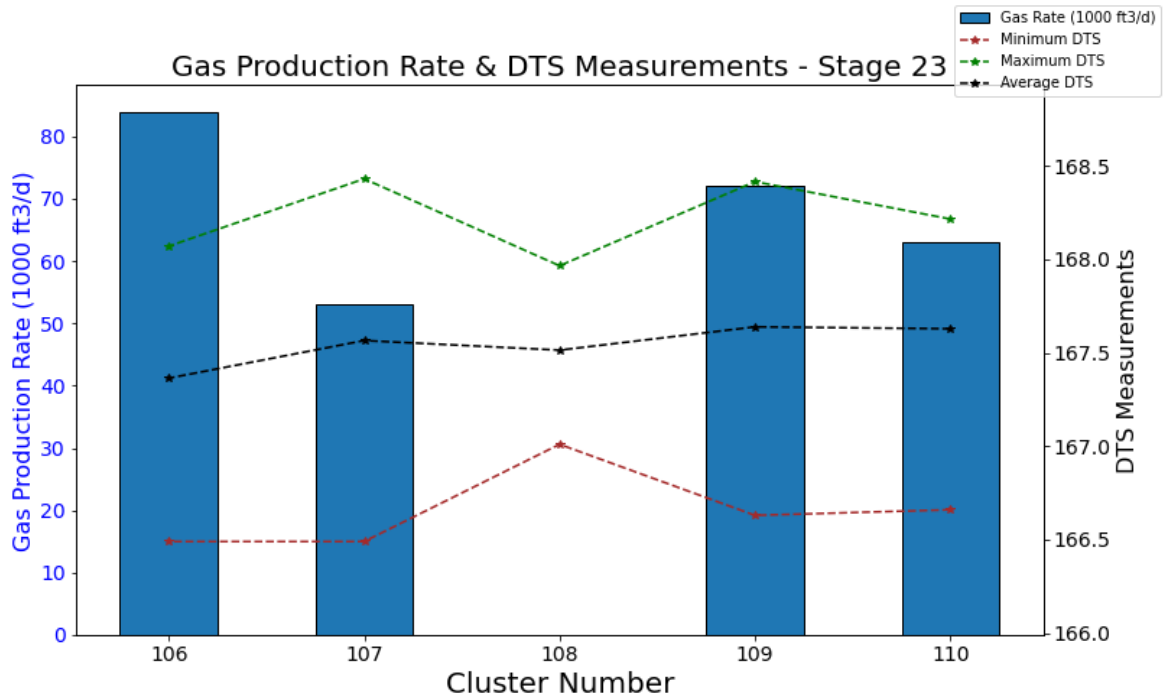
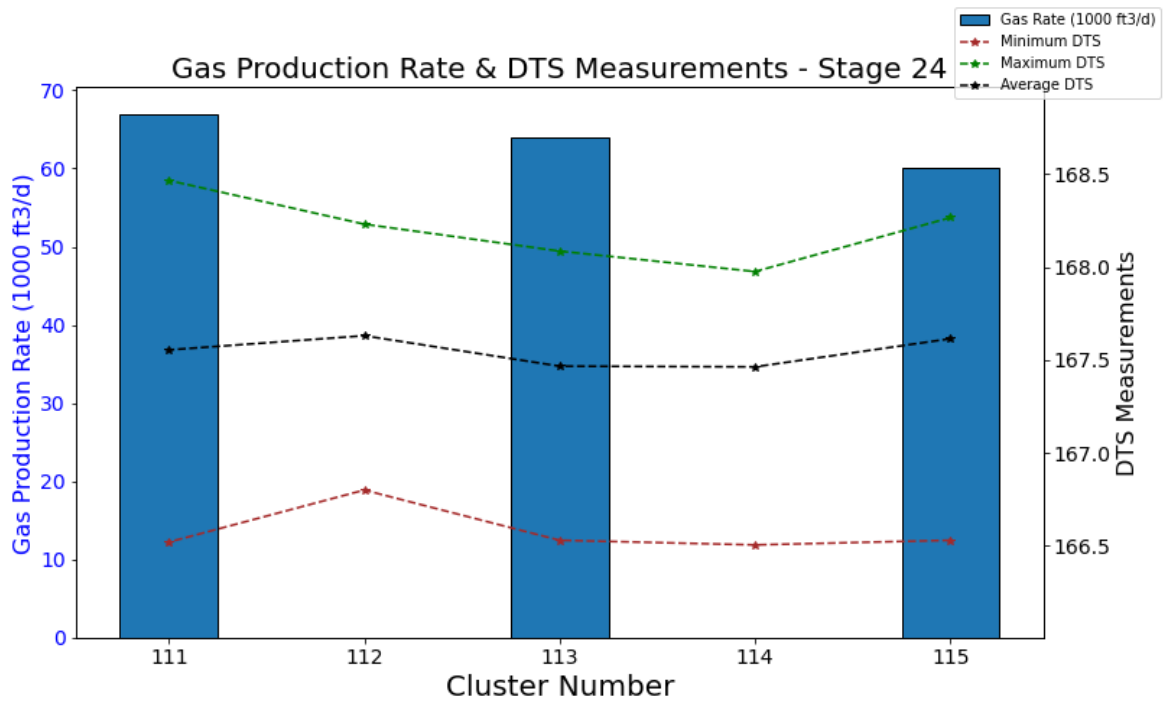


Figure 58: DTS Measurements in Stage 22 on Day of Production Log



*Figure 59: DTS Measurements in Stage 23 on Day of Production Log*



*Figure 60: DTS Measurements in Stage 24 on Day of Production Log*

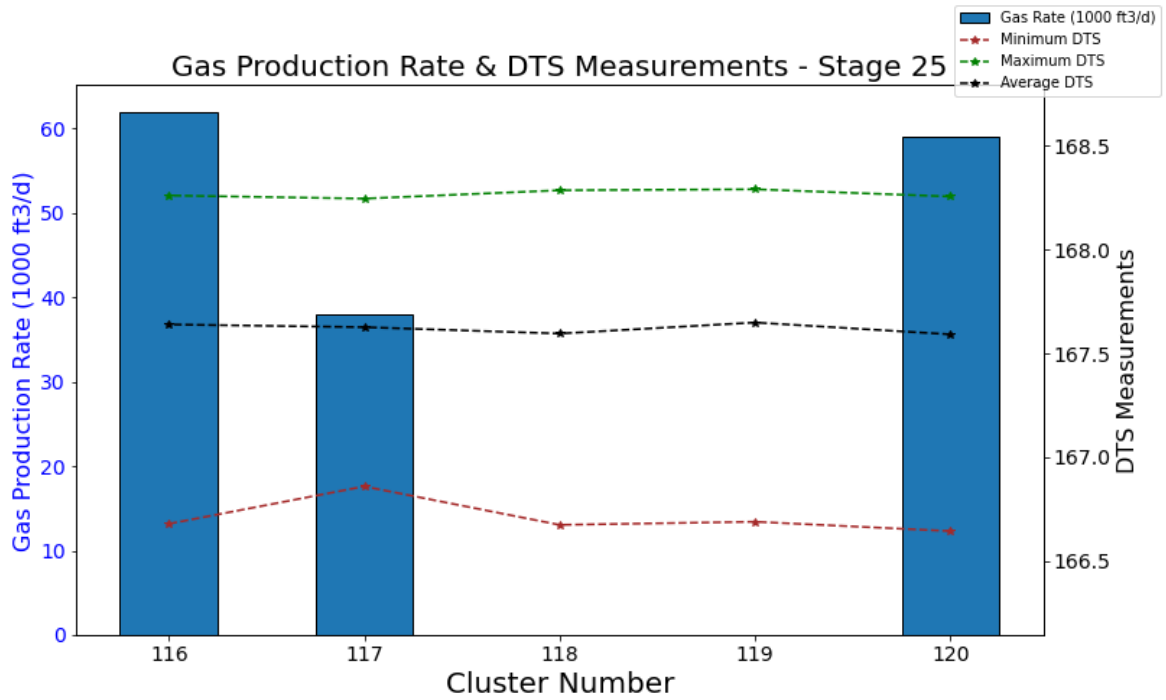


*Figure 61: DTS Measurements in Stage 25 on Day of Production Log*

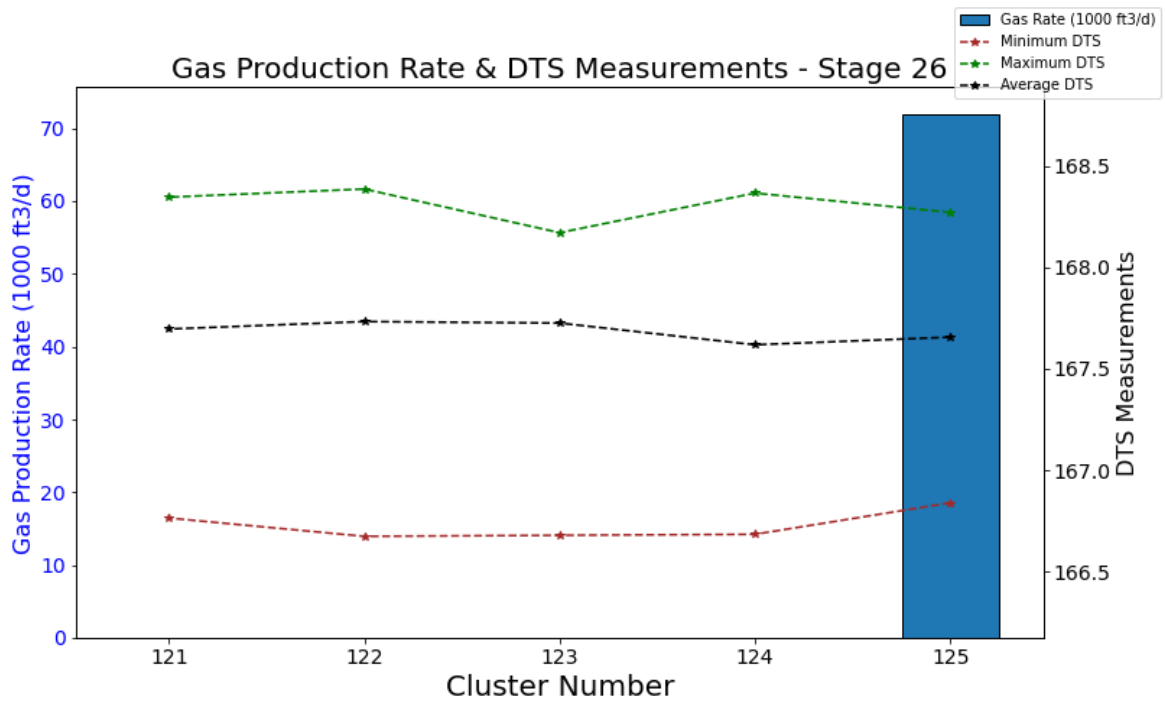


*Figure 62: DTS Measurements in Stage 26 on Day of Production Log*

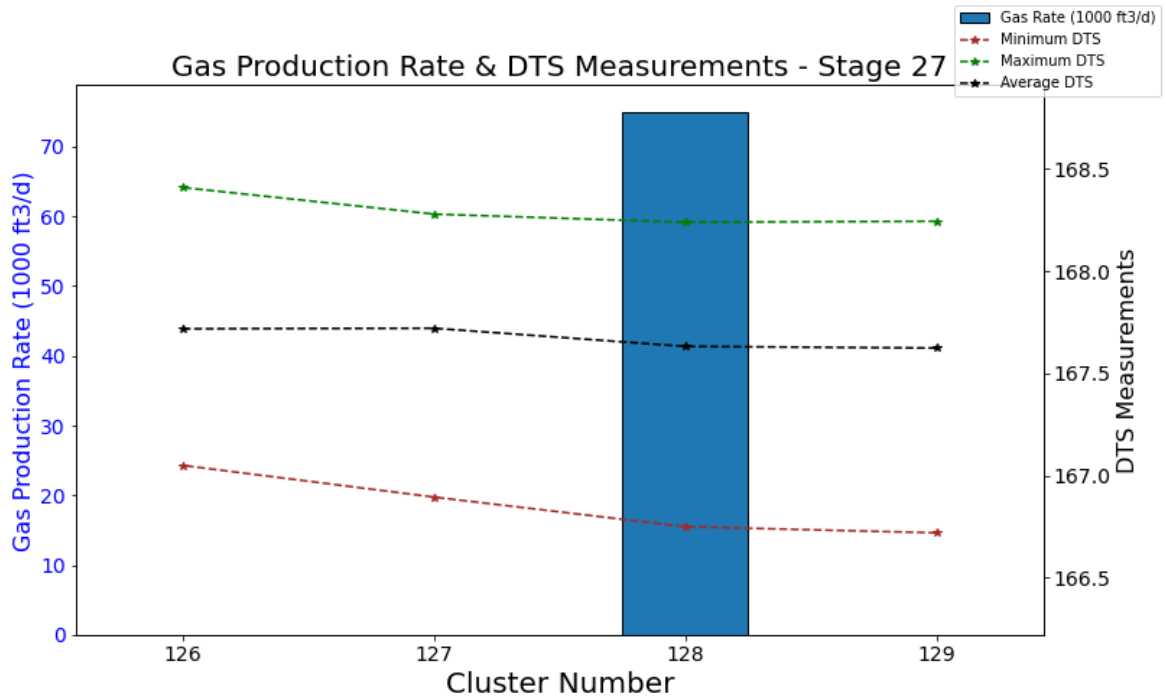


Figure 63: DTS Measurements in Stage 27 on Day of Production Log

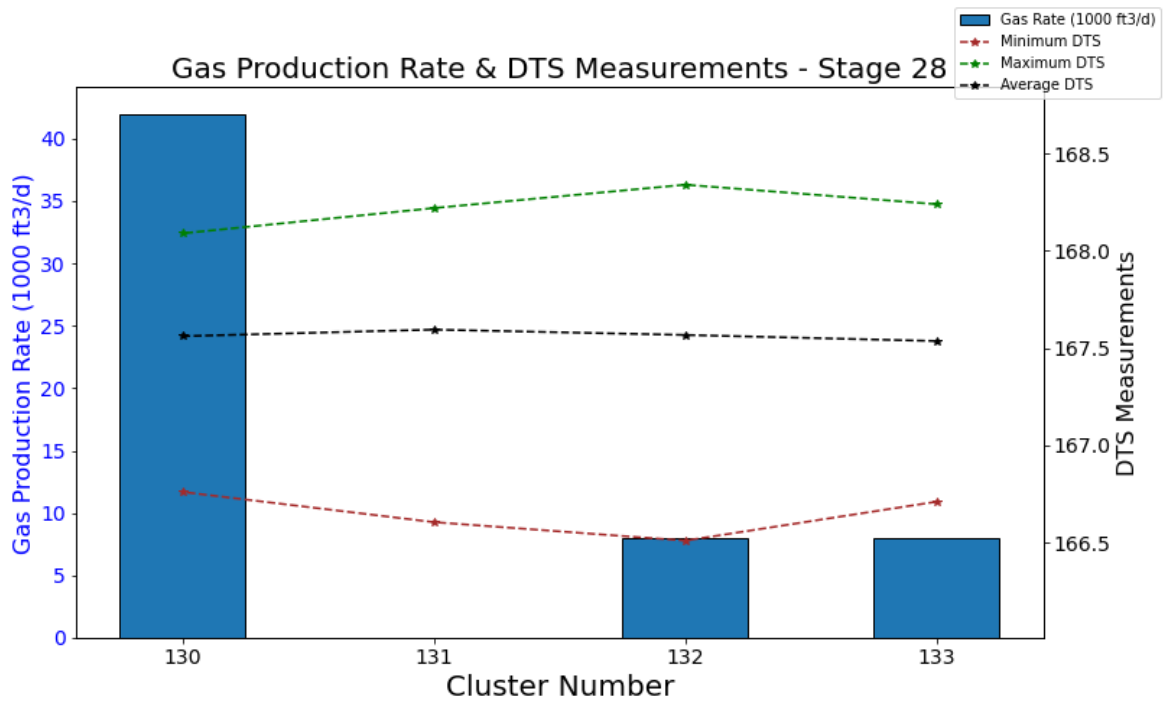


Figure 64: DTS Measurements in Stage 28 on Day of Production Log